TD-07-012
LARP-DSnote_2006

Corresponding author: Giorgio Ambrosio
Fermi National Accelerator Laboratory
Technical Division
Magnet System Department
Mail stop 315
P.O. Box 500
Batavia, Illinois • 60510

TD-07-012
LARP_DSnote_2006
9/26/2006

STUDY OF MECHANICAL DESIGNS FOR 110-mm APERTURE QUADRUPOLE WITH 230-T/m GRADIENT

G. Ambrosio

Fermi National Accelerator Laboratory, Batavia IL 60510, USA

Abstract:

The LHC Accelerator Research Program (LARP) is developing Nb_3Sn quadrupole magnet models for a luminosity upgrade of the Large Hadron Collider (LHC). A major milestone in this development is to assemble and test a series of quadrupole cold masses with 90-mm aperture and gradient larger than 200 T/m during 2006 and 2007.

Aiming at exploring designs with significantly larger apertures, a study of different mechanical designs for a high gradient quadrupole with 110 mm aperture has been performed and is presented in this report. The focus of this study is to understand how to handle the very large forces of such magnet exploring different concepts more than looking for the optimization of a design.

This report presents the magnetic design and forces at maximum gradient (228 T/m), some analytical studies, simple models of collared coils with rigid boundary conditions or external force on the mid-planes, a comparison among several models with interference at the coil-pole interface, detailed solutions of some of these models, study of collaring, a series of models with interference on the coil mid-planes, and conclusions.

1. INTRODUCTION

The LHC Accelerator Research Program (LARP) is developing, Nb_3Sn quadrupole magnet models for a luminosity upgrade of the Large Hadron Collider (LHC). A major milestone in this development is to assemble and test a series of quadrupole cold masses with 90-mm aperture and gradient larger than 200 T/m during 2006 and 2007. In the following years (2008 and 2009) a series of 4m long quadrupole cold masses with the same aperture will be fabricated and tested. Aiming at exploring designs with significantly larger apertures, a study of different mechanical designs for a high gradient quadrupole with 110 mm aperture has been performed and is presented in this report.

In this study we have taken a magnetic design with 110 mm aperture and 228 T/m gradient, and performed a series of analysis in order to evaluate the magnetic forces, the stresses induced in the coils under different conditions, and stresses and deformations with different mechanical designs based on collars. The main goal of this study is the comparison of these mechanical designs in order to find/develop the best suited for this very high level of forces. The next step, based on the results of this study, should be the final optimization of the design (magnetic, mechanical and quench protection) and the assembly procedure.

2. MAGNETIC DESIGN

The magnetic design is based on two double-pancakes resulting in four layers with grading between the two innermost and outermost layers. The conductor parameters are shown in Table I. The magnetic analysis was performed assuming 15 mm spacing for collars between the outer coil radius and the iron, and J_c = 2400 A/mm^2 @ 4.2K , 12 T. The peak field on each layer is shown in table II and the field distribution on each turn is shown in Figure 1. The main parameters of the magnet are presented in Table III, further details can be found in [1].

Table I: Conductor parameters.

Parameter	Unit	110 mm design	
		Inner	Outer
Number of strands	-	24	18
Strand diameter	mm	1.000	1.000
Cable bare width	mm	12.329	9.230
Bare inner edge thickness	mm	1.587	1.662
Bare outer edge thickness	mm	1.943	1.867
Cabling angle	deg.	14.5	14.5
Keystone angle	deg.	1.655	1.273
Average packing factor	%	89.0	89.0
Inner edge compression	%	20.6	16.9
Outer edge compression	%	2.8	6.6
Width compression	%	0.0	0.0
Radial insulation thickness	mm	0.18	0.18
Azimuthal insulation thickness	mm	0.18	0.18
Copper to non-copper ratio	-	1.2	1.2

Table II: Peak field on each layer at quench current.

*Block #	Peak field, T
1	11.59
2	12.83
3	13.51
4	12.76
5	14.04
Current, kA	12.938

*Block numbering starts from the outermost layer.

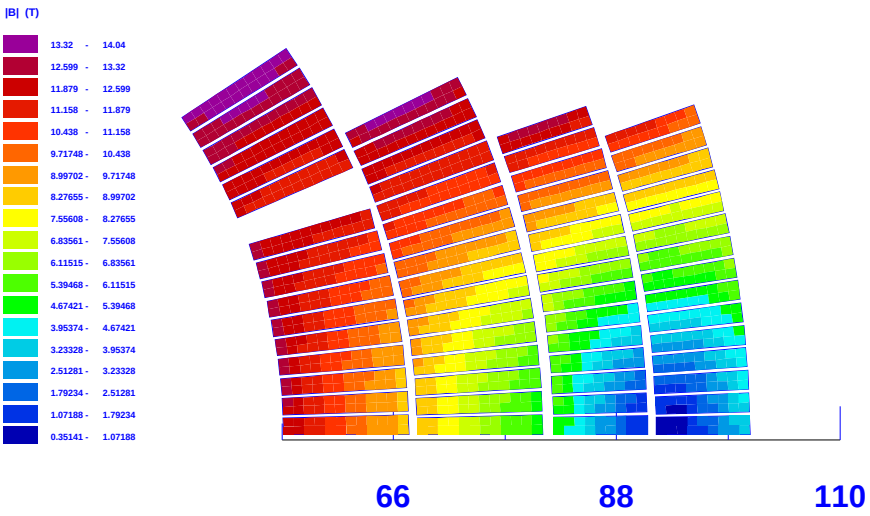

Fig.1: Field distribution in the coil computed by ROXIE.

Table III: Main magnet parameters.

Parameter	Unit	
N of layers		4
N of turns		248
Coil area (Cu + nonCu)	cm^2	84.88
NonCu Jc at 12 T, 4.5 K	A/mm^2	2400
Quench gradient	T/m	228
Quench current	kA	12.94
Peak field in the coil at quench	T	14.04
Inductance	mH/m	17.46
Stored energy	kJ/m	1461

Table IV: Magnetic forces per octant at 228 T/m compared with other quadrupoles.

	HGQ† (MN/m)	TQ* (MN/m)	110 mm (MN/m) ROXIE	110 mm (MN/m) ANSYS
Fx	**1.6**	**1.4**	**4.24**	**4.16**
Fy	**-1.9**	**-2.0**	**-4.23**	**-4.1**
Fr				**2.8**
F_θ				**-5**

† KEK design scaled to 228 T/m
* TQC scaled to 228 T/m

The magnetic forces used for this study were computed using ANSYS and compared with the previous results (obtained by ROXIE). The results by ANSYS are very close to those by ROXIE. The field distribution by ANSYS is shown in Fig 2. The maximum field computed by ANSYS is slightly lower because in ANSYS the current is distributed on the whole shell (made of the cable turns and the insulation between turns). The magnetic forces, shown in Table V, are very close (see comparison in Table IV). Fig. 3 shows the magnetic forces at maximum gradient (228 T/m). The length of each vector in this plot depends on the mesh (force density time element surface), therefore it can be used only for comparison within each coil layer.

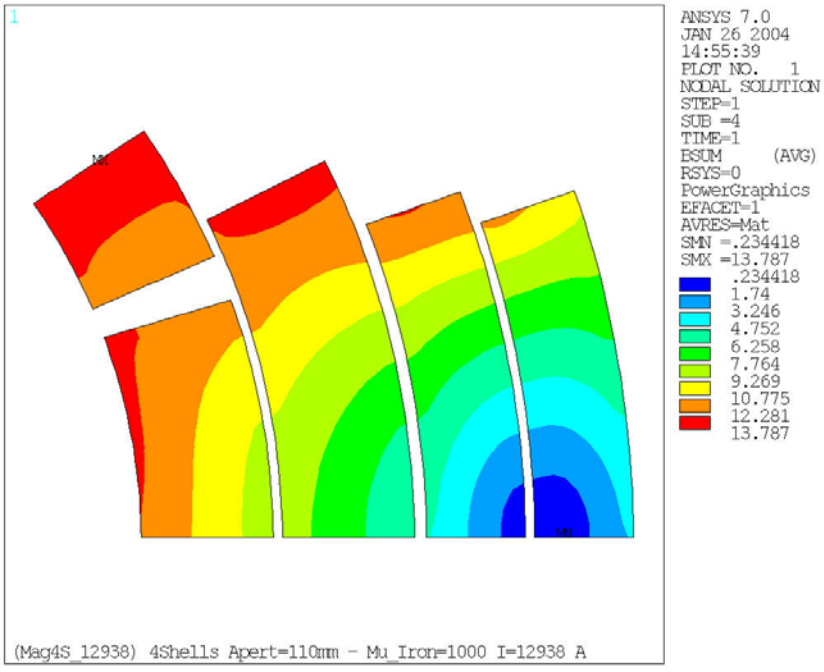

Fig.2: Field distribution in the coil computed by ANSYS

Table V: magnetic forces (N/m) at quench current computed by ANSYS

SELECT	COMPONENT CO1D	SELECT	COMPONENT CO1D
FX	0.133427E+07	FR	0.121418E+07
FY	-389475.	FTH	-614402.
SELECT	COMPONENT CO1U	SELECT	COMPONENT CO1U
FX	740593.	FR	346012.
FY	-606634.	FTH	-887203.
SELECT	COMPONENT CO2	SELECT	COMPONENT CO2
FX	0.146865E+07	FR	0.107740E+07
FY	-0.111281E+07	FTH	-0.139791E+07
SELECT	COMPONENT CO3	SELECT	COMPONENT CO3
FX	705948.	FR	430255.
FY	-0.102205E+07	FTH	-0.113054E+07
SELECT	COMPONENT CO4	SELECT	COMPONENT CO4
FX	-86563.4	FR	-305998.
FY	-971600.	FTH	-947889.
SELECT	COMPONENT COILS (TOTAL)	SELECT	COMPONENT COILS (TOTAL)
FX	0.416290E+07	FR	0.276185E+07
FY	-0.410257E+07	FTH	-0.497795E+07

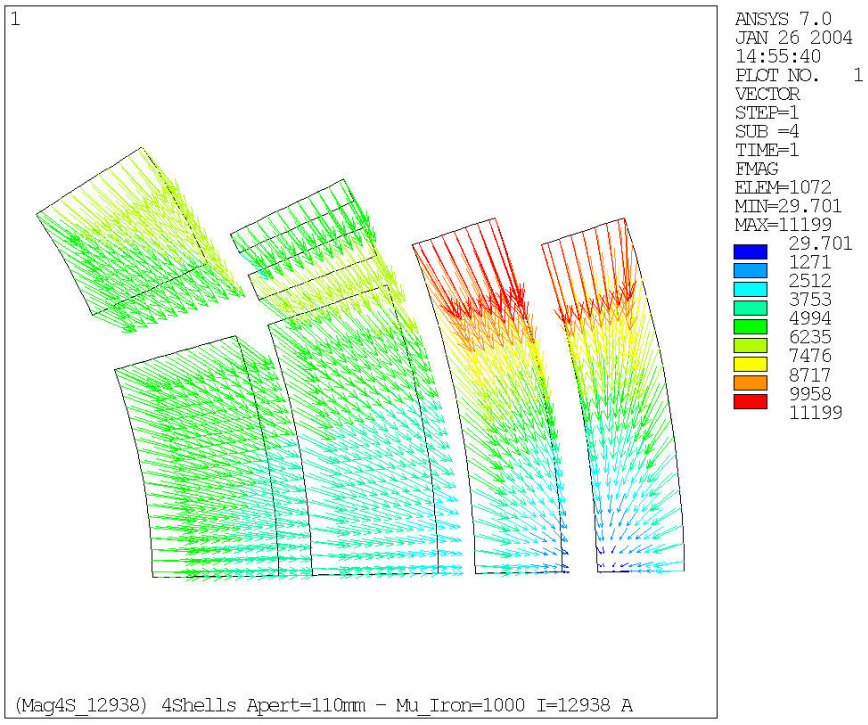

Fig.3: Distribution of magnetic forces at 228 T/m

3. ANALYTICAL STUDIES

A few simple analytical observations, based on the magnetic forces presented in the previous section, can show the feasibility and the complexity of a mechanical design for this magnet.

The azimuthal component of the magnetic force on the first layer (lower and upper blocks) is 1.5 MN/m. Since the cable width is 12.3 mm it results in a transverse pressure of 122 MPa. Therefore this is the minimum average pressure expected on the midplane turn unless the pole turn is glued to the pole and it goes under tension (scenario that should be avoided because could result in very long training). Any coil bending (unavoidable under magnetic forces) will further increase the peak stress on this turn.

In order to have a first order estimate of the coil bending under magnetic forces we can assume that the coil is divided in two equal-surface parts by an horizontal line, and look at the effect of the horizontal component of the force. On the lower half the force is 1.7 MN/m. The coil, with respect of the force in radial direction, is a stack of cable layers (50 GPa elastic module) and insulation layers (14 GPa module). Taking into account the thickness of these layers, including the ground insulation, it's possible to compute the displacement under 1.7 MN/m that results in 87 μm. This has been computed assuming a uniform force distribution on the lower half coil. In reality the force is higher on the midplane, and so should be the deformation on the midplane. In the upper half of the coil the top layers cannot be displaced because they are supported by the pole component. Therefore the coil radial deformation (difference between the radial displacement on the innermost radius of the coil at the midplane and at the pole) should be larger than 87 μm in case of an infinitely rigid mechanical structure. This deformation will increase the peak stress in the first layer previously computed.

4. F.E.M. MATERIAL PROPERTIES

Table VI presents the properties of the materials used in the FE models presented in this report. All analyses have been performed using ANSYS 9.0. The following figures (M1 and M2) show the mesh and the materials in the whole model and in the coil area.

The mechanical properties of the cable stack are from [2]. The cable stack thermal contraction coefficient in azimuthal direction is consistent with measurement performed on Nb_3Sn cable stacks insulated with Kapton and excessive for Nb_3Sn cable stacks insulated with ceramic or S2-glass fiber reinforced epoxy. This problem was found during the development of this study, and it was decided not to fix it for consistency and easy comparisons among the different cases presented. The goal of this study is in fact a comparison among different mechanical designs and a feasibility study. The use of a thermal contraction coefficient higher than expected makes more difficult to find an acceptable solution and is therefore a conservative approximation.

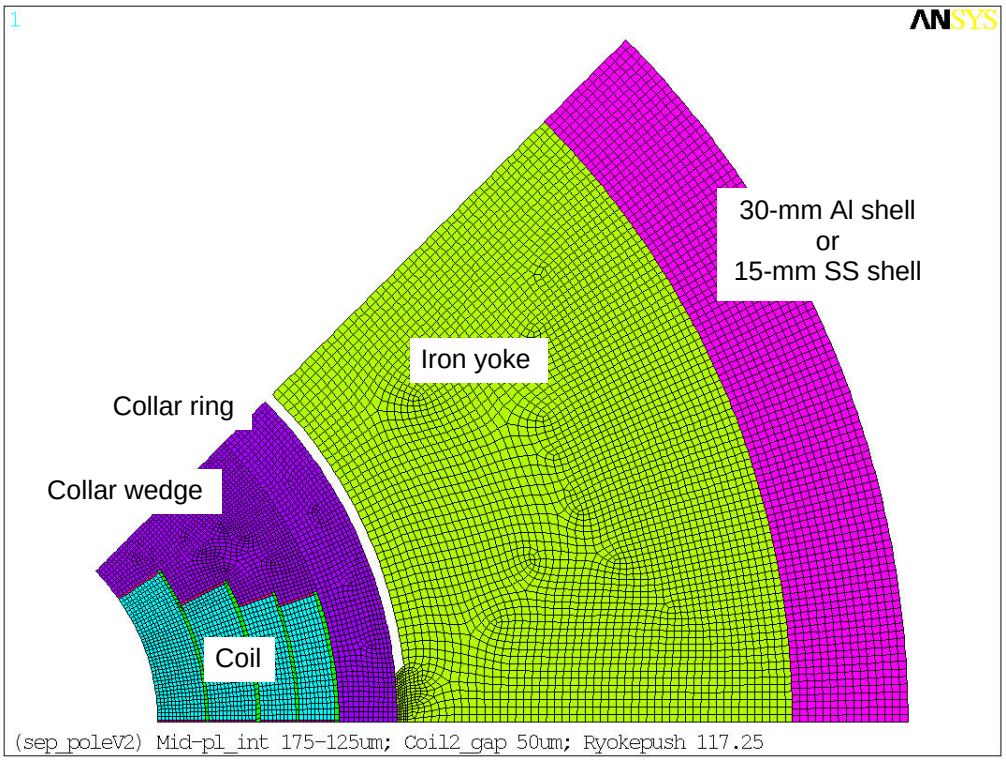

Fig. M1: FEM model with 30-mm Al shell showing mesh and materials (different colors)

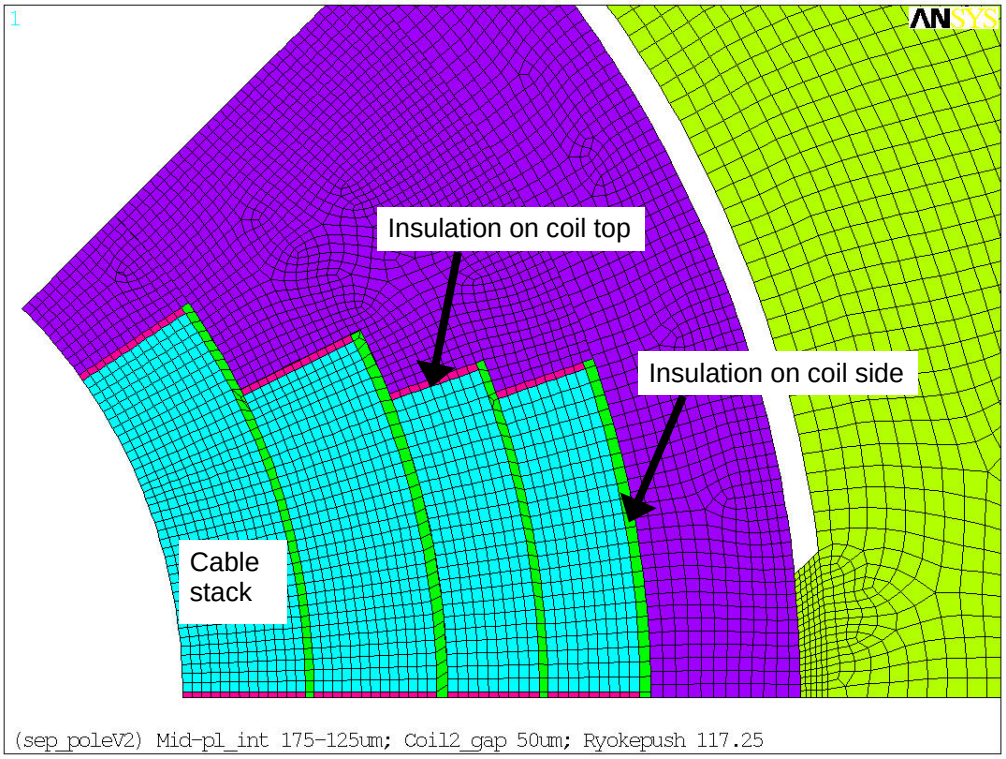

Fig. M2: Detail of the FEM model showing mesh and materials (different colors) in the coil

Table VI: Material Properties (in radial coordinates) used in the analyses presented in this report.

Magnet Component		Elasticity Modulus				Thermal Contraction Coefficient			
		293 K [GPa]		4.2 K [GPa]		293–4.2K [mm/m]		per 1 K [μm/m/K]*	
		X	Y	X	Y	X	Y	X	Y
Cable stack	Impregn. Cu/Nb_3Sn, + ceramic ins.	40	38	50	38	3.3	4.3	11.4	15
Layer-layer & ground insul. on coil side	G10	14	18	14	18	7.62	2.75	26.4	9.5
Mid-plane & ground insul. on coil top	G10	18	14	18	14	2.75	7.62	9.5	26.4
Collar wedge & ring, SS outer shell	Stainless Steel 316	210	210	225	225	2.97	2.97	10.3	10.3
Yoke	Iron	210	210	225	225	2.04	2.04	6.9	6.9
Al outer shell	Aluminum	70	70	81.6	81.6	4.23	4.23	14.3	14.3

(*calculated from integrated contraction between 293 and 4.2 K, assuming a linear contraction coefficient)

5. SIMPLE MODELS

The first analysis uses a simple model consisting of coils (all layers glued together) and stainless steel collars with infinitely rigid boundary conditions on the outer surface of the collars (see Fig. 4). The collars are made of two pieces (pole and outer ring) without modeling the laminations. No pre-stress is applied to the coils and all material properties are at 4.2 K. When the magnetic forces are applied the coil deflection (88 μm) increases the azimuthal stress on the midplane close to the aperture resulting in 152 MPa peak stress (see Fig. 5).

The second analysis uses the same model without the infinitely rigid boundary condition. In this case some pre-stress (80-90 MPa) is applied at room temperature by azimuthal interferences (between coil and collar-wedge) and radial interference (between coil and collar-ID). The cooldown is simulated by changing temperature and material properties starting from the solution at 300 K. During cooldown an external force of 2 MN/m is applied to the collar outer surface on the midplane resulting in a bending inward of the coil ID of 34 μm. The coil stress after cooldown is acceptable except for a stress concentration point on the midplane at the contact between coil and collar (see Fig. 6). When magnetic forces are applied the azimuthal stress on the midplane of the coil ID remains below 140 MPa (see Fig. 7). Higher stresses can be found close to the stress concentration point on the midplane of the coil OD but remedies can easily be found (such as the distribution of the external force on a large surface, or the use of a dummy turn on the midplane of the outer layer).

The coil inner radius on the midplane moves outward by 203 μm under magnetic forces (this change will be called “coil displacement” in the following) and the final coil deflection is 103 mm (it cannot be easily compared to the deflection of the previous case because of the cooldown and because of slightly different material properties).

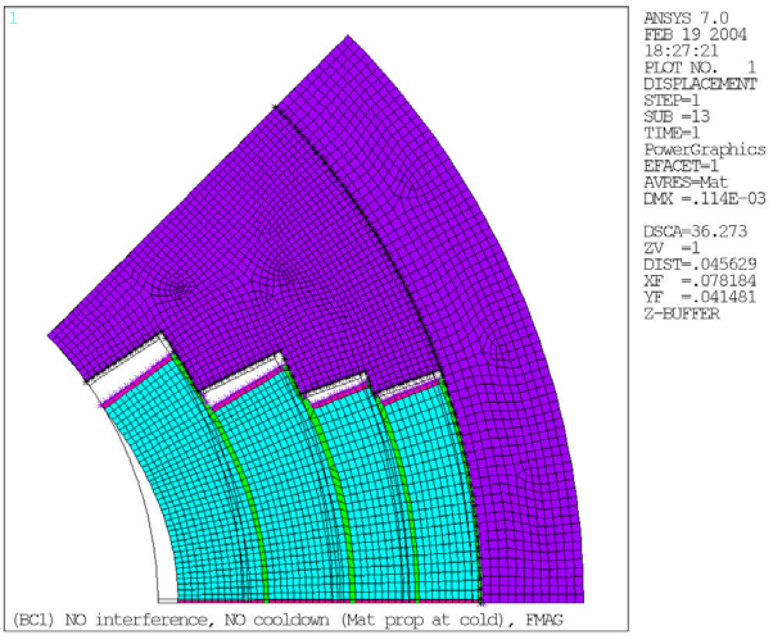

Fig.4: Simple model #1: Coils and collars with infinitely rigid boundary condition on the OD. The plot shows the coil deformation (enhanced) under magnetic forces.

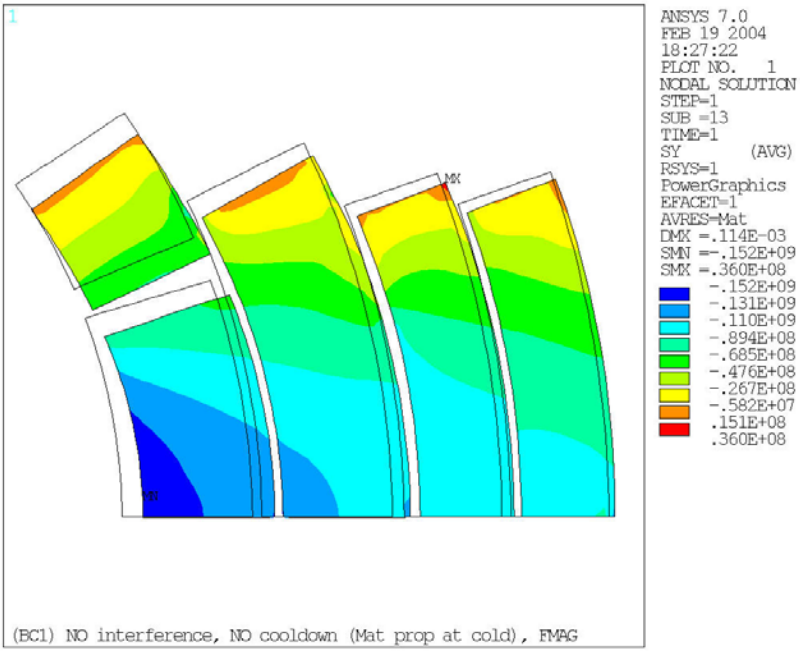

Fig.5: Simple model #1: Coils and collars with infinitely rigid boundary condition on the OD. The plot shows the azimuthal stress under magnetic forces.

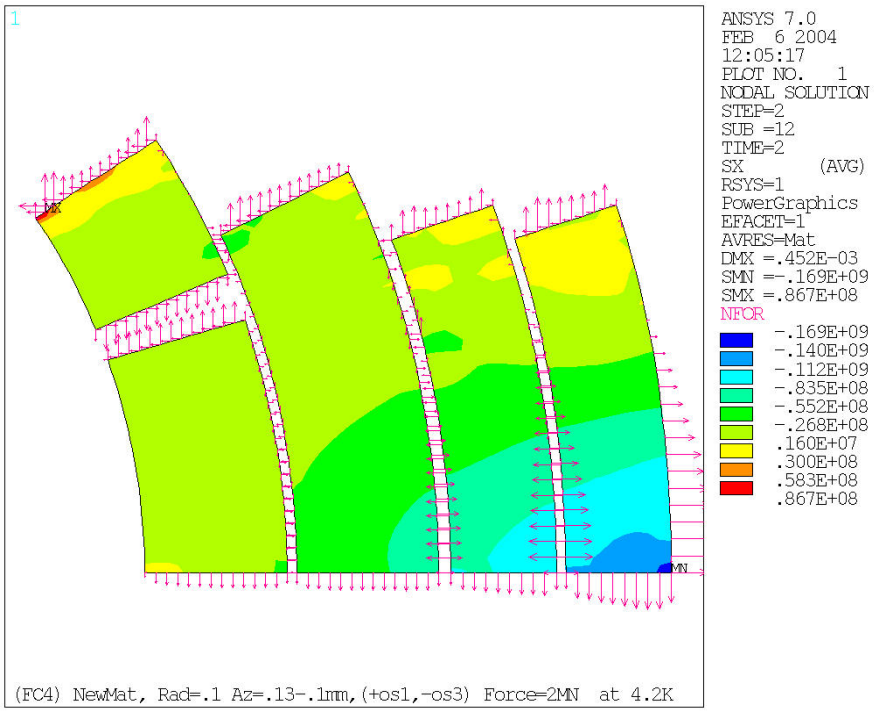

Fig.6: Simple model #2: Coils and collars with external load on the midplane. The plot shows coil radial stress after cooldown

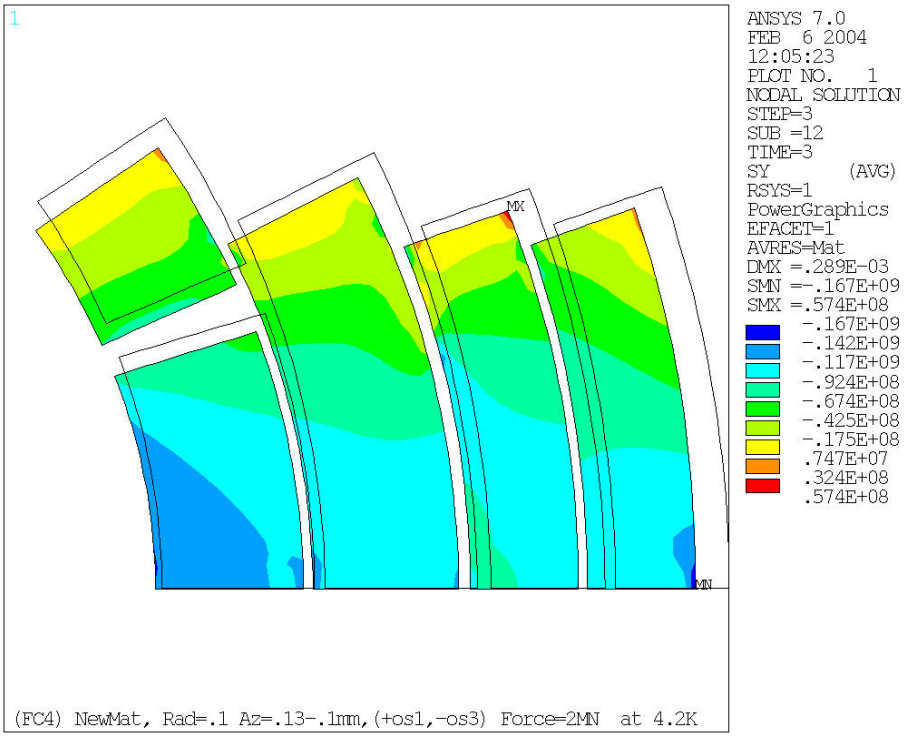

Fig.7: Simple model #2: Coils and collars with external load on the midplane. The plot shows coil azimuthal stress under magnetic forces.

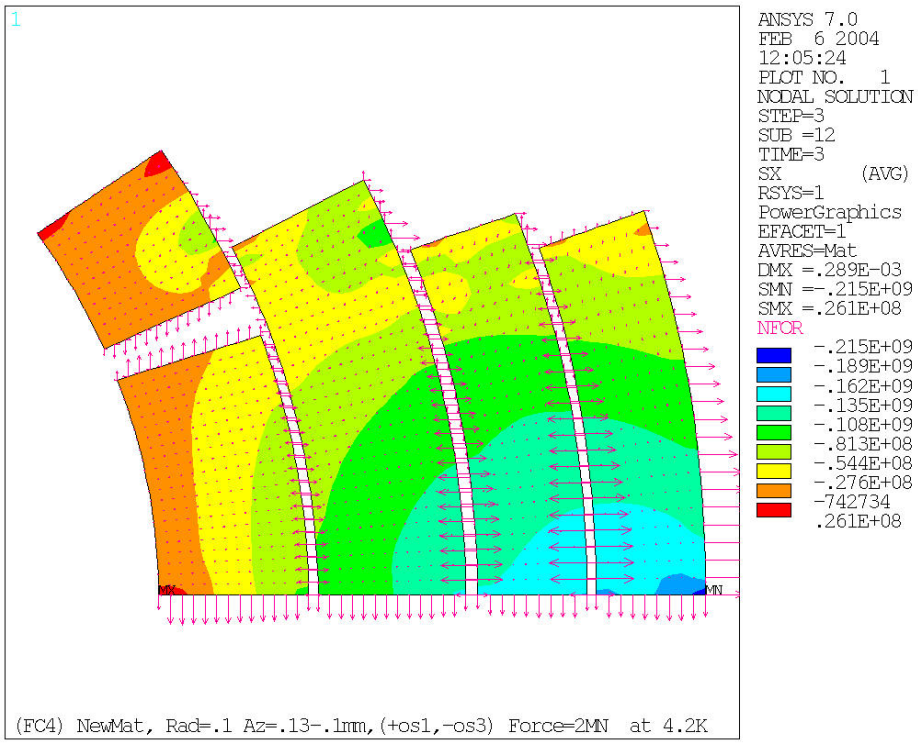

Fig.8: Simple model #2: Coils and collars with external load on the midplane. The plot shows coil radial stress under magnetic forces, and nodal forces.

6. 1st SERIES – F.E. MODELS WITH INTERFERENCE AT COIL-POLE

The results of the previous sections show that the mechanical design should provide a very rigid structure with additional force on the mid-planes in order to reduce the coil bending. Several models have been developed and compared aiming at this goal. They are based on the following concept:

- almost stand-alone stainless steel collars, which can provide sufficient pre-stress at room temperature
- additional support on the mid-planes by the outer shell, which provides additional pre-stress during cooldown and avoids excessive coil bending under magnetic forces.

Table VII presents the list of models. In all these models the four layers of the coil are glued together (as if impregnated together) and the collars are made of a 15-mm thick collar ring and a collar wedge (without modeling the laminations). Pre-stress is applied by coil-collar interferences (azimuthal interference on coil top, and radial interference on coil OD) to simulate the collaring, and by yoke-skin interference to simulate the skin welding or the Al-shell pre-load. The Al-shell pre-load can be achieved by using bladders (in the yoke gap at 45°) and shims (on the mid-plane at the contact between collars and yoke). The contact between collars and yoke extends from the mid-plane up to 6°.

The yoke gap is open at room temperature in all models. It closes completely during cooldown in the last two models. In the first models the yoke gap closes only in the center of the gap (radially) where 10-mm long shims are located after the bladder inflation (yoke ID and OD are 120 and 220 mm respectively).

Fig. 9 shows the model with 15-mm thick stainless steel outer shell.

Table VII: 1st series models and main results

Model:	***Gap***	***Max Stress***	**Coil displacement†:** ***Cooldown – G = 228 T/m***
Al shell (30 mm)	**Closed at shim**	**<150 Mpa***	**131 μm**
Thick Al shell (60 mm)	**Open**	**“**	**153 μm**
Al shell (30 mm)	**Open**	**“**	**167 μm**
Stainless steel shell (15 mm)	**Open**	**“**	**158 μm**
Al shell (30 mm)	**Closed**	**“**	**120 μm**
Stainless steel shell (15 mm)	**Closed**	**“**	**124 μm**

* Except lowest turn on the outermost coil

† At the coil inner radius on the mid-plane

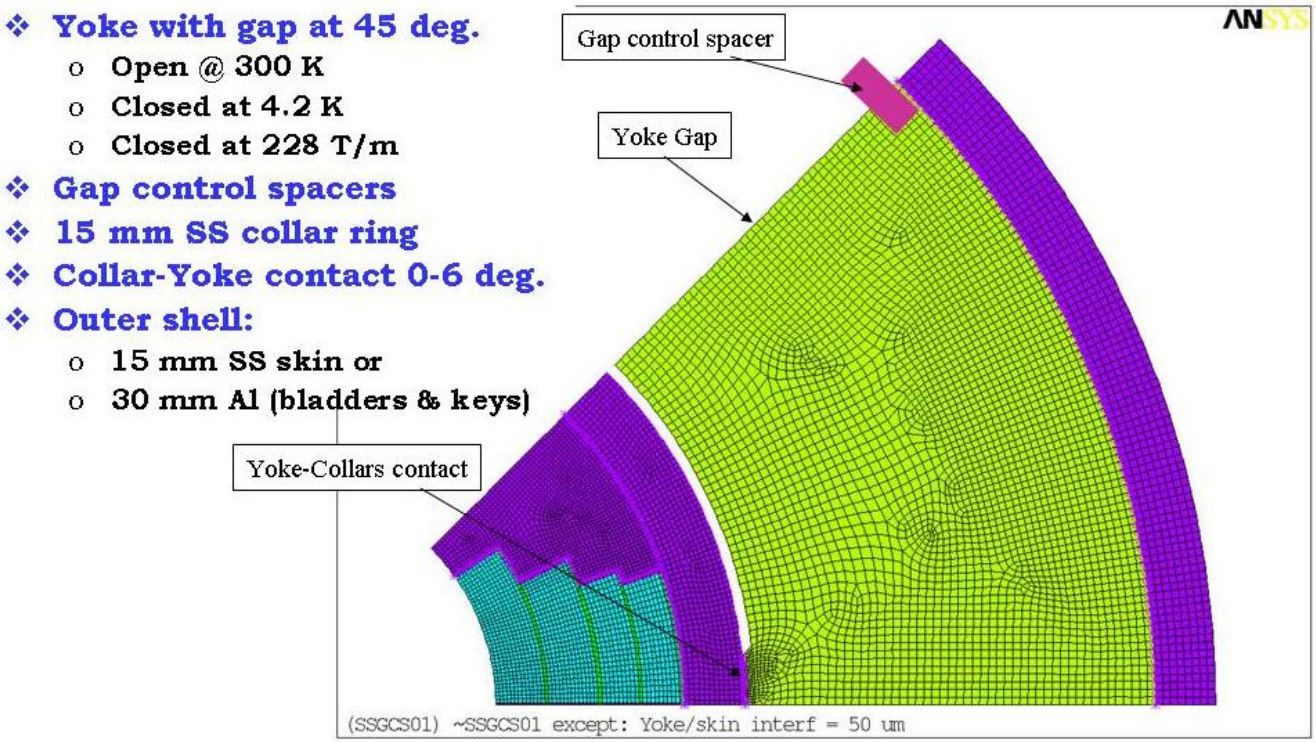

Fig.9: 1st series model with 15-mm stainless steel shell.

Table VI shows that in all models it's possible to keep the maximum stress below 150 MPa during all stages of operation (pre-stress application at 300 K, cooldown, maximum forces).

A stress concentration point is present on the mid-plane at the coil-collar interface as in the second analysis presented in the previous section. The solutions presented for that case (optimization of collar-coil contact, and/or dummy turn) can be adopted for all these models.

The largest difference among these models is the coil displacement (see definition in the previous section) that goes from 120 to 167 μm. The more rigid is the structure the smaller is the deformation. The smallest deformations (acceptable from a field quality point of view) have been obtained by closing the yoke gap during cooldown with sufficient force to keep it closed under maximum magnetic forces. Small coil displacements are associated with small coil deformations (defined as the difference between the coil inner radius on the midplane and the coil inner radius on the pole turn). The yoke gap closing also prevents excessive coil pre-stress from the shell. Both a 15-mm stainless steel shell (welded under a press) and a 30-mm aluminum shell (preloaded by using bladders and keys) can be used to achieve this goal. Gap control spacers (as developed during the R&D for the 1st generation of LHC main dipoles) should be used to preserve yoke alignment and assure that the gaps close at the right time during cooldown with uniform pre-stress.

7. 1st SERIES BEST SOLUTIONS

Examples of analysis using a 15-mm steel shell (see 7.1) and a 30-mm aluminum shell (see 7.2 and 7.3) are shown in the following pages. The first and second models have interferences optimized for each coil layer. They are: (S1) 0.13-0.18, (S2) 0.12-0.12 (S3) 0.12-0.07, (S4) 0.12-0.12 mm; where for each layer (starting from the innermost layer) the numbers show the interference thickness at the inner and outer layer edge (if the two numbers are the same, there is a rectangular interference, if the are different there is a wedge-like interference). The third model has the same interference on each layer.

The main parameters of these models have been previously described. The yoke ID and OD are respectively 120 and 220 mm.

The following plots show for each stage of the analysis (after pre-stress application, after cooldown, and under maximum forces):

- Radial displacement (in meter) along the aperture starting from the midplane up to the mid-pole. The displacement is computed with respect to the geometry at room temperature before pre-stress application. This plot is useful to evaluate the coil deformation (difference between the displacement at the mid-plane and the displacement at the coil pole turn [at about 3.4 cm]), and to evaluate the coil displacement under magnetic forces (difference between the displacement after cooldown and the displacement under magnetic forces).
- Detail of the model showing the coils, the collars ring and wedge, part of the yoke, and the contact elements (black lines and asterisks). Displacements and deformations are scaled up in order to show trends.
- Azimuthal stress in the coil.
- Radial stress in the coil and nodal forces (i.e. the forces applied from the coil boundaries against the othrer parts of the model not shown in this plot.
- Radial coil displacements with respect to coil shape before pre-stress application (shown by black lines).

- Equivalent stress in all parts of the model and nodal forces acting against boundaries used to enforce symmetry conditions.
- At the end of the second model (Al-shell with interferences optimized for each shell) the reaction forces are plotted (together with the equivalent stress) after each step of the solution, showing that the yoke gap is open at room temperature, closed after cooldown , and that it remains closed at maximum gradient.
- The last plot shows the equivalent stress in the coil under maximum forces

These models are not fully optimized (because this wasn't the goal of this study), nonetheless they show that it's possible to find acceptable solutions:

- Max stress in the coil lower than 150 MPa at all stages (using a dummy turn on the mid-plane of the outermost coil)
- Acceptable coil displacement and deformation (105 and 87 μm in case of stainless steel and aluminum shell respectively) under magnetic forces
- Pole turns still under compression (in the solution with 30-mm aluminum shell), or under very small tension (in the solution with 15-mm stainless steel shell).

The first two models (7.1 and 7.2) show more uniform pre-stress at room temperature and after cooldown than the last one (7.3) because coil-collar interference shims were optimized for each layer. In case of the last model the same interference was used for all layers. A comparison between the second and third model shows the advantage of optimizing the interference for each layer.

The yoke gap under max force is partially open in the first model, it remains completely closed in the second and third models.

7.1 15-mm stainless steel skin - Yoke closes during cooldown - Yokegap=0.01,

Coil/Coll radial interference : 0.1 mm, Yoke/skin radial interference = 50 μm,
Azim. interference = (S1) 0.13-0.18, (S2) 0.12-0.12 (S3) 0.12-0.07, (S4) 0.12-0.12

Prestress:

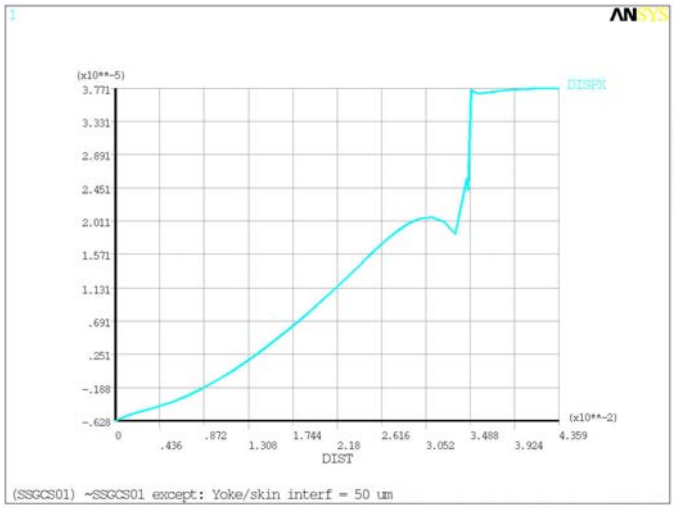

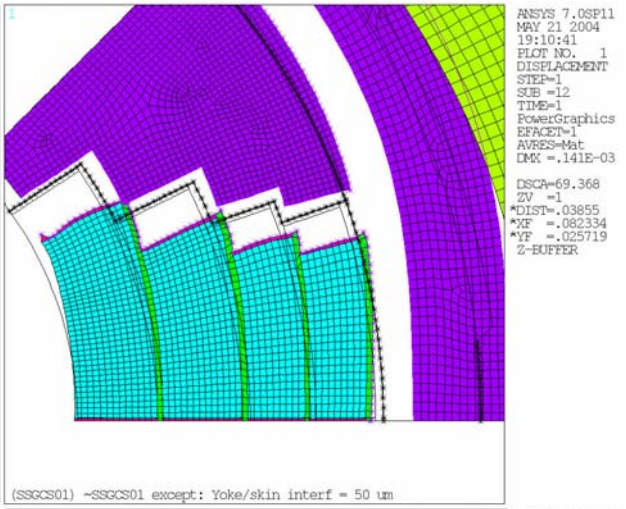

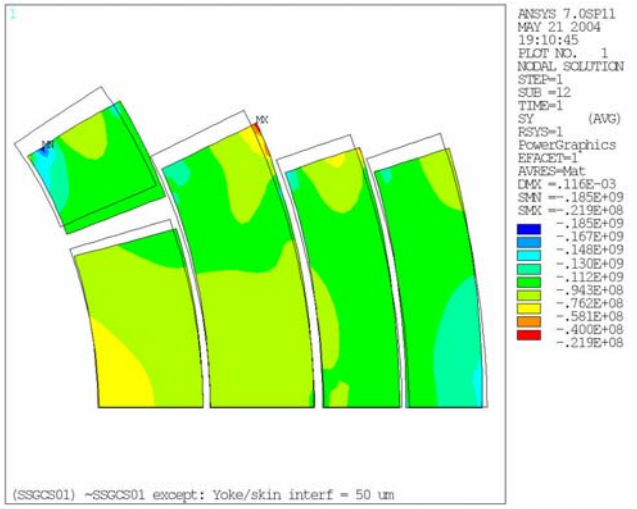

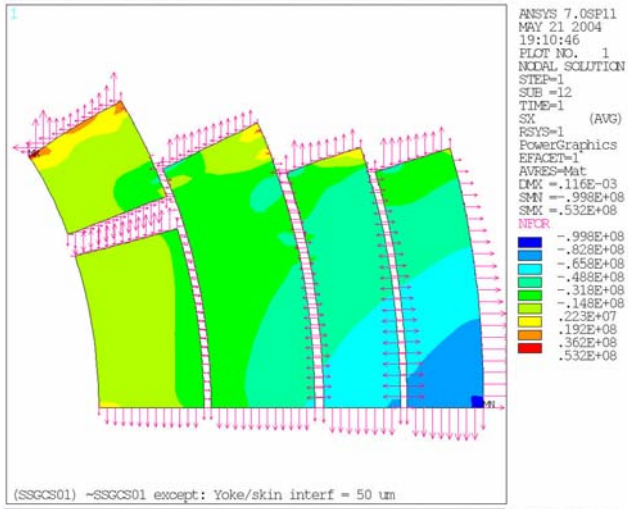

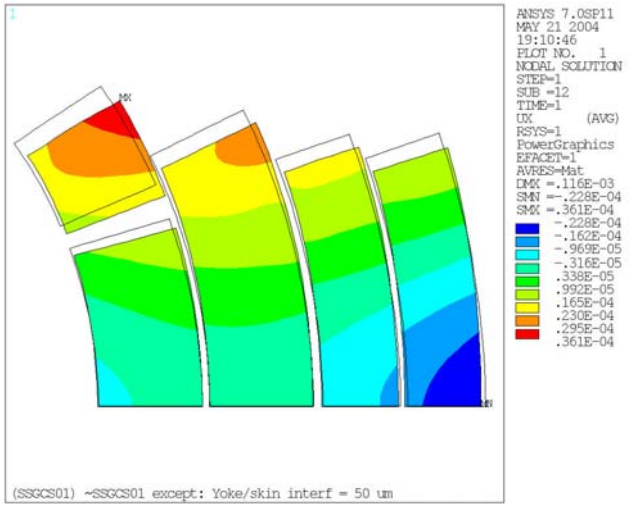

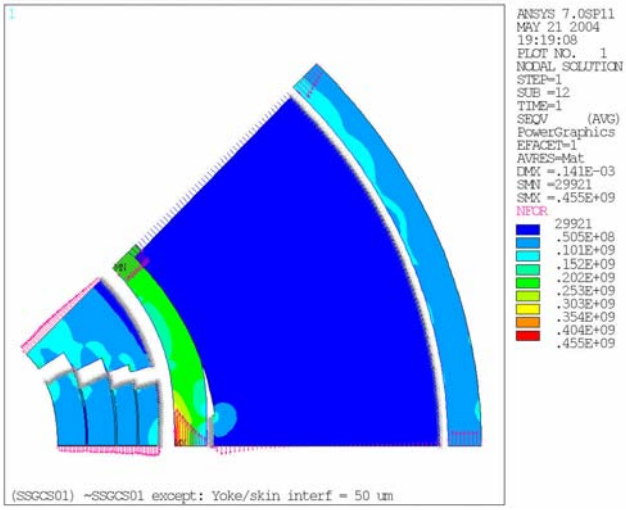

After Cooldown

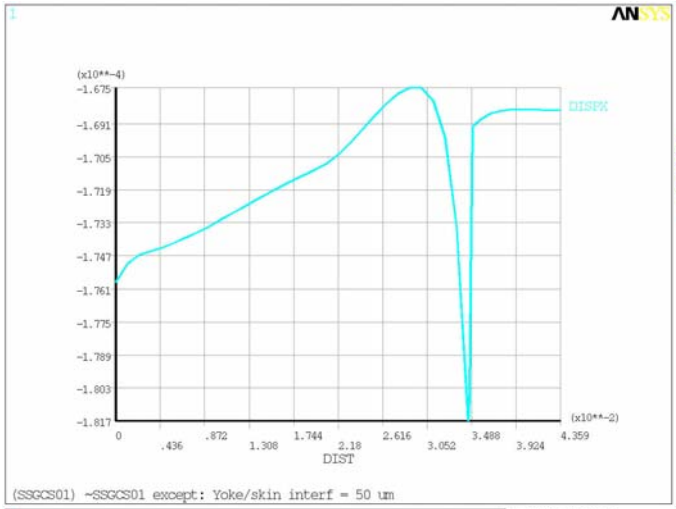

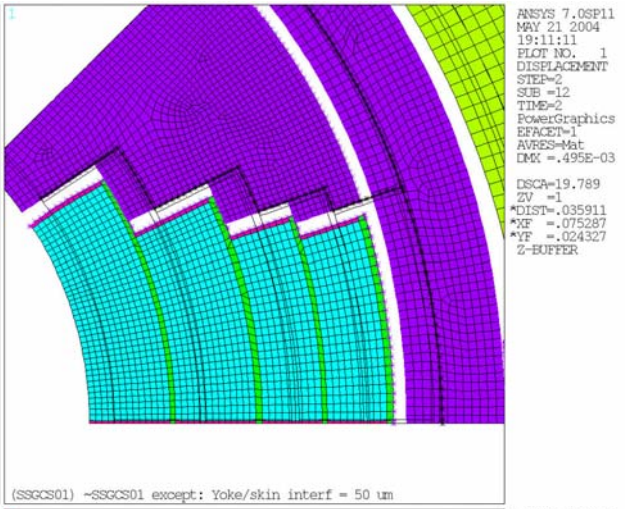

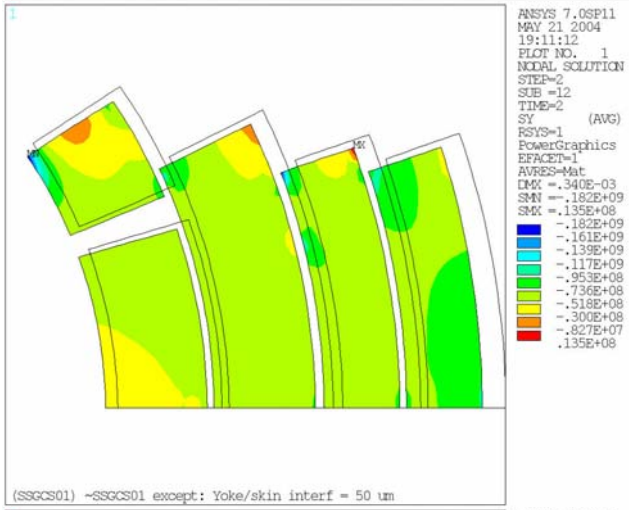

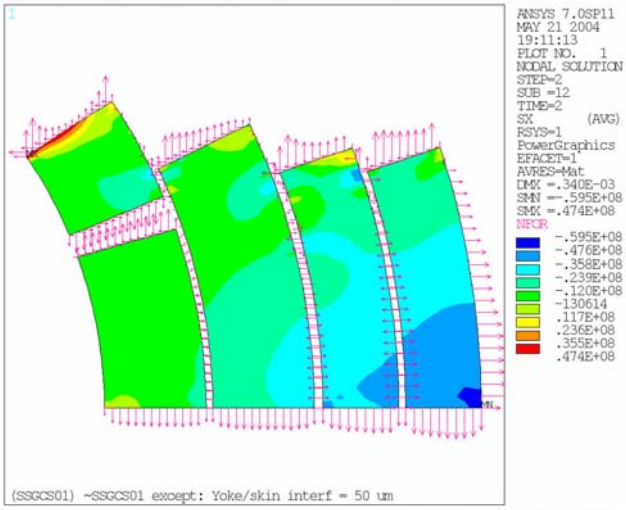

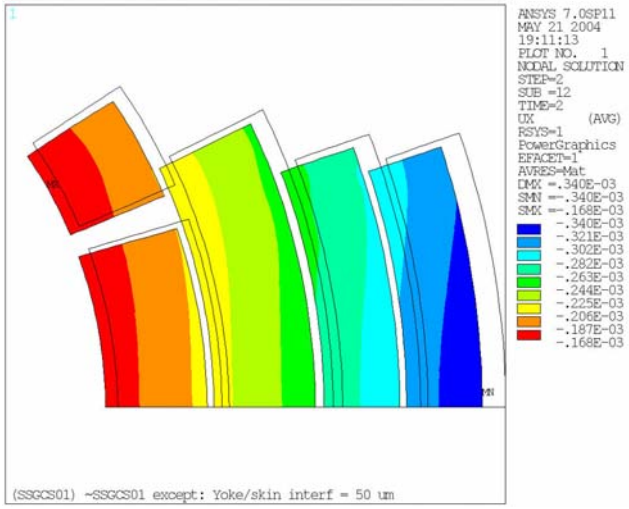

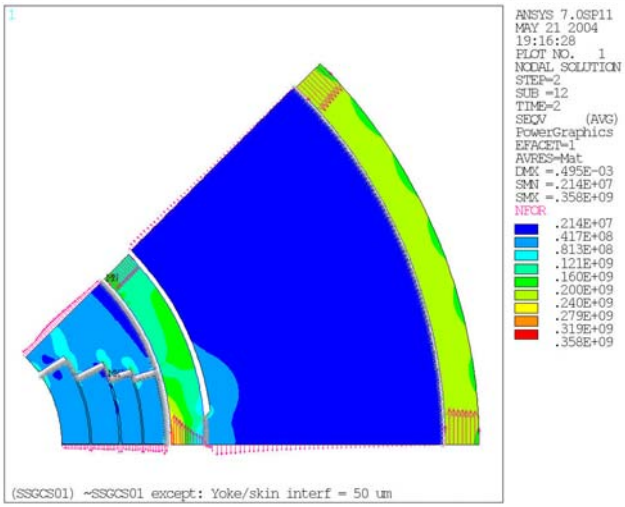

At 228 T/m

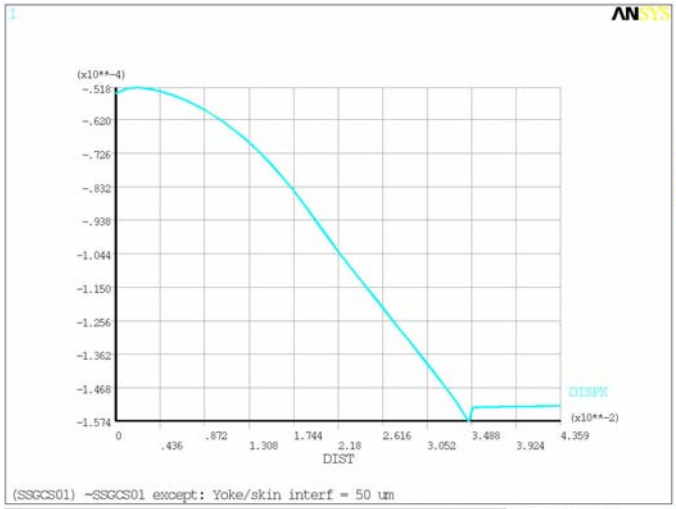
ANSYS
(x10**-4)
-.518
-.620
-.726
-.832
-.938
-1.044
-1.150
-1.256
-1.362
-1.468
-1.574
DISPX
(x10**-2)
0
.436
.872
1.308
1.744
2.18
2.616
3.052
3.488
3.924
4.359
DIST
(SSGCS01) ~SSGCS01 except: Yoke/skin interf = 50 um

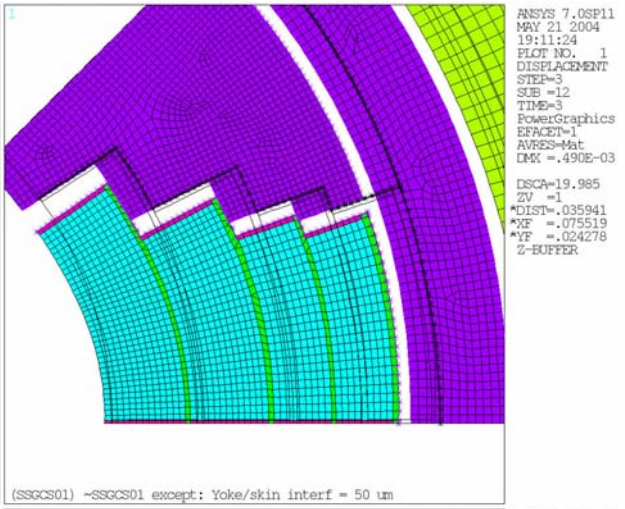
ANSYS 7.0SP11
MAY 21 2004
19:11:24
PLOT NO. 1
DISPLACEMENT
STEP=3
SUB =12
TIME=3
PowerGraphics
EFACET=1
AVRES=Mat
DMX =.490E-03
DSCA=19.985
ZV =1
*DIST=.035941
*XF =.075519
*YF =.024278
Z-BUFFER
(SSGCS01) ~SSGCS01 except: Yoke/skin interf = 50 um

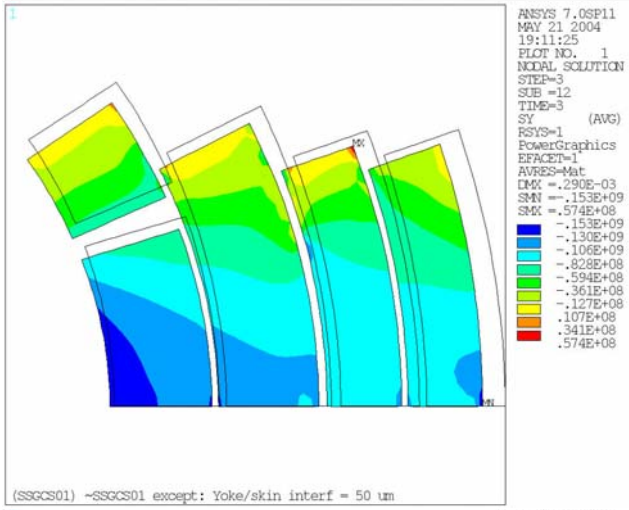
ANSYS 7.0SP11
MAY 21 2004
19:11:25
PLOT NO. 1
NODAL SOLUTION
STEP=3
SUB =12
TIME=3
SY (AVG)
RSYS=1
PowerGraphics
EFACET=1
AVRES=Mat
DMX =.290E-03
SMN =-.153E+09
SMX =.574E+08
-.153E+09
-.130E+09
-.106E+09
-.828E+08
-.594E+08
-.361E+08
-.127E+08
.107E+08
.341E+08
.574E+08
(SSGCS01) ~SSGCS01 except: Yoke/skin interf = 50 um

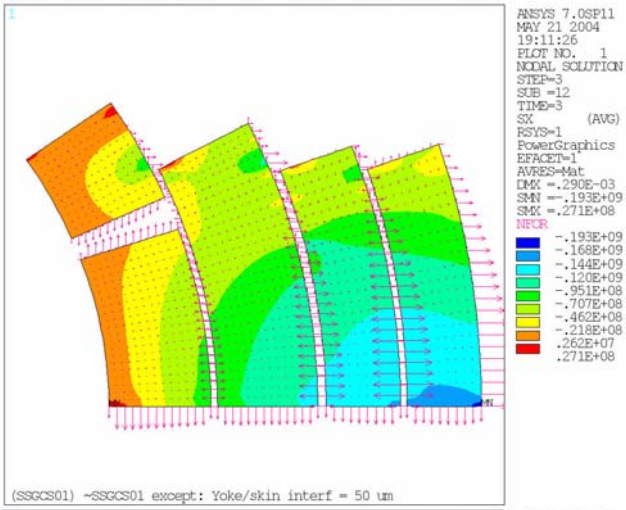
ANSYS 7.0SP11
MAY 21 2004
19:11:26
PLOT NO. 1
NODAL SOLUTION
STEP=3
SUB =12
TIME=3
SX (AVG)
RSYS=1
PowerGraphics
EFACET=1
AVRES=Mat
DMX =.290E-03
SMN =-.193E+09
SMX =.271E+08
NFOR
-.193E+09
-.168E+09
-.144E+09
-.120E+09
-.951E+08
-.707E+08
-.462E+08
-.218E+08
.262E+07
.271E+08
(SSGCS01) ~SSGCS01 except: Yoke/skin interf = 50 um

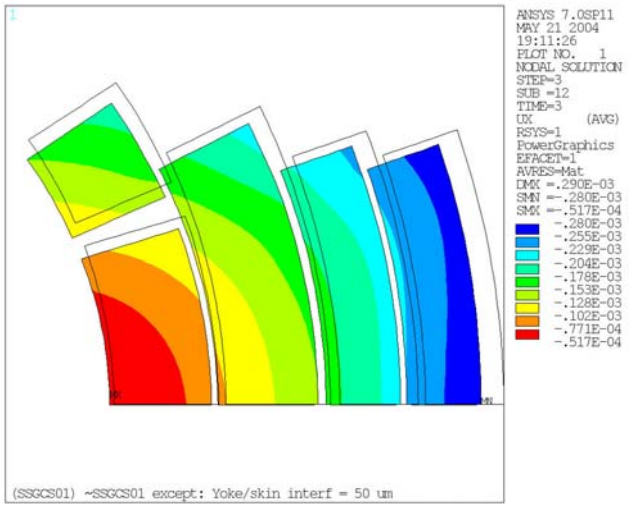
ANSYS 7.0SP11
MAY 21 2004
19:11:26
PLOT NO. 1
NODAL SOLUTION
STEP=3
SUB =12
TIME=3
UX (AVG)
RSYS=1
PowerGraphics
EFACET=1
AVRES=Mat
DMX =.290E-03
SMN =-.280E-03
SMX =-.517E-04
-.280E-03
-.255E-03
-.229E-03
-.204E-03
-.178E-03
-.153E-03
-.128E-03
-.102E-03
-.771E-04
-.517E-04
(SSGCS01) ~SSGCS01 except: Yoke/skin interf = 50 um

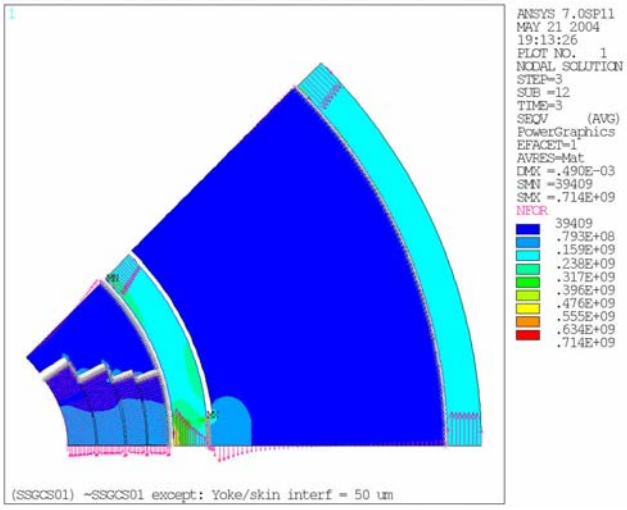
ANSYS 7.0SP11
MAY 21 2004
19:13:26
PLOT NO. 1
NODAL SOLUTION
STEP=3
SUB =12
TIME=3
SEQV (AVG)
PowerGraphics
EFACET=1
AVRES=Mat
DMX =.490E-03
SMN =39409
SMX =.714E+09
NFOR
39409
.793E+08
.159E+09
.238E+09
.317E+09
.396E+09
.476E+09
.555E+09
.634E+09
.714E+09
(SSGCS01) ~SSGCS01 except: Yoke/skin interf = 50 um

Von Mises stress at F Max

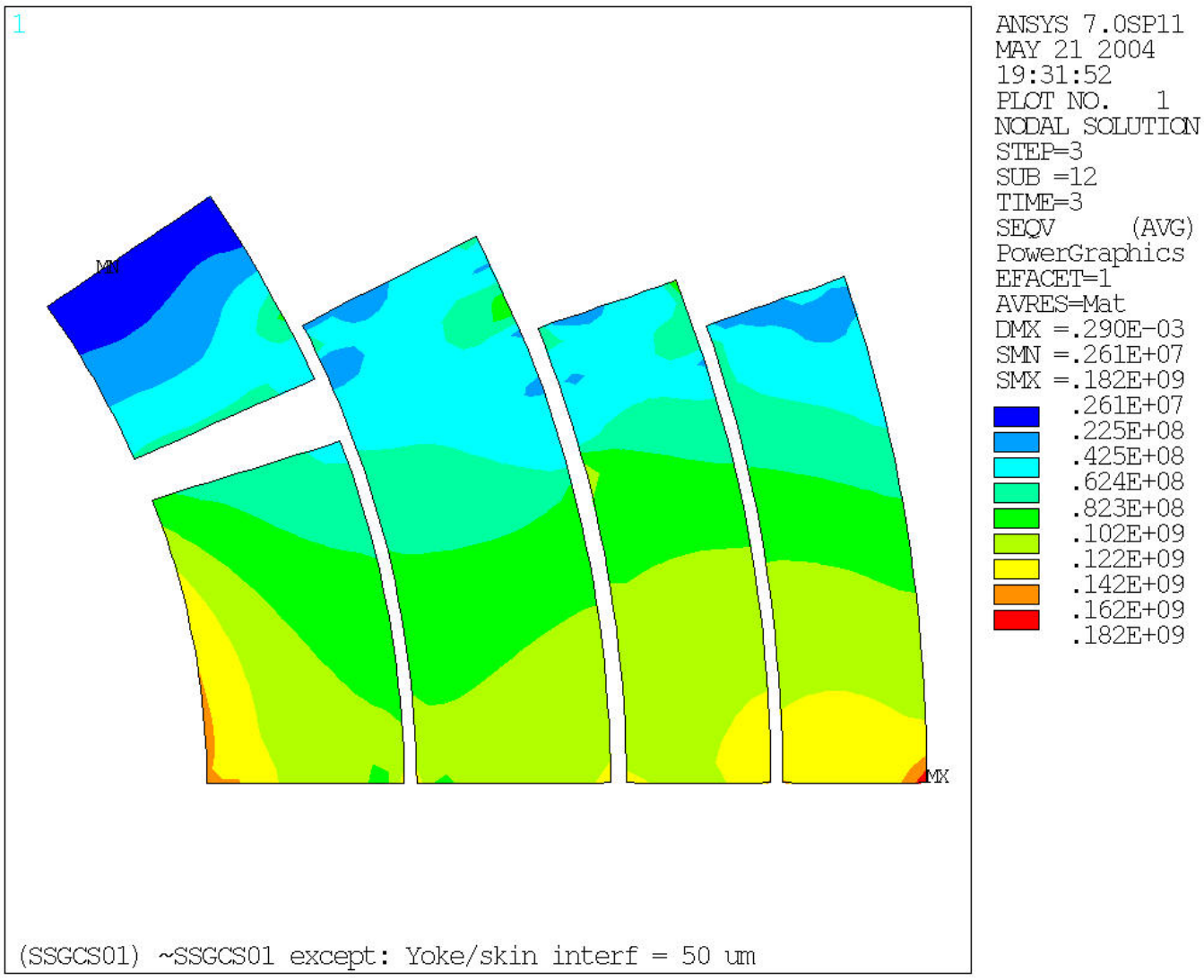

7.2 30-mm aluminum shell – Yoke closes during cooldown –

Coil/Coll radial interference: 0.1 mm, - Yoke/skin radial interference: 0.2 mm
Azim. Interference = (S1) 0.13-0.18, (S2) 0.12-0.12 (S3) 0.12-0.07, (S4) 0.12-0.12

Prestress:

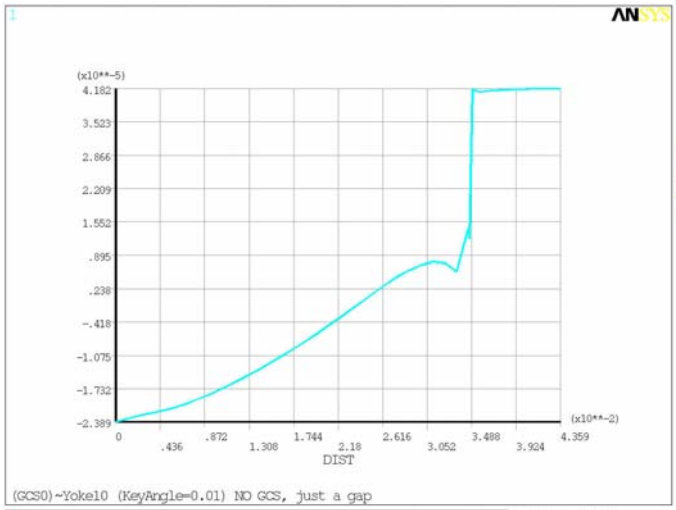

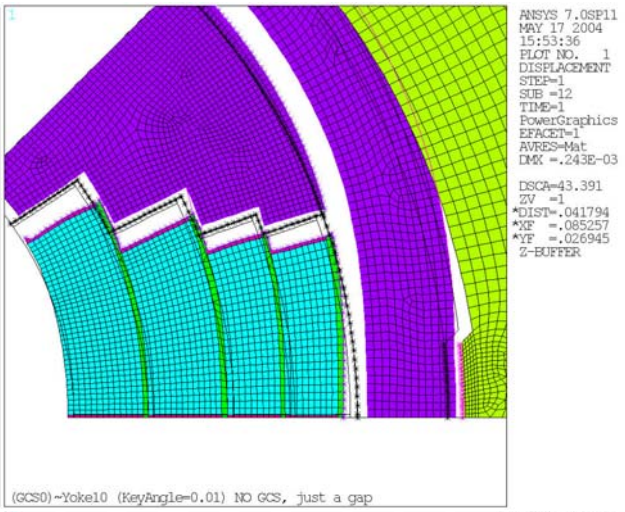

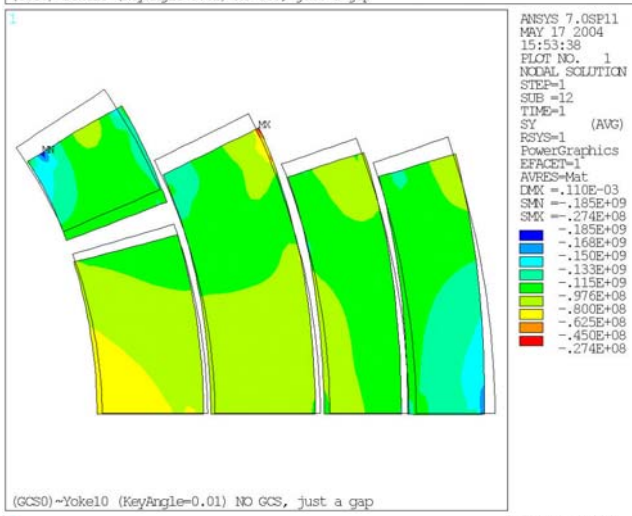

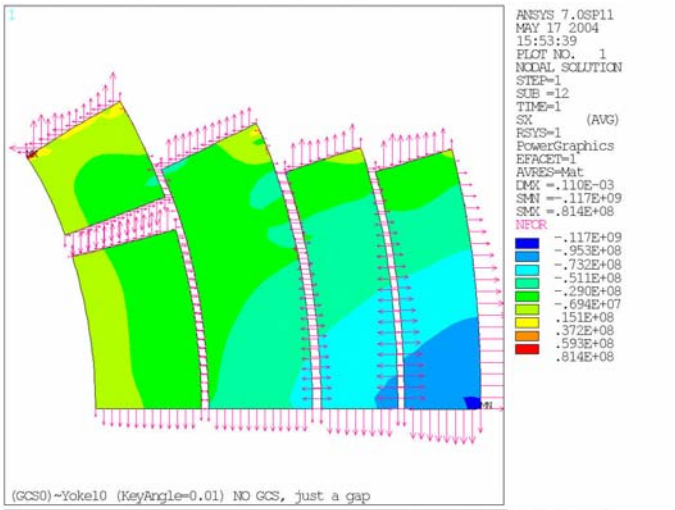

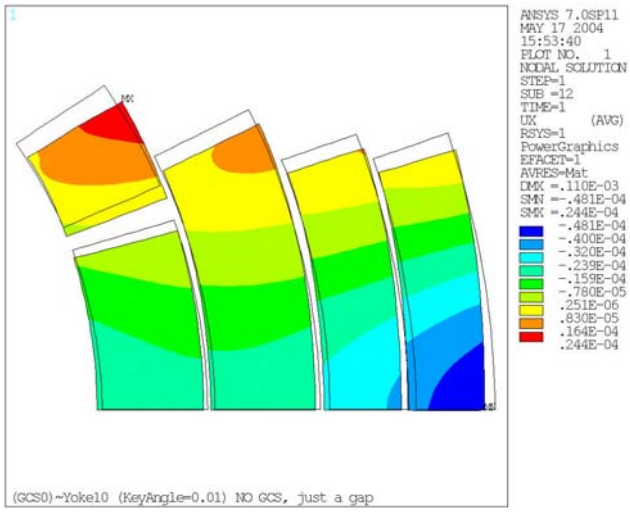

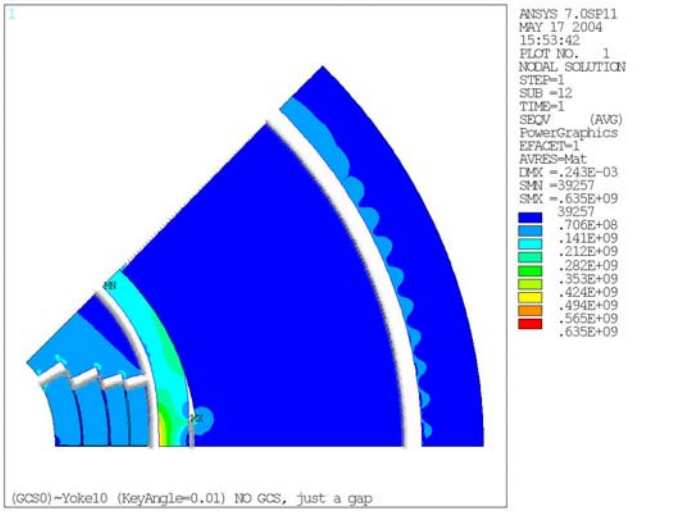

After Cooldown

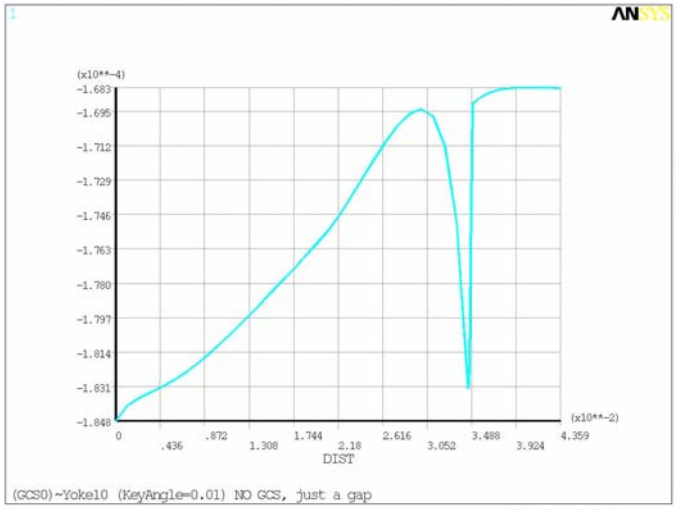

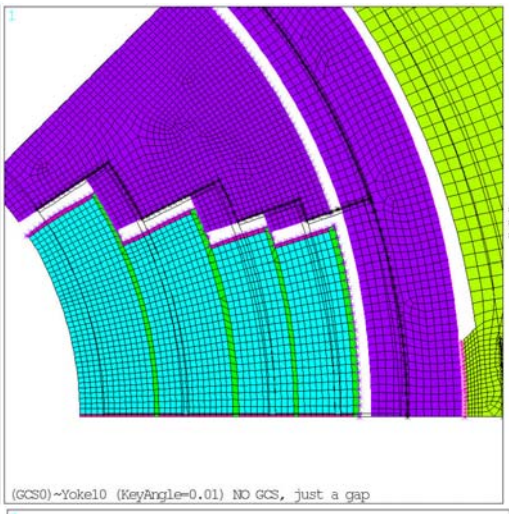

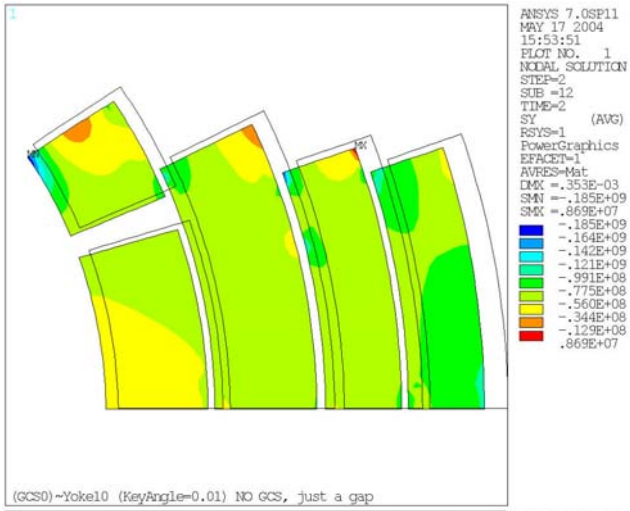

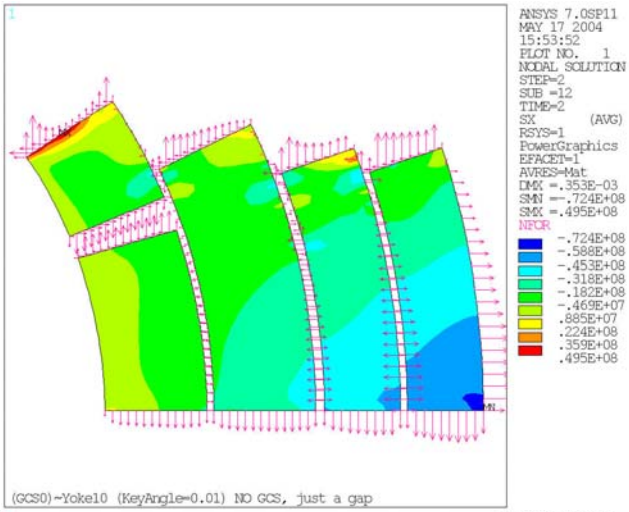

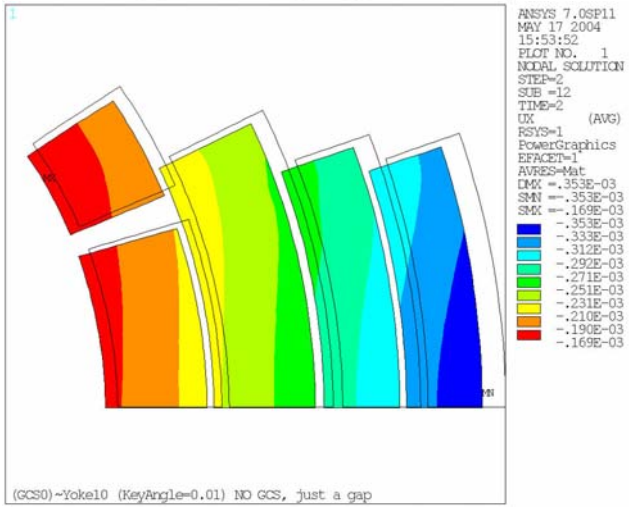

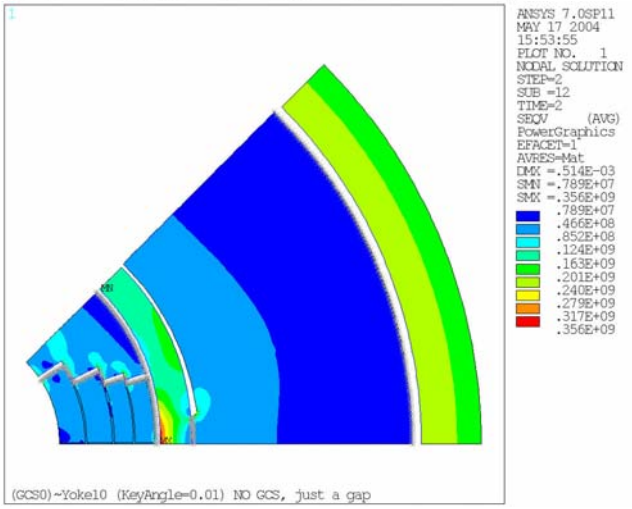

At 228 T/m

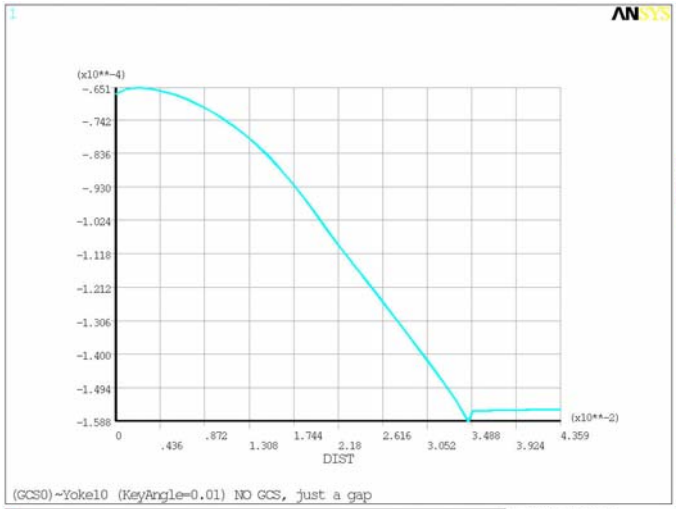
(x10**-4)
-.651
-.742
-.836
-.930
-1.024
-1.118
-1.212
-1.306
-1.400
-1.494
-1.588
0
.436
.872
1.308
1.744
2.18
2.616
3.052
3.488
3.924
4.359
(x10**-2)
DIST
(GCS0)~Yoke10 (KeyAngle=0.01) NO GCS, just a gap

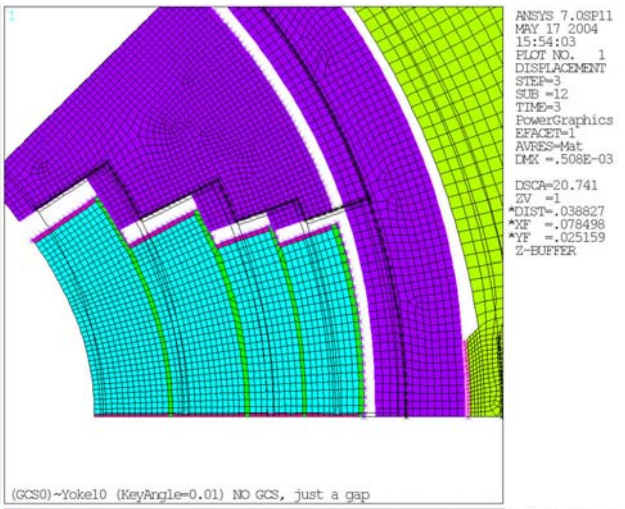
ANSYS 7.0SP11
MAY 17 2004
15:54:03
PLOT NO. 1
DISPLACEMENT
STEP=3
SUB =12
TIME=3
PowerGraphics
EFACET=1
AVRES=Mat
DMX =.508E-03
DSCA=20.741
ZV =1
*DIST=.038827
*XF =.078498
*YF =.025159
Z-BUFFER
(GCS0)~Yoke10 (KeyAngle=0.01) NO GCS, just a gap

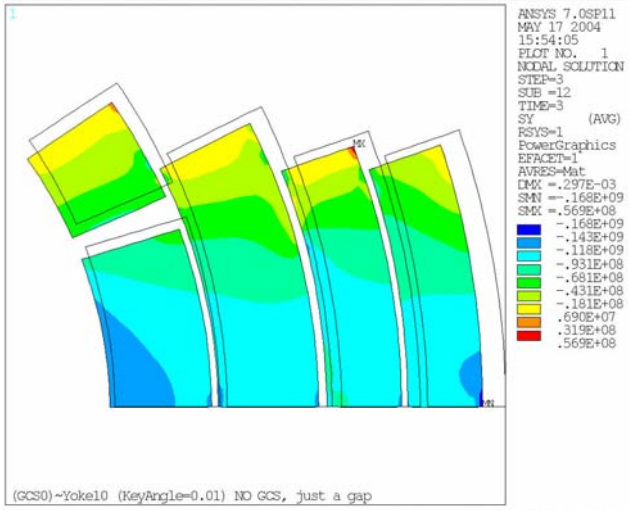
ANSYS 7.0SP11
MAY 17 2004
15:54:05
PLOT NO. 1
NODAL SOLUTION
STEP=3
SUB =12
TIME=3
SY (AVG)
RSYS=1
PowerGraphics
EFACET=1
AVRES=Mat
DMX =.297E-03
SMN =-.168E+09
SMX =.569E+08
-.168E+09
-.143E+09
-.118E+09
-.931E+08
-.681E+08
-.431E+08
-.181E+08
.690E+07
.319E+08
.569E+08
(GCS0)~Yoke10 (KeyAngle=0.01) NO GCS, just a gap

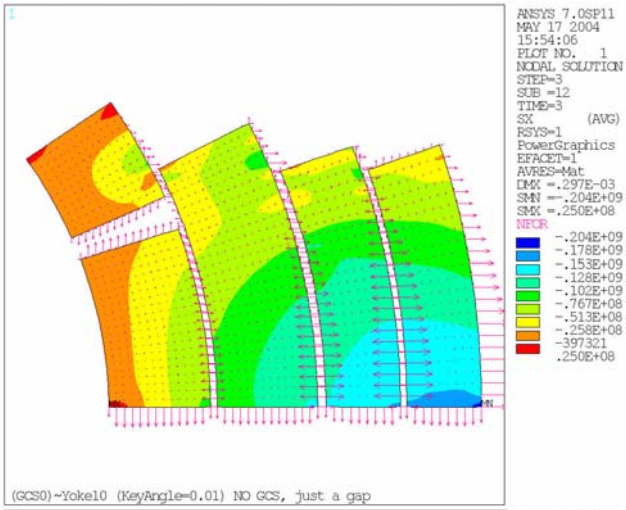
ANSYS 7.0SP11
MAY 17 2004
15:54:06
PLOT NO. 1
NODAL SOLUTION
STEP=3
SUB =12
TIME=3
SX (AVG)
RSYS=1
PowerGraphics
EFACET=1
AVRES=Mat
DMX =.297E-03
SMN =-.204E+09
SMX =.250E+08
NFOR
-.204E+09
-.178E+09
-.153E+09
-.128E+09
-.102E+09
-.767E+08
-.513E+08
-.258E+08
-397321
.250E+08
(GCS0)~Yoke10 (KeyAngle=0.01) NO GCS, just a gap

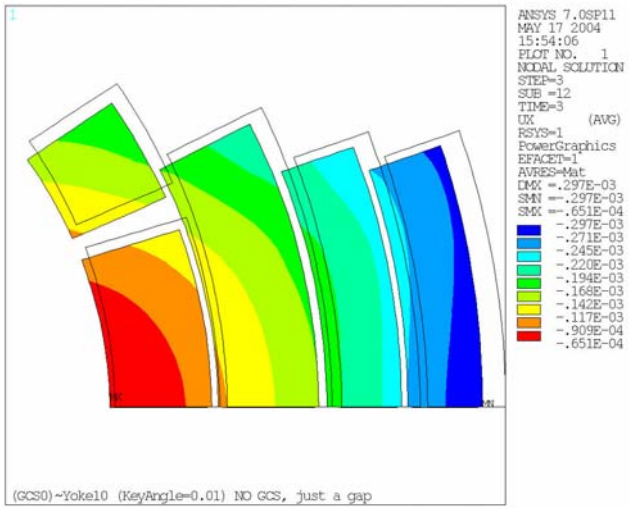
ANSYS 7.0SP11
MAY 17 2004
15:54:06
PLOT NO. 1
NODAL SOLUTION
STEP=3
SUB =12
TIME=3
UX (AVG)
RSYS=1
PowerGraphics
EFACET=1
AVRES=Mat
DMX =.297E-03
SMN =-.297E-03
SMX =-.651E-04
-.297E-03
-.271E-03
-.245E-03
-.220E-03
-.194E-03
-.168E-03
-.142E-03
-.117E-03
-.909E-04
-.651E-04
(GCS0)~Yoke10 (KeyAngle=0.01) NO GCS, just a gap

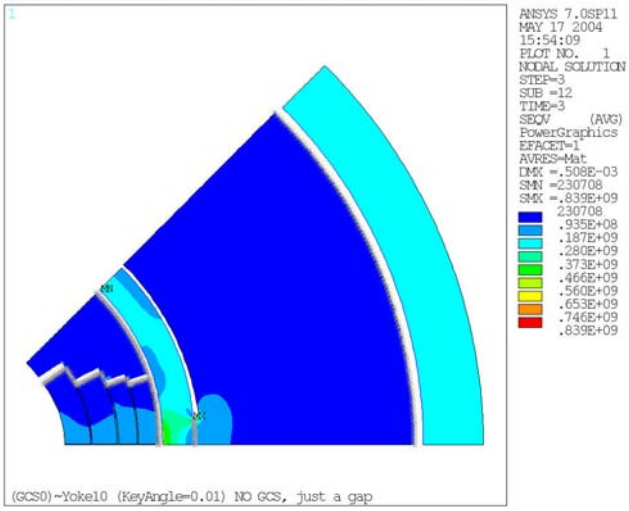
ANSYS 7.0SP11
MAY 17 2004
15:54:09
PLOT NO. 1
NODAL SOLUTION
STEP=3
SUB =12
TIME=3
SEQV (AVG)
PowerGraphics
EFACET=1
AVRES=Mat
DMX =.508E-03
SMN =230708
SMX =.839E+09
230708
.935E+08
.187E+09
.280E+09
.373E+09
.466E+09
.560E+09
.653E+09
.746E+09
.839E+09
(GCS0)~Yoke10 (KeyAngle=0.01) NO GCS, just a gap

Reaction forces:

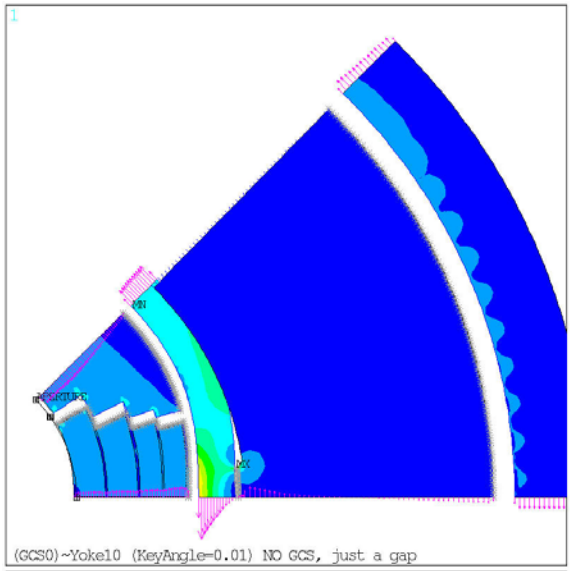

ANSYS 7.0SP11
MAY 17 2004
17:10:52
PLOT NO. 1
NODAL SOLUTION
STEP=1
SUB =12
TIME=1
SEQV (AVG)
PowerGraphics
EFACET=1
AVRES=Mat
DMX =.243E-03
SMN =39257
SMX =.635E+09
RFOR
PATH
39257
.706E+08
.141E+09
.212E+09
.282E+09
.353E+09
.424E+09
.494E+09
.565E+09
.635E+09

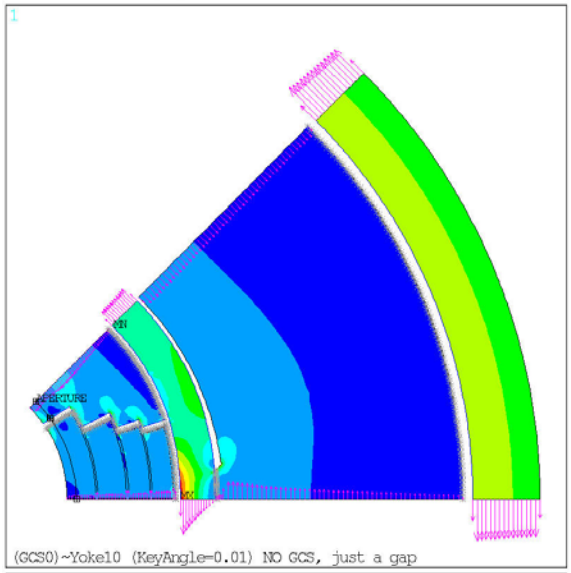

ANSYS 7.0SP11
MAY 17 2004
16:13:32
PLOT NO. 1
NODAL SOLUTION
STEP=2
SUB =12
TIME=2
SEQV (AVG)
PowerGraphics
EFACET=1
AVRES=Mat
DMX =.514E-03
SMN =.789E+07
SMX =.356E+09
RFOR
PATH
.789E+07
.466E+08
.852E+08
.124E+09
.163E+09
.201E+09
.240E+09
.279E+09
.317E+09
.356E+09

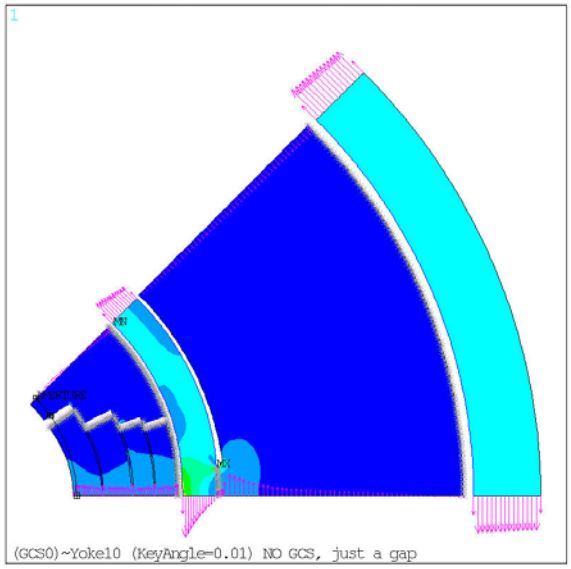

ANSYS 7.0SP11
MAY 17 2004
16:11:00
PLOT NO. 1
NODAL SOLUTION
STEP=3
SUB =12
TIME=3
SEQV (AVG)
PowerGraphics
EFACET=1
AVRES=Mat
DMX =.508E-03
SMN =230708
SMX =.839E+09
RFOR
PATH
230708
.935E+08
.187E+09
.280E+09
.373E+09
.466E+09
.560E+09
.653E+09
.746E+09
.839E+09

Von Mises stress at F Max

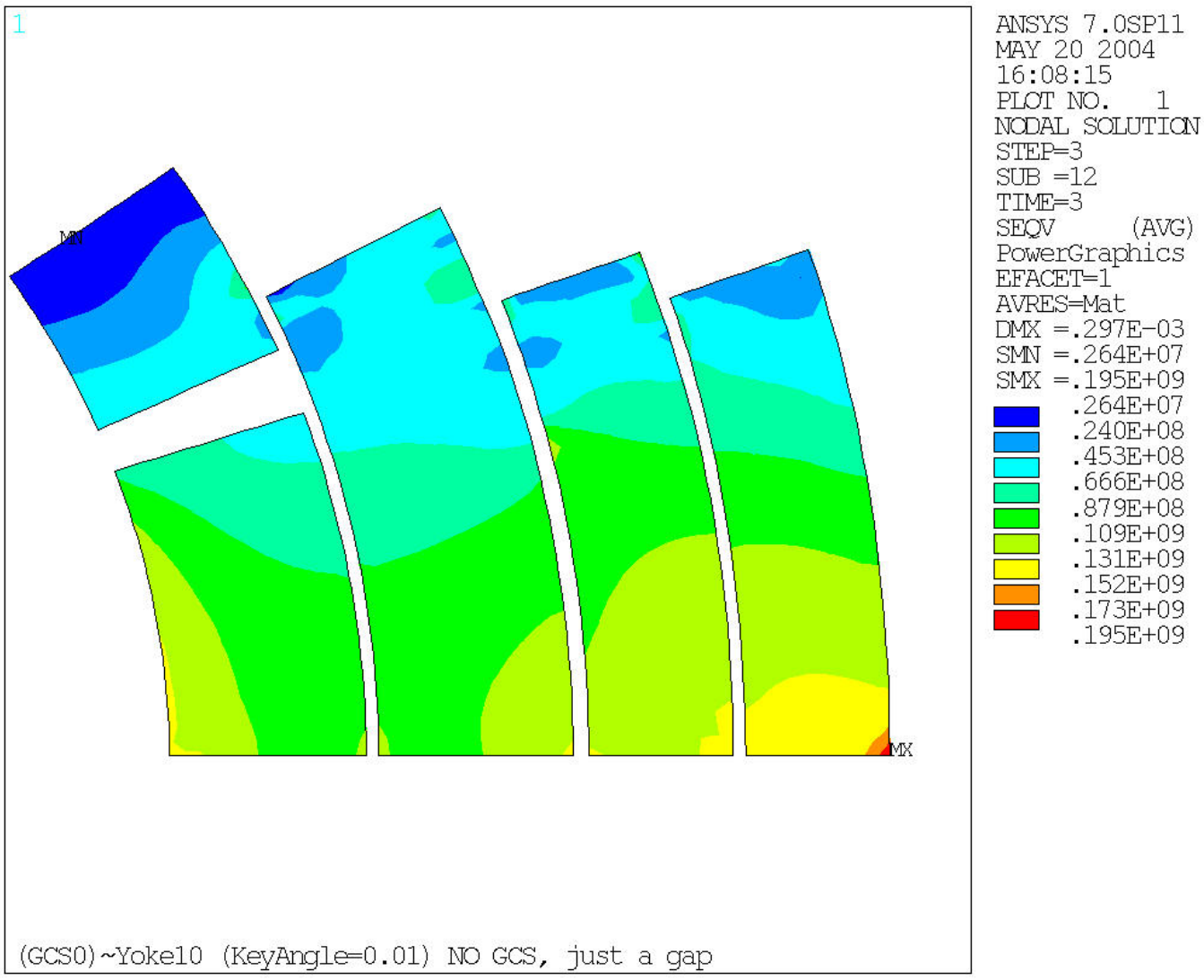

7.3 30-mm aluminum shell with uniform coil Interference (125 μm)

Yoke closes during cooldown
Coil/Coll radial Int : 0.1 mm,

Prestress:

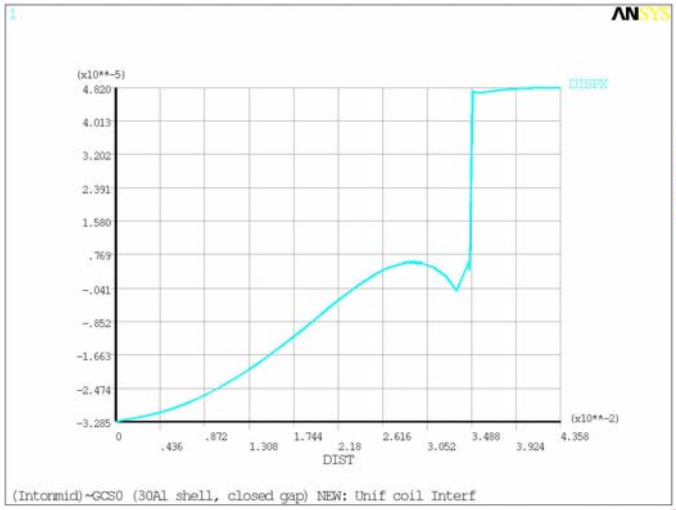

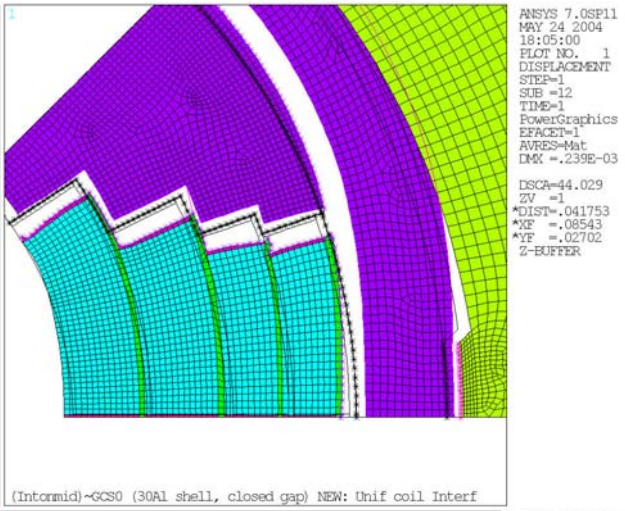

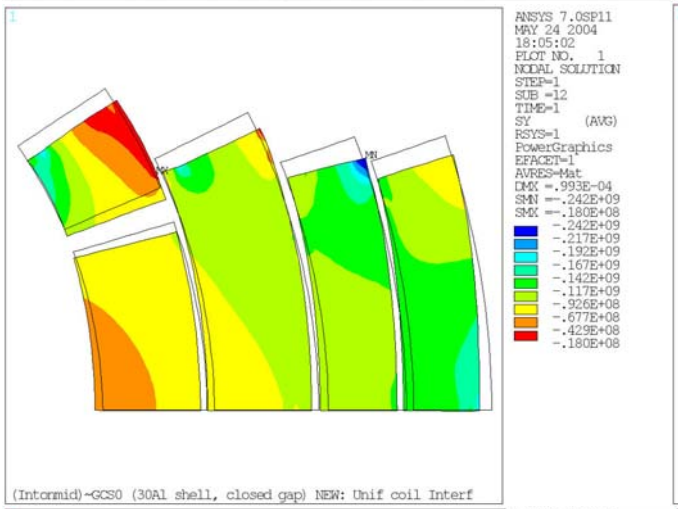

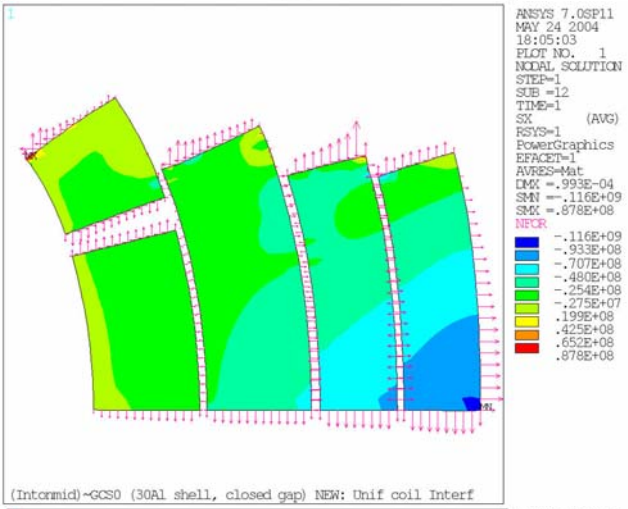

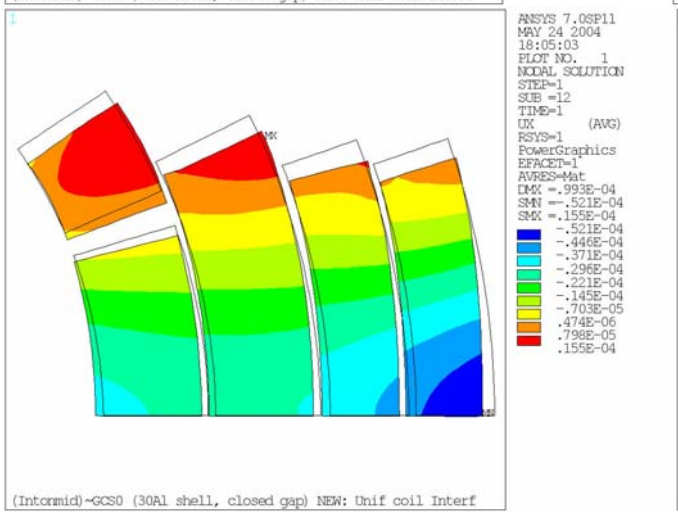

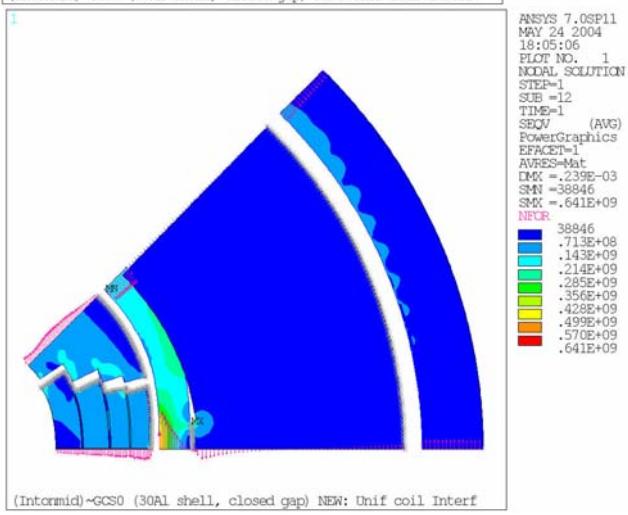

After Cooldown

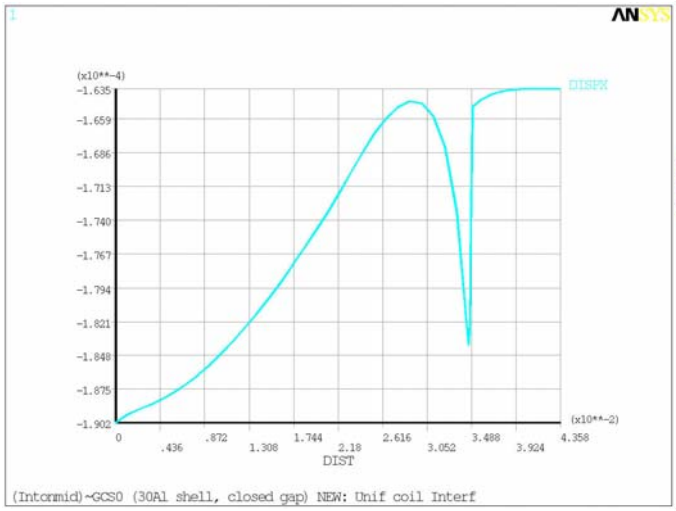

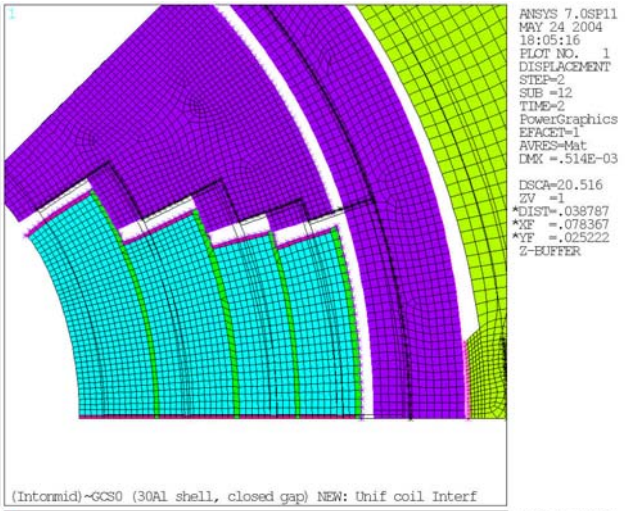

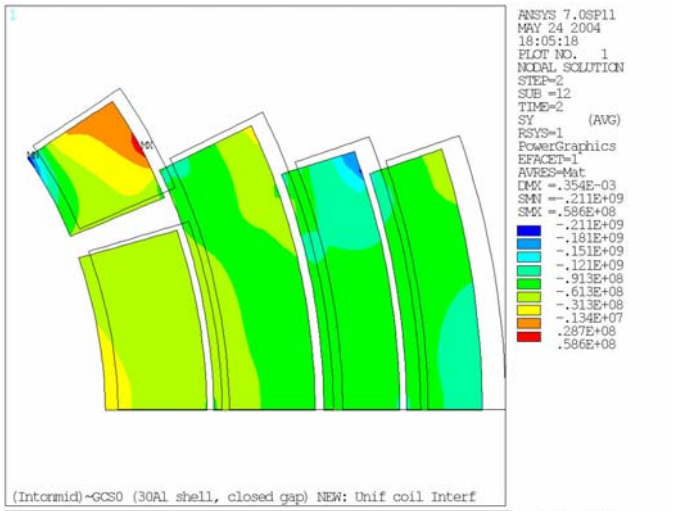

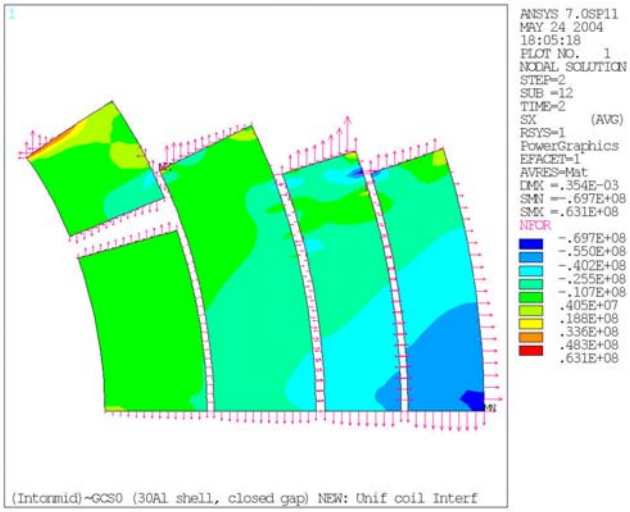

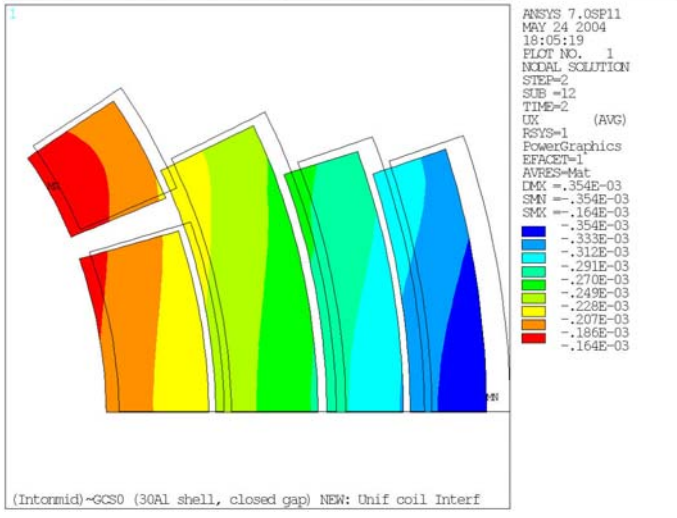

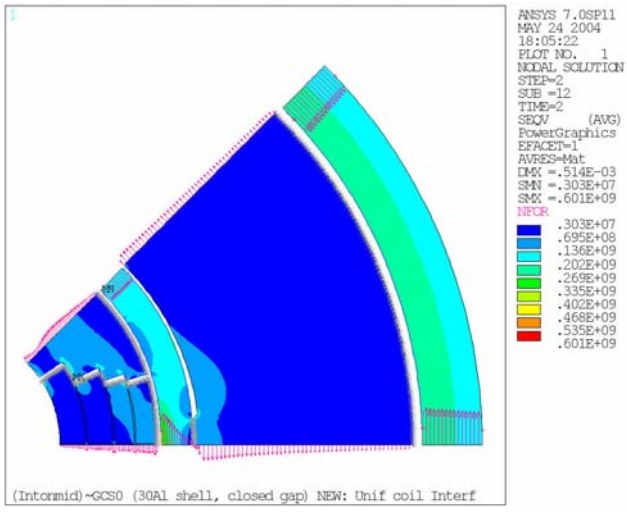

At 228 T/m

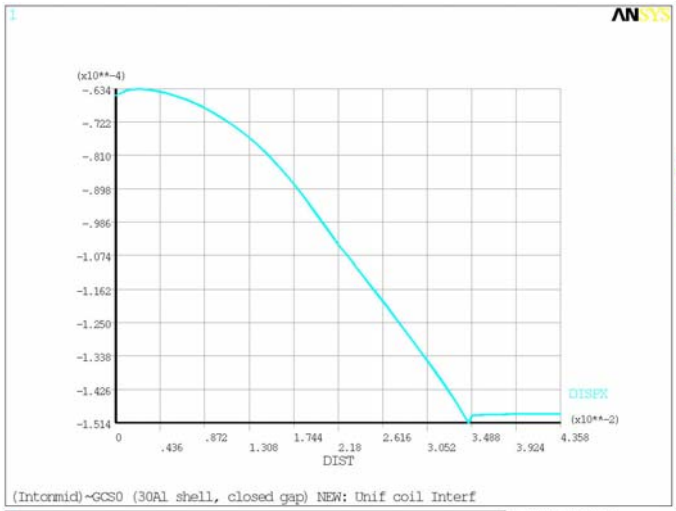
ANSYS
(x10**-4)
-.634
-.722
-.810
-.898
-.986
-1.074
-1.162
-1.250
-1.338
-1.426
-1.514
DISPX
(x10**-2)
0
.436
.872
1.308
1.744
2.18
2.616
3.052
3.488
3.924
4.358
DIST
(Intonmid)~GCS0 (30Al shell, closed gap) NEW: Unif coil Interf

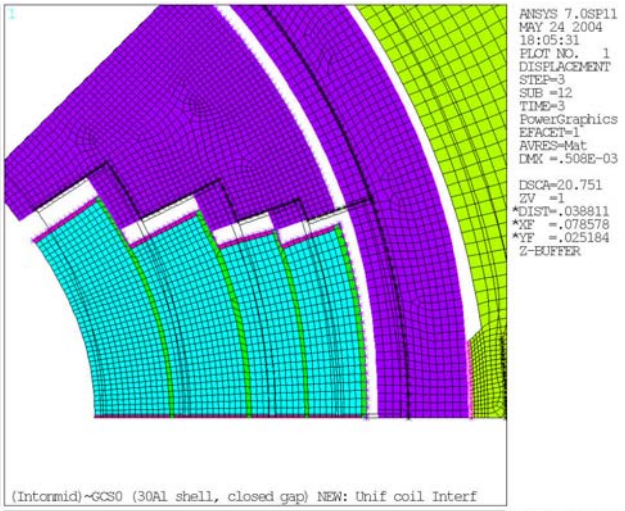
ANSYS 7.0SP11
MAY 24 2004
18:05:31
PLOT NO. 1
DISPLACEMENT
STEP=3
SUB =12
TIME=3
PowerGraphics
EFACET=1
AVRES=Mat
DMX =.508E-03
DSCA=20.751
ZV =1
*DIST=.038811
*XF =.078578
*YF =.025184
Z-BUFFER
(Intonmid)~GCS0 (30Al shell, closed gap) NEW: Unif coil Interf

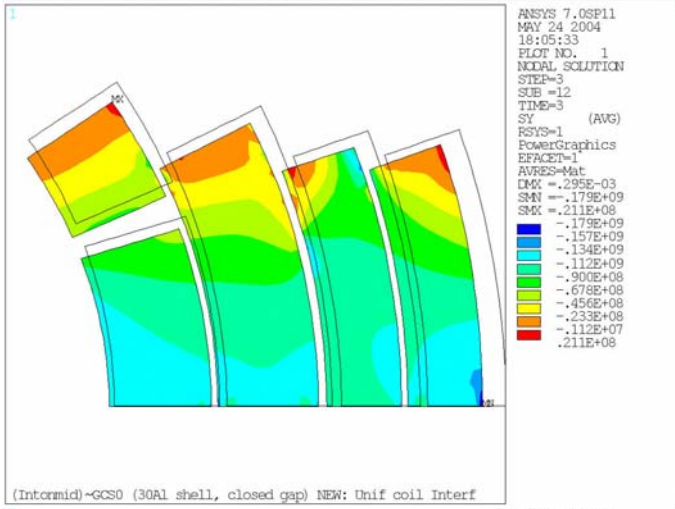
ANSYS 7.0SP11
MAY 24 2004
18:05:33
PLOT NO. 1
NODAL SOLUTION
STEP=3
SUB =12
TIME=3
SY (AVG)
RSYS=1
PowerGraphics
EFACET=1
AVRES=Mat
DMX =.295E-03
SMN =-.179E+09
SMX =.211E+08
-.179E+09
-.157E+09
-.134E+09
-.112E+09
-.900E+08
-.678E+08
-.456E+08
-.233E+08
-.112E+07
.211E+08
(Intonmid)~GCS0 (30Al shell, closed gap) NEW: Unif coil Interf

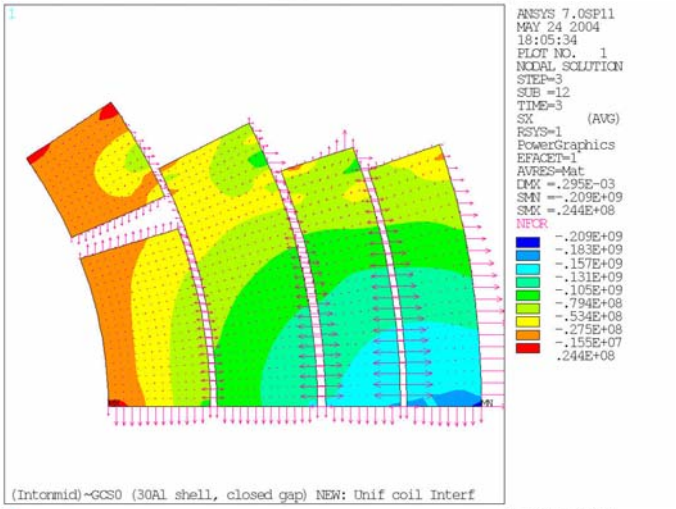
ANSYS 7.0SP11
MAY 24 2004
18:05:34
PLOT NO. 1
NODAL SOLUTION
STEP=3
SUB =12
TIME=3
SX (AVG)
RSYS=1
PowerGraphics
EFACET=1
AVRES=Mat
DMX =.295E-03
SMN =-.209E+09
SMX =.244E+08
NFOR
-.209E+09
-.183E+09
-.157E+09
-.131E+09
-.105E+09
-.794E+08
-.534E+08
-.275E+08
-.155E+07
.244E+08
(Intonmid)~GCS0 (30Al shell, closed gap) NEW: Unif coil Interf

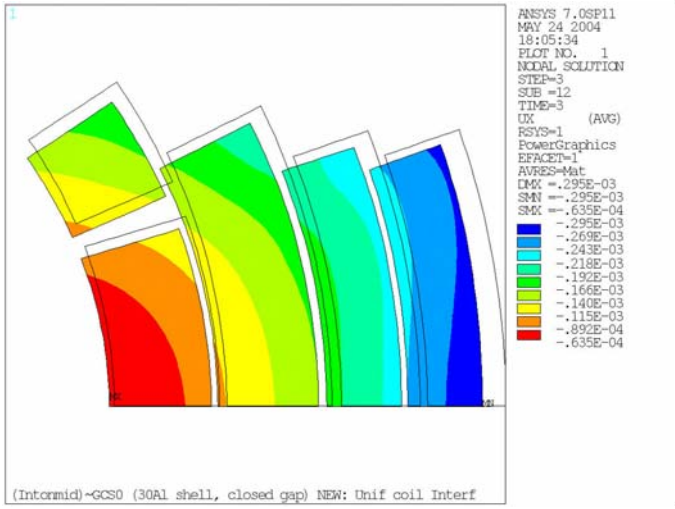
ANSYS 7.0SP11
MAY 24 2004
18:05:34
PLOT NO. 1
NODAL SOLUTION
STEP=3
SUB =12
TIME=3
UX (AVG)
RSYS=1
PowerGraphics
EFACET=1
AVRES=Mat
DMX =.295E-03
SMN =-.295E-03
SMX =-.635E-04
-.295E-03
-.269E-03
-.243E-03
-.218E-03
-.192E-03
-.166E-03
-.140E-03
-.115E-03
-.892E-04
-.635E-04
(Intonmid)~GCS0 (30Al shell, closed gap) NEW: Unif coil Interf

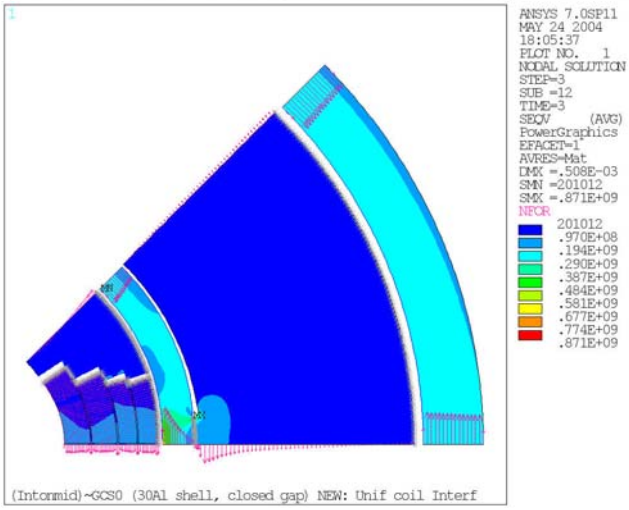
ANSYS 7.0SP11
MAY 24 2004
18:05:37
PLOT NO. 1
NODAL SOLUTION
STEP=3
SUB =12
TIME=3
SEQV (AVG)
PowerGraphics
EFACET=1
AVRES=Mat
DMX =.508E-03
SMN =201012
SMX =.871E+09
NFOR
201012
.970E+08
.194E+09
.290E+09
.387E+09
.484E+09
.581E+09
.677E+09
.774E+09
.871E+09
(Intonmid)~GCS0 (30Al shell, closed gap) NEW: Unif coil Interf

Von Mises stress at F Max

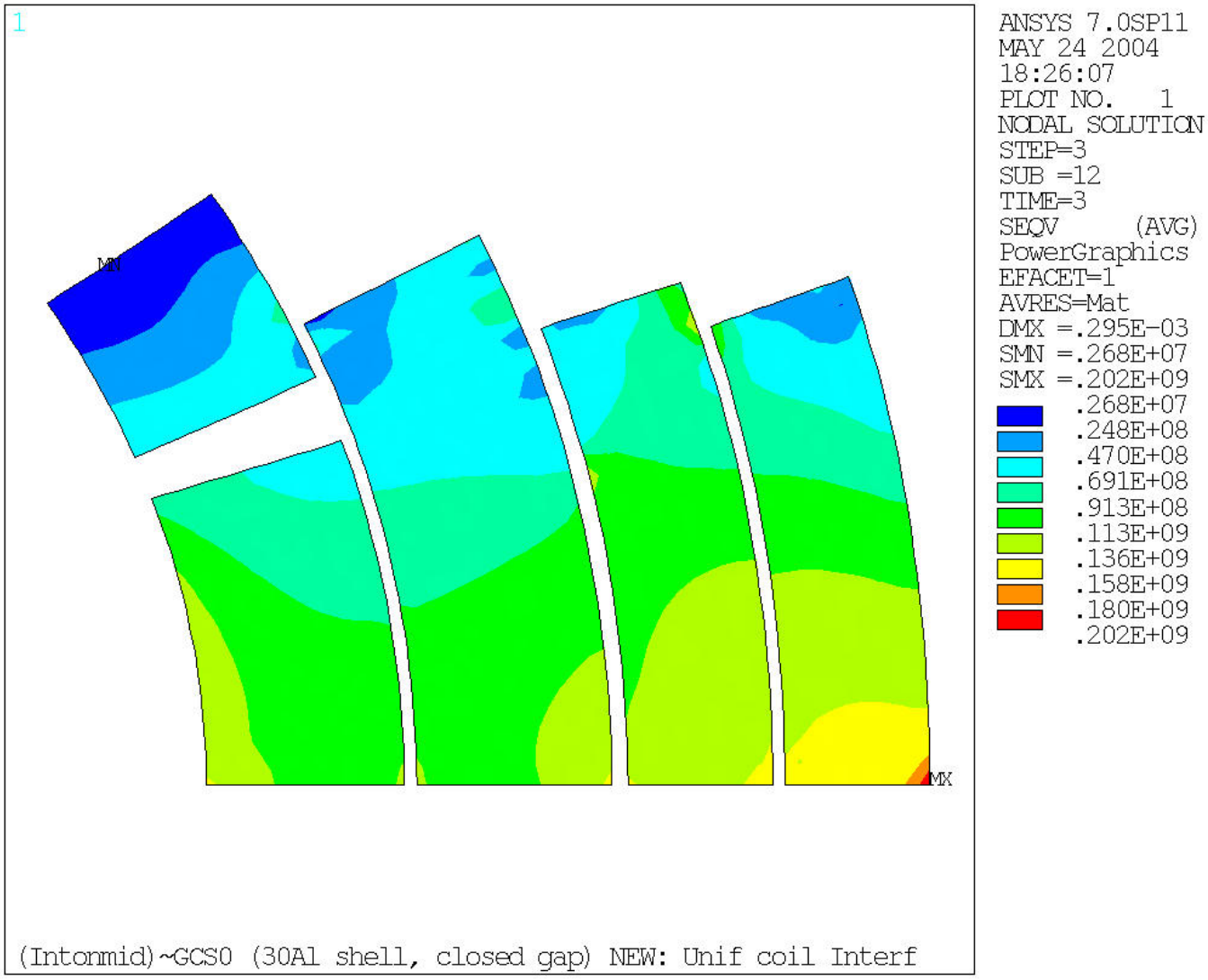

8. COLLARING

In the solutions presented the pre-stress is applied by the collars and the shell. The results at room temperature show coils stresses after magnet assembly is completed (i.e. after skin welding in case of stainless steel shell, and after key insertion and bladder deflation in case of aluminum shell). The collaring procedure should be optimized in order to avoid excessive pre-stress during collaring. In the following we present the results of two analyses that should give guidelines for the collaring procedure. The FE model for these analyses consists of the coils, the collar wedge and ring used in all previous FE models. The coil-pole interferences are the same used to apply pre-stress in the first two models presented in the previous section (interferences optimized for each layer).

The first analysis looked at the stresses in the coil and collars after collaring. The following plots show:

- Azimuthal stress in the coil (lower than 117 MPa)
- Azimuthal stress in the collar ring (lower than 280 MPa)
- Equivalent stresses in the whole model
- Radial displacement in the whole model.

In the second analysis rigid boundary conditions, applied to the outer surface of the collar ring, were added to the same model previously used (with the same interferences). This was done in order to simulate the stresses in the coils before spring back. This is a conservative case corresponding to a collaring procedure where the collars and the coils are so much precompressed that the collar keys can be introduced without any force. For this analysis the following plots show:

- Azimuthal stress in the coil (mostly between 160 and 180 MPa, some spots close to 190 MPa)
- Radial stress in the coil (lower than 100 MPa)

In this case the azimuthal stresses are above our target (150 MPa), but not excessively. Therefore the use of tapered keys introduced under load should solve this problem by stretching the collars during collaring and allowing lower stresses in the coils.

Stresses after collaring:

Interferences (mm): Rad=0.1

Azim=(SI) 0.13-0.18, (S2) 0.12-0.12 (S3) 0.12-0.07, (S4) 0.12-0.12

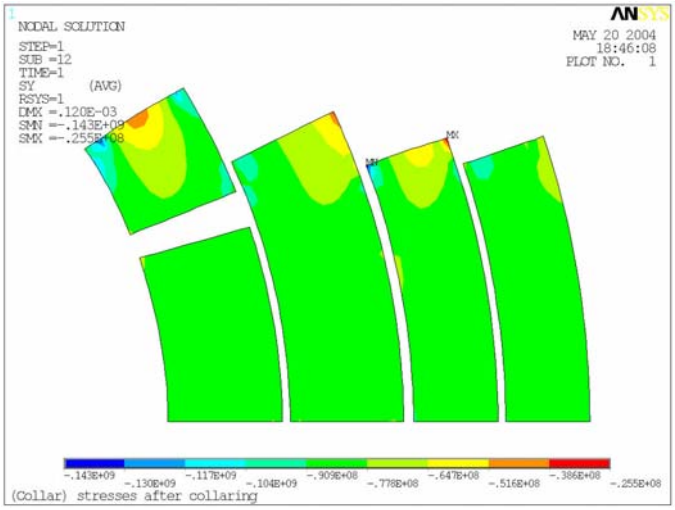

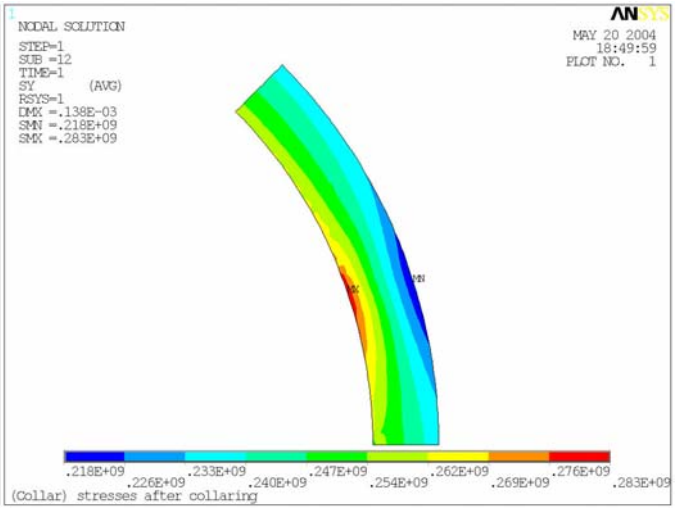

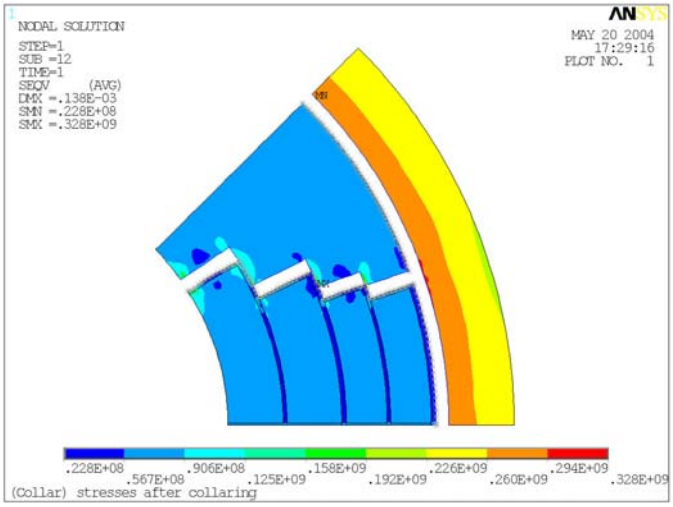

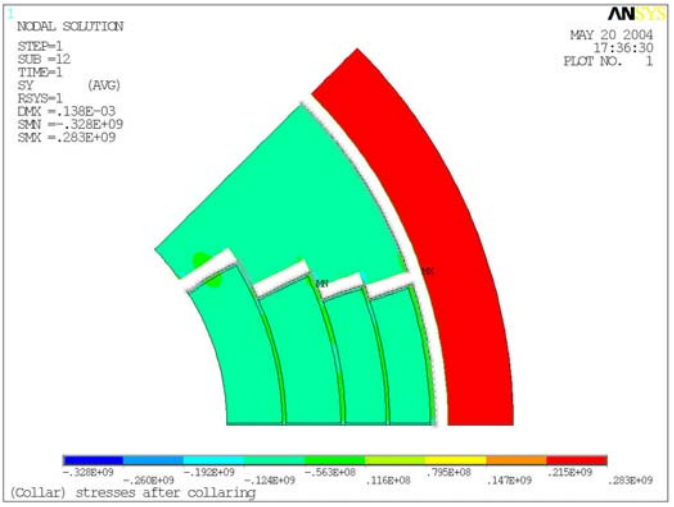

Stresses during collaring before spring-back:

Note: conservative analysis because there is NO stretching of the collars

Interferences (mm): Rad=0.1

Azim=(SI) 0.13-0.18, (S2) 0.12-0.12 (S3) 0.12-0.07, (S4) 0.12-0.12

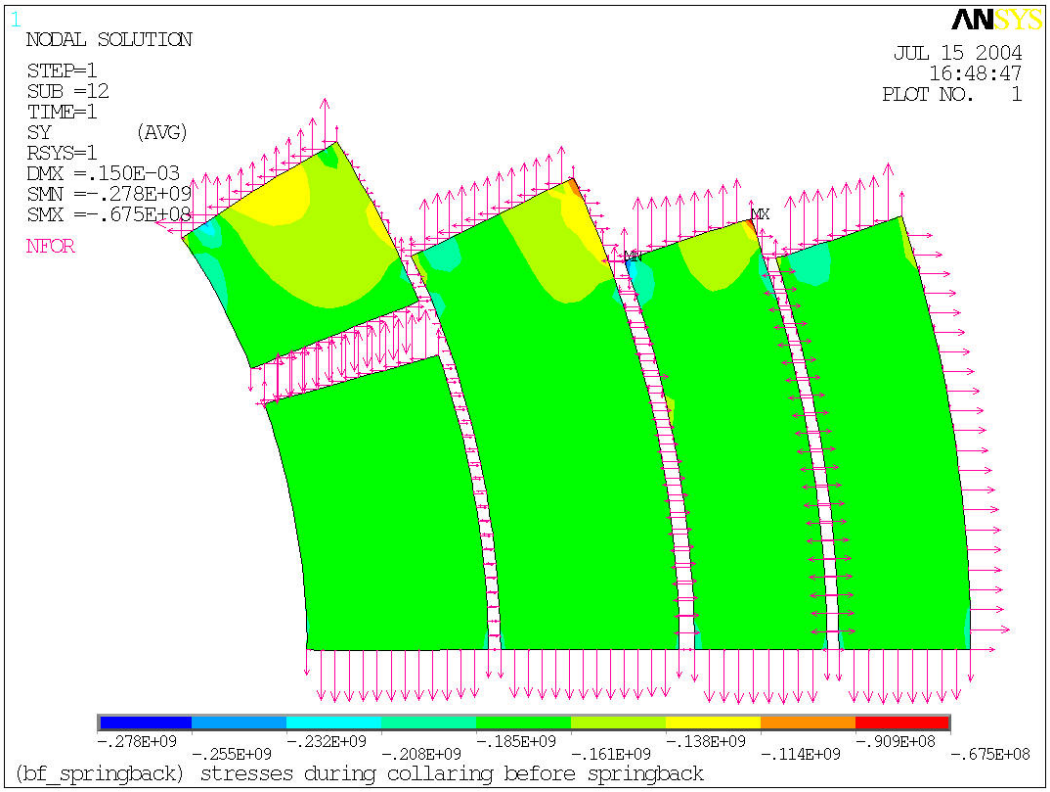

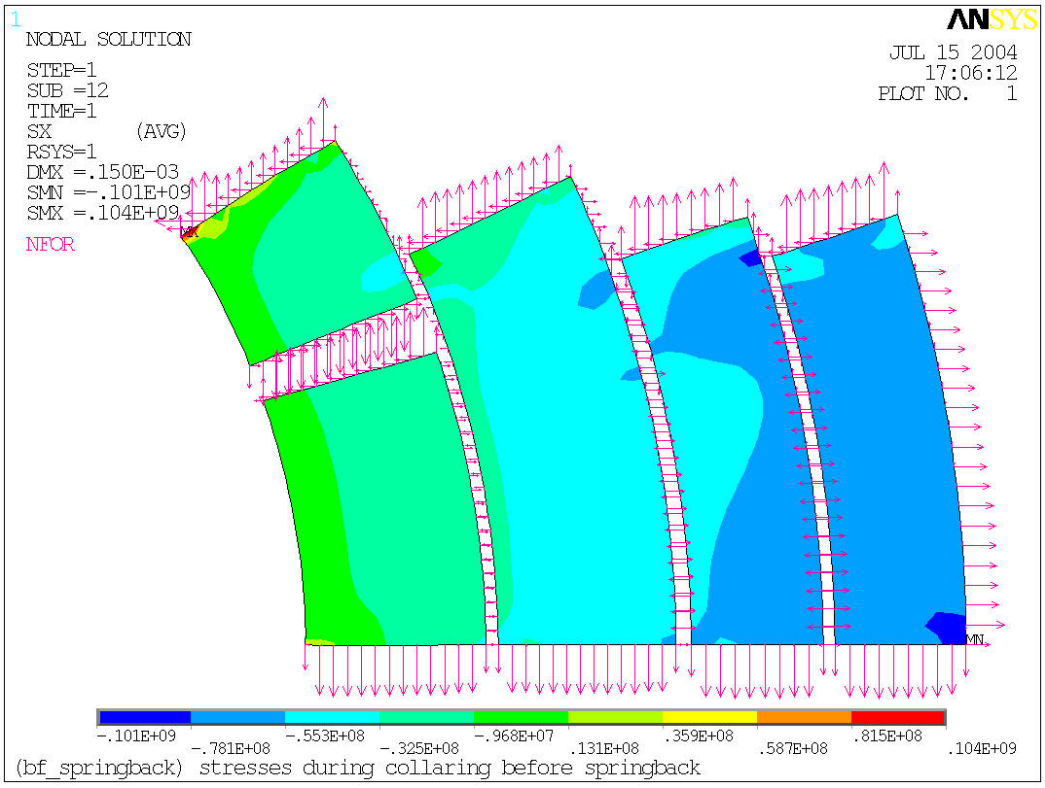

9. 2nd SERIES – F.E. MODELS WITH INTERFERENCE AT COIL MID-PLANE

In the previous models part of the pre-stress was simulated by coil-collar interferences at the boundary between the top of each coil shell and the collar wedge. This simulation corresponds to a real case if interference shims are placed on the top of each layer after impregnation. This can be done, but has some impact on the coil fabrication technology because it doesn't allow having the pole glued to any shell of the coil. In order to explore a pre-stress application allowing glued pole the following analyses were performed. In all these cases the interferences were set on the coil mid-plane, simulating shims set between coils during magnet assembly.

The first analysis (shown in 9.1) presents a case very similar to the case of 30-aluminum shell with uniform interference shown above (in 7.3). The only differences are: (i) the interference (125 μm as in the previous case) is applied on the mid-plane instead of at the coil-wedge interface; (ii) the coils are glued to the collar-wedge. For an easy comparison the same six plots described in section 6 are shown in the following for each stage of the analysis. It can be seen that under maximum forces the top of the first and second layers goes under tension. This can be explained by a low efficiency of the mid-plane shims in pre-loading the pole turns of the inner layers, aggravated by the fact that they are higher than the other layers. The last factor makes difficult to transfer sufficient pres-tress to the top of the inner layers because the pre-stress is intercepted by the collar wedge on the outer layers. The higher thermal contraction of the coils with respect to the collar wedge further decreases the pole turn pre-load of the innermost layers after cooldown.

The coil displacement at the mid-plane was 93 μm and the coil deformation (Rmax - Rmin) was 39 μm.

The results of this analysis clearly show the need of separating layer 1 & 2 from layer 3 & 4 in order to allow different pre-loads by using different shims.

9.1 Equal to 7.3 except for <u>mid-plane</u> coil interference (125 μm)

Coil/Coll radial Int : 0.1 mm,

Prestress:

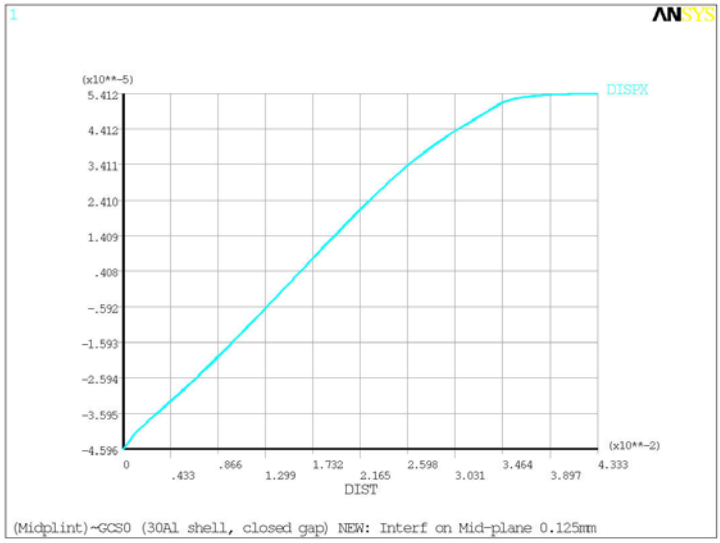

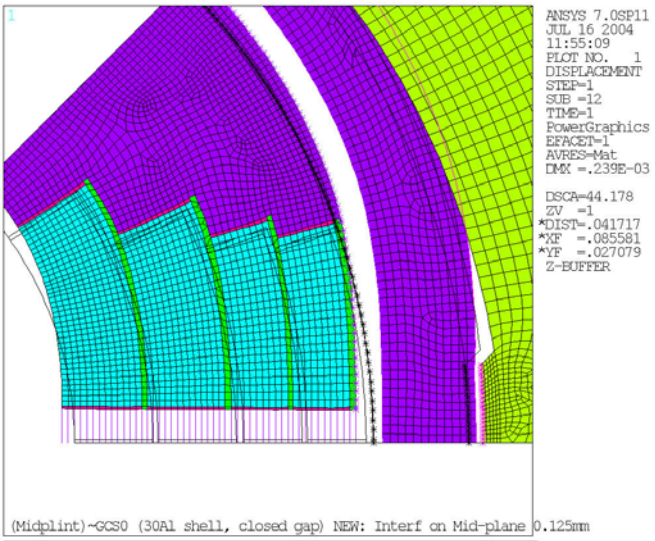

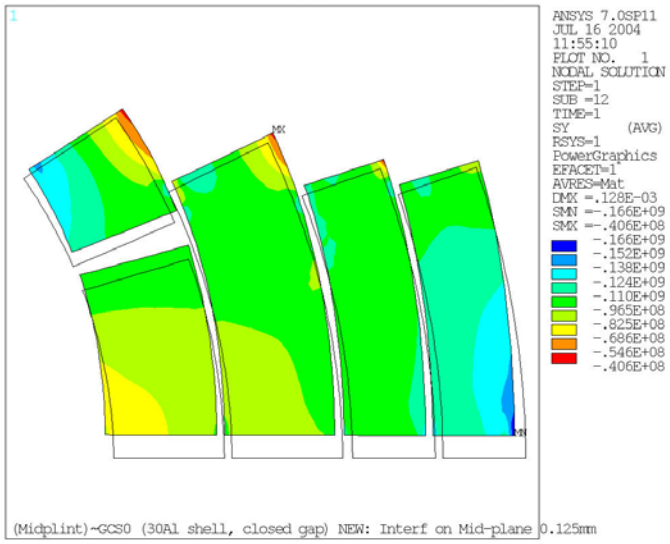

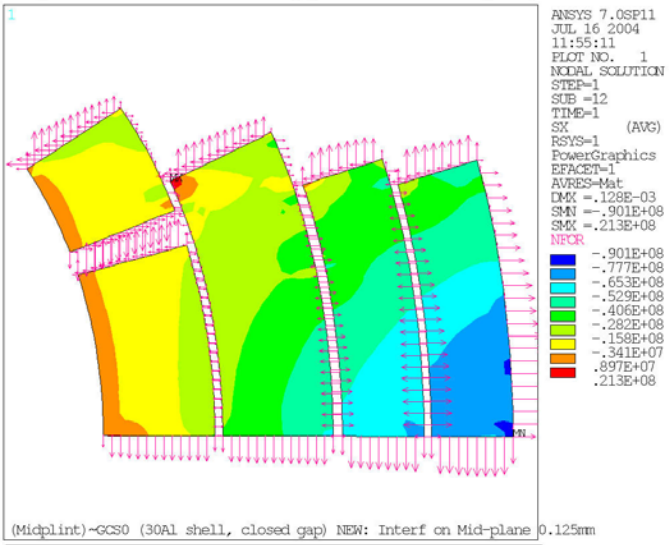

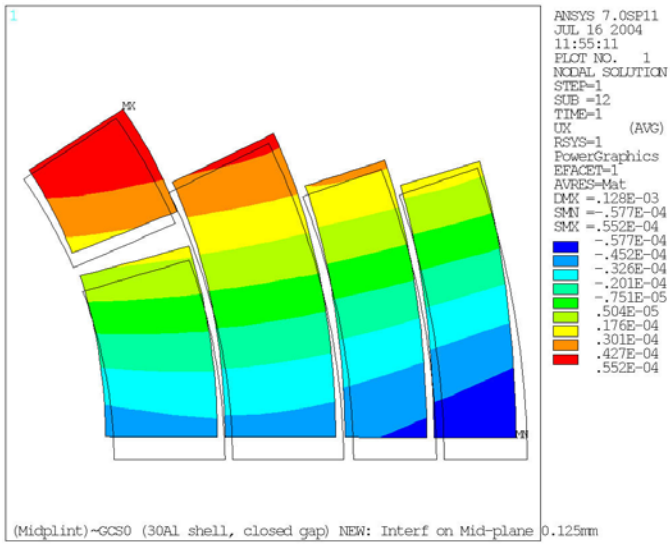

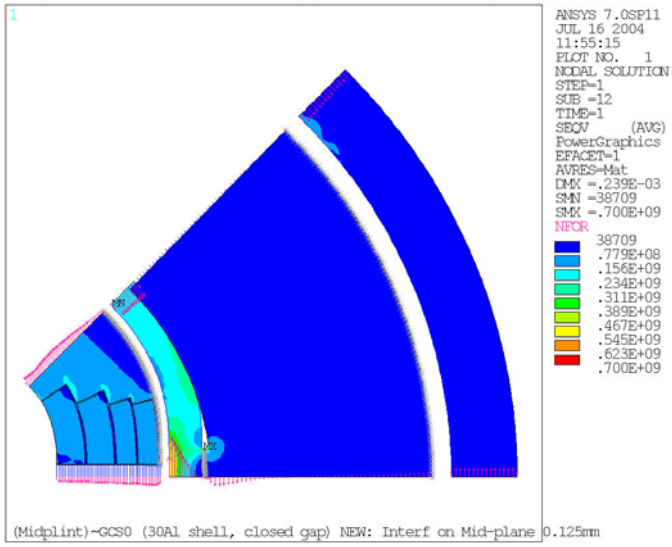

After Cooldown

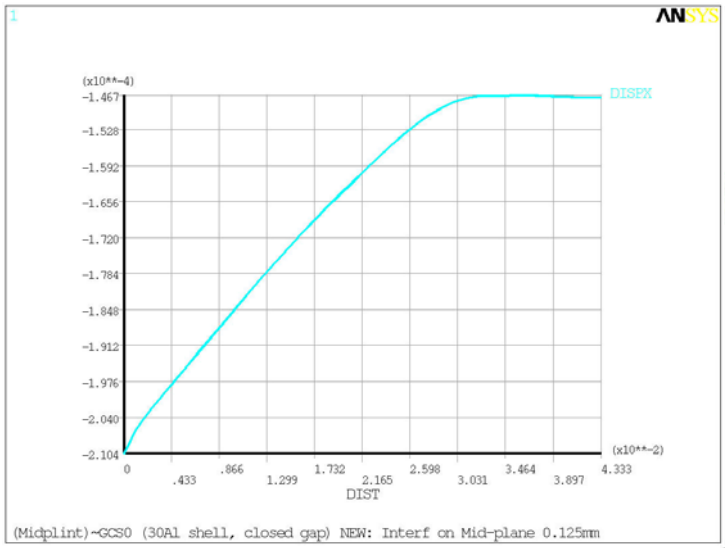

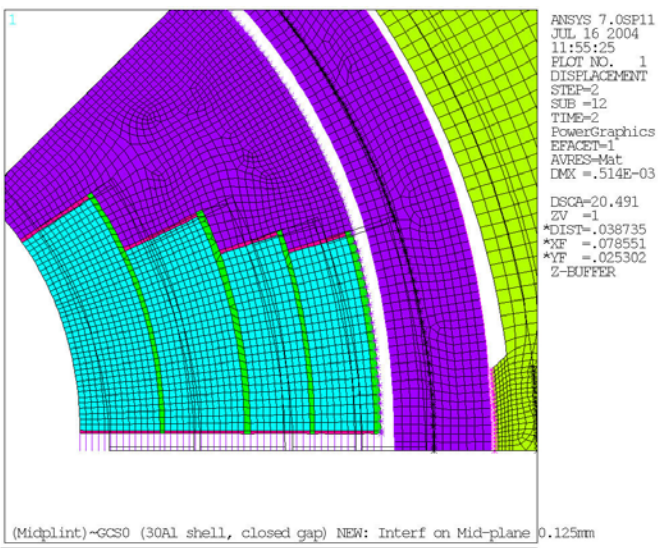

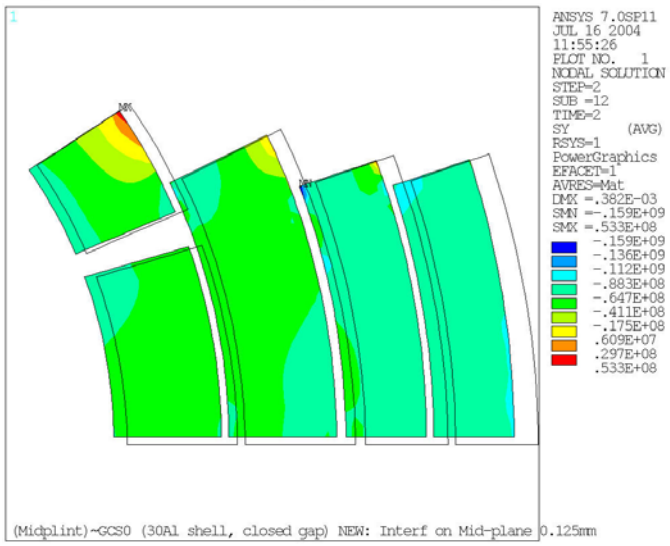

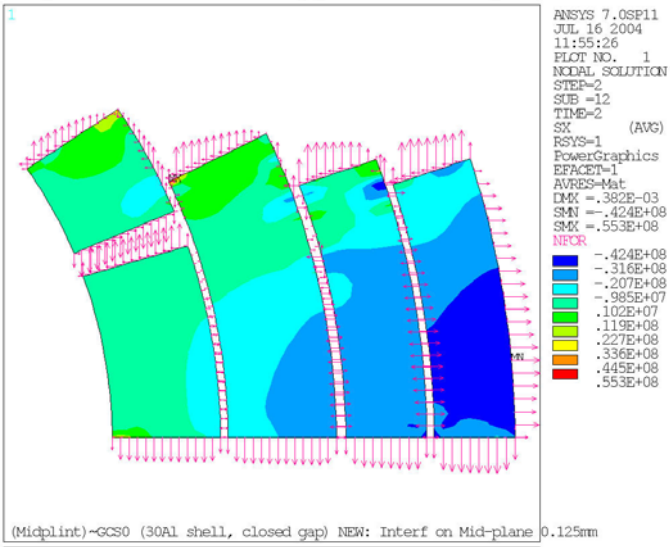

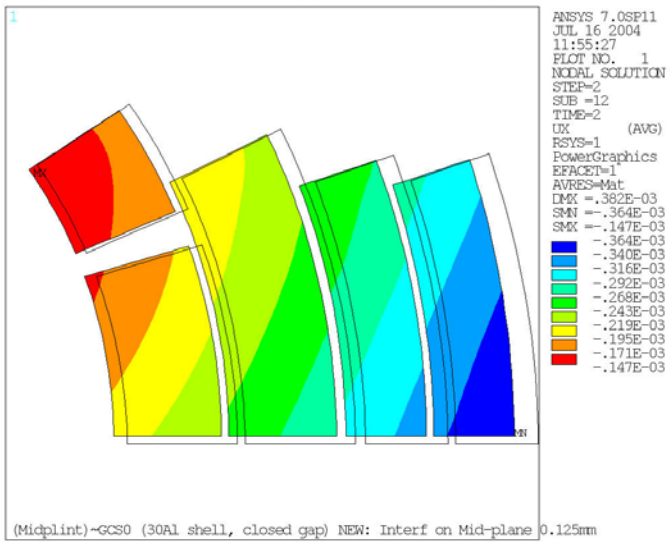

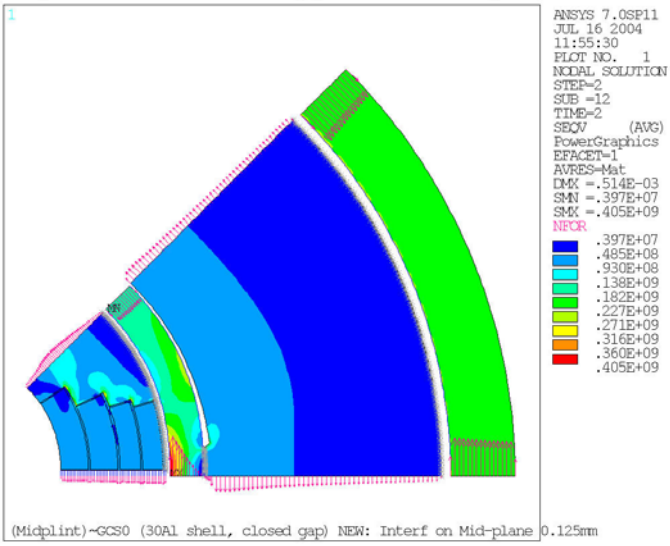

At 228 T/m

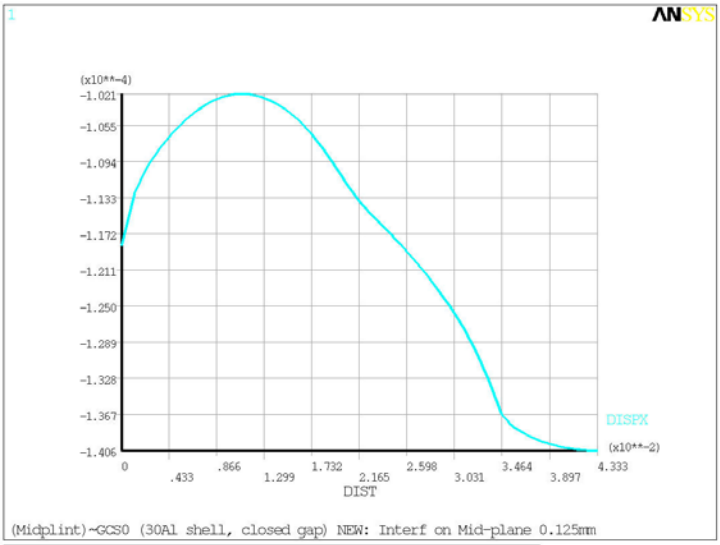
ANSYS
(x10**-4)
-1.021
-1.055
-1.094
-1.133
-1.172
-1.211
-1.250
-1.289
-1.328
-1.367
-1.406
0
.433
.866
1.299
1.732
2.165
2.598
3.031
3.464
3.897
4.333
DIST
DISPX
(x10**-2)
(Midplint)-GCS0 (30Al shell, closed gap) NEW: Interf on Mid-plane 0.125mm

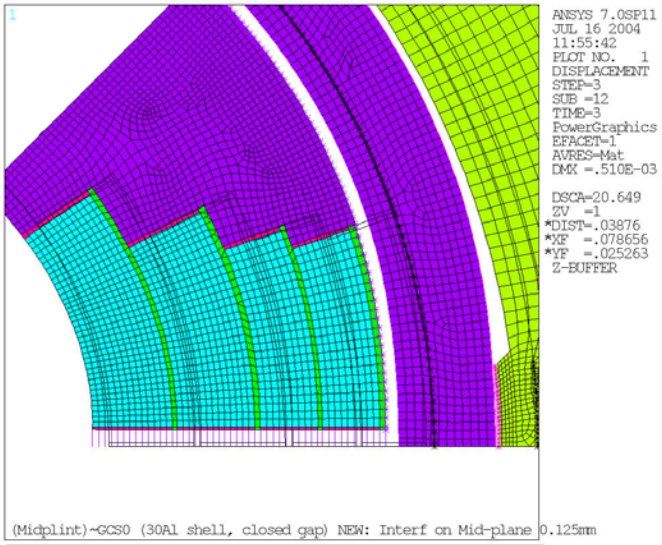
ANSYS 7.0SP11
JUL 16 2004
11:55:42
PLOT NO. 1
DISPLACEMENT
STEP=3
SUB =12
TIME=3
PowerGraphics
EFACET=1
AVRES=Mat
DMX =.510E-03
DSCA=20.649
ZV =1
*DIST=.03876
*XF =.078656
*YF =.025263
Z-BUFFER
(Midplint)-GCS0 (30Al shell, closed gap) NEW: Interf on Mid-plane 0.125mm

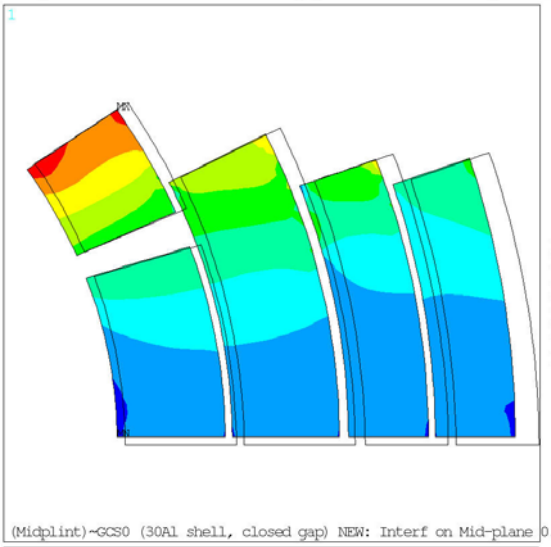
ANSYS 7.0SP11
JUL 16 2004
11:55:43
PLOT NO. 1
NODAL SOLUTION
STEP=3
SUB =12
TIME=3
SY (AVG)
RSYS=1
PowerGraphics
EFACET=1
AVRES=Mat
DMX =.343E-03
SMN =-.139E+09
SMX =.112E+09
-.139E+09
-.111E+09
-.827E+08
-.550E+08
-.272E+08
607185
.284E+08
.562E+08
.839E+08
.112E+09
(Midplint)-GCS0 (30Al shell, closed gap) NEW: Interf on Mid-plane 0.125mm

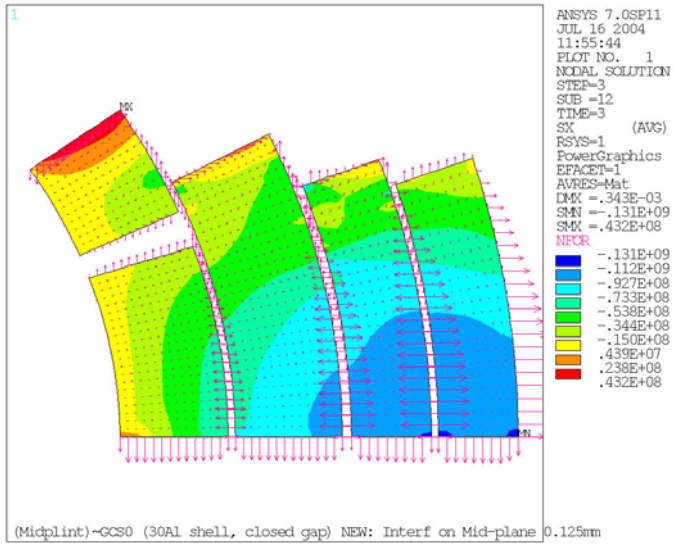
ANSYS 7.0SP11
JUL 16 2004
11:55:44
PLOT NO. 1
NODAL SOLUTION
STEP=3
SUB =12
TIME=3
SX (AVG)
RSYS=1
PowerGraphics
EFACET=1
AVRES=Mat
DMX =.343E-03
SMN =-.131E+09
SMX =.432E+08
NFOR
-.131E+09
-.112E+09
-.927E+08
-.733E+08
-.538E+08
-.344E+08
-.150E+08
.439E+07
.238E+08
.432E+08
(Midplint)-GCS0 (30Al shell, closed gap) NEW: Interf on Mid-plane 0.125mm

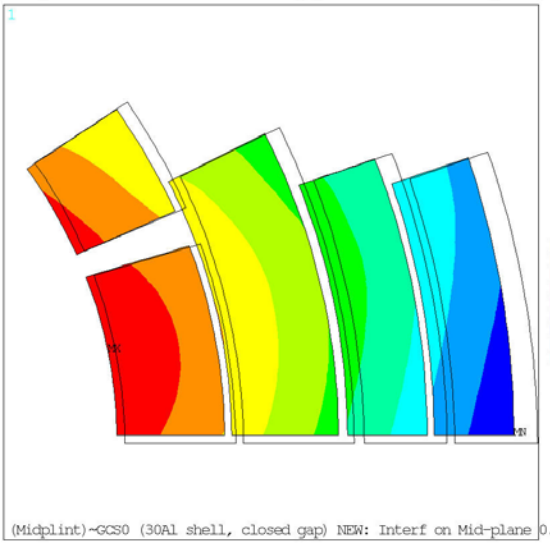
ANSYS 7.0SP11
JUL 16 2004
11:55:45
PLOT NO. 1
NODAL SOLUTION
STEP=3
SUB =12
TIME=3
UX (AVG)
RSYS=1
PowerGraphics
EFACET=1
AVRES=Mat
DMX =.343E-03
SMN =-.323E-03
SMX =-.102E-03
-.323E-03
-.299E-03
-.274E-03
-.250E-03
-.225E-03
-.200E-03
-.176E-03
-.151E-03
-.127E-03
-.102E-03
(Midplint)-GCS0 (30Al shell, closed gap) NEW: Interf on Mid-plane 0.125mm

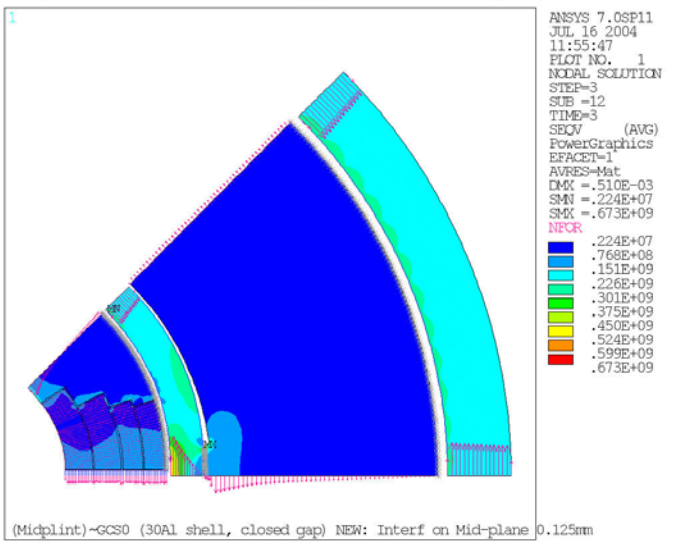
ANSYS 7.0SP11
JUL 16 2004
11:55:47
PLOT NO. 1
NODAL SOLUTION
STEP=3
SUB =12
TIME=3
SEQV (AVG)
PowerGraphics
EFACET=1
AVRES=Mat
DMX =.510E-03
SMN =.224E+07
SMX =.673E+09
NFOR
.224E+07
.768E+08
.151E+09
.226E+09
.301E+09
.375E+09
.450E+09
.524E+09
.599E+09
.673E+09
(Midplint)-GCS0 (30Al shell, closed gap) NEW: Interf on Mid-plane 0.125mm

9.2 Separation between layer 2 and 3

The following results show the analysis of a model with separation between layers 2 and 3 (layers 1&2 on a side and layers 3&4 on the other side are still glued together). It corresponds to a real case when the coils are wound and impregnated as double-layers. The mid-plane interference is 175 μm for layers 1&2 (by 50 μm higher than in the previous case) and 125 μm for layers 3&4 (as in the previous case). The radial interference between coil and collars was the same: 0.1 mm.

The results show some improvements (layer 2 was under compression at maximum gradient) but layer 1 was still under tension at maximum gradient. The azimuthal stress after cooldown shows that part of the pole turns of layer 1 are already under tension after the cooldown. These results suggested the need to have a sliding surface between the side of shell 1 and the collar wedge.

The coil displacement at the mid-plane was 91 μm and the coil deformation (Rmax - Rmin) was 30 μm.

Equal to 9.1 except for: **Layers 1&2 separate from 2&3**
Mid-plane interference: 175 (1&2) – 125 (3&4) μm

Coil/Coll radial Int : 0.1 mm,

Prestress:

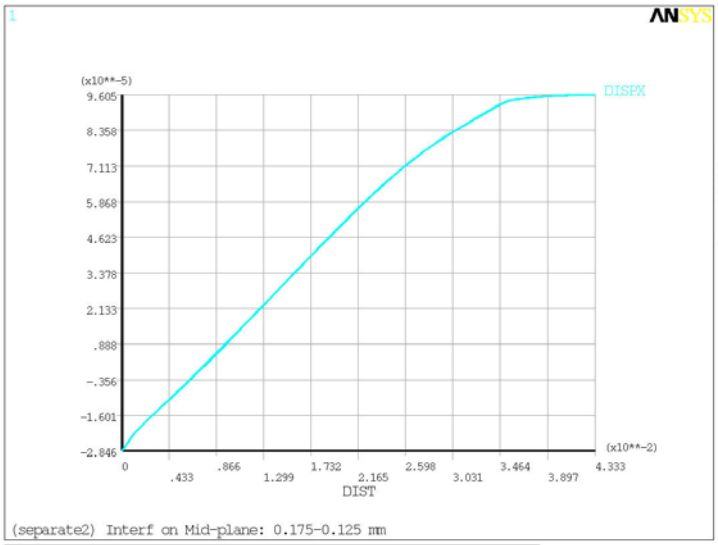

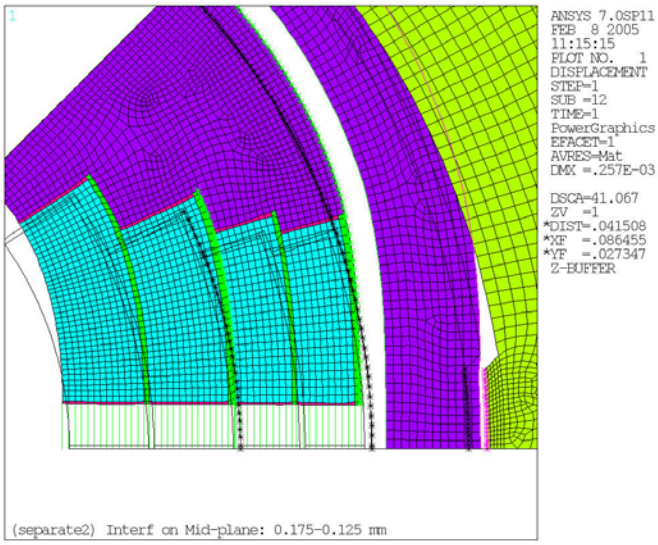

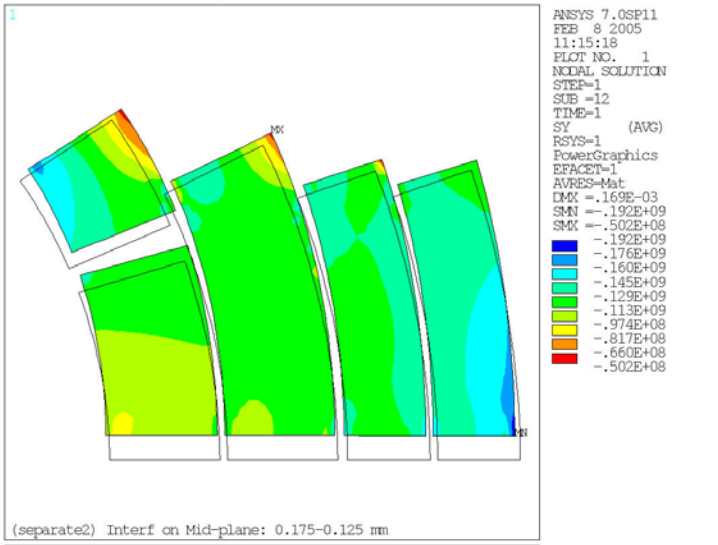

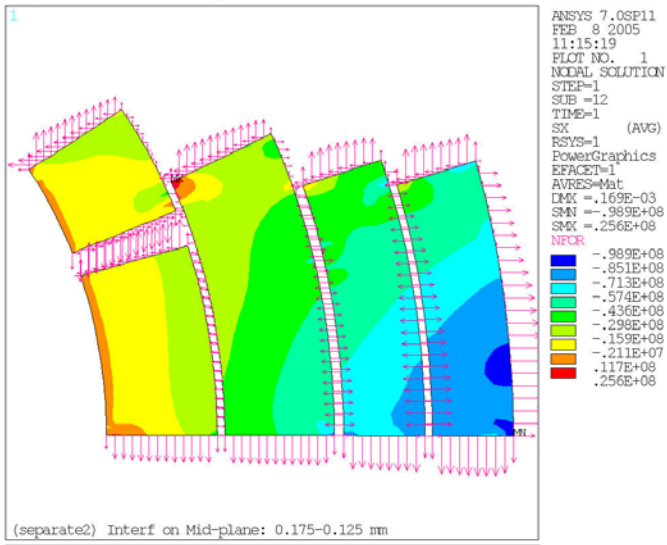

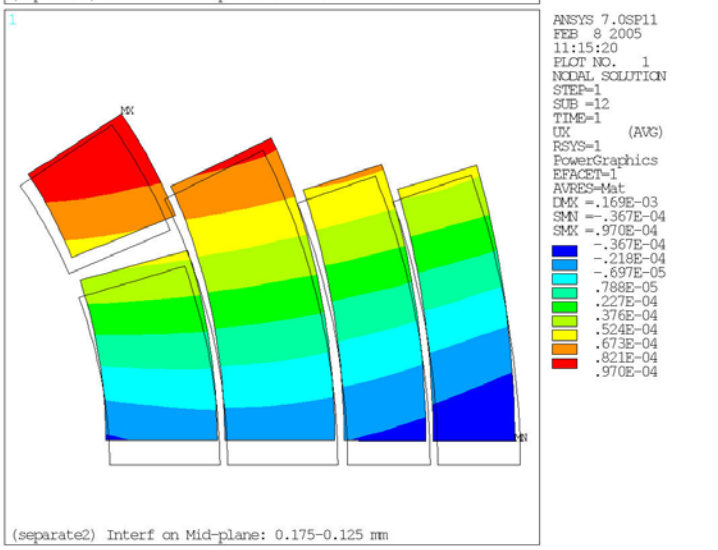

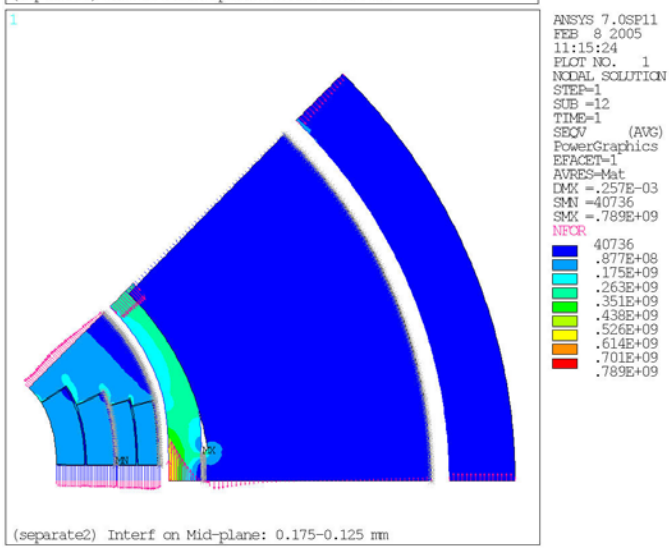

After Cooldown

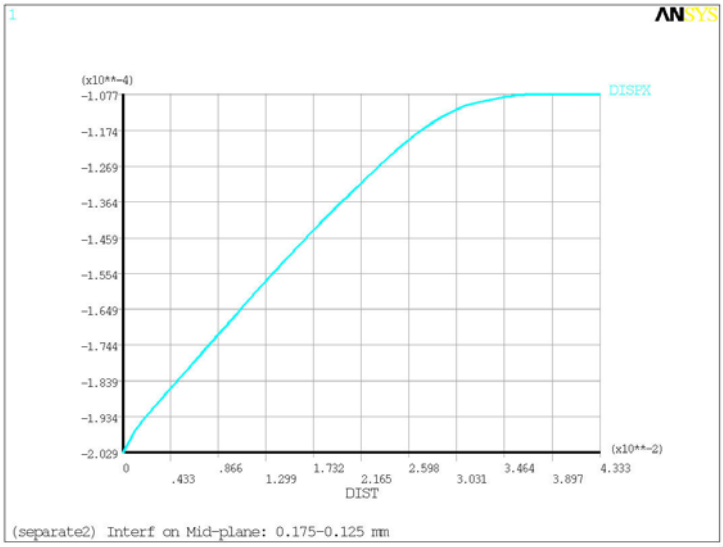

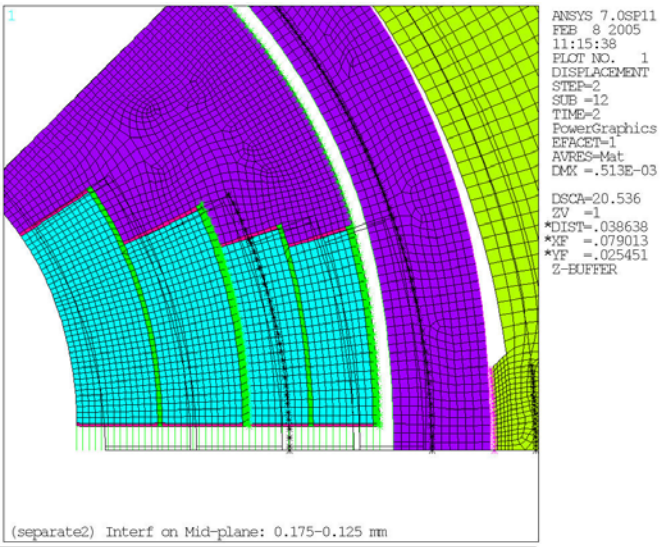

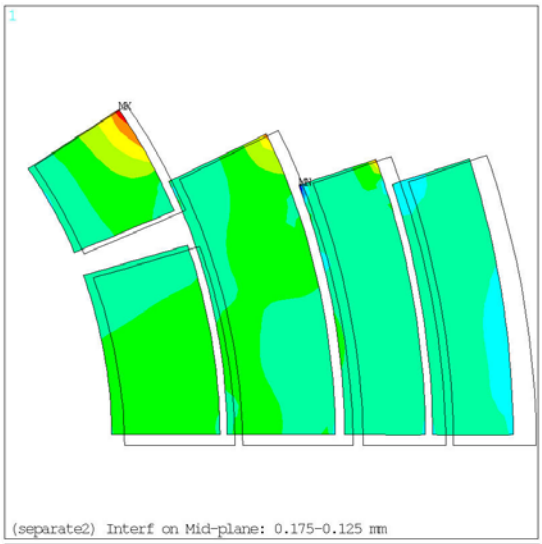

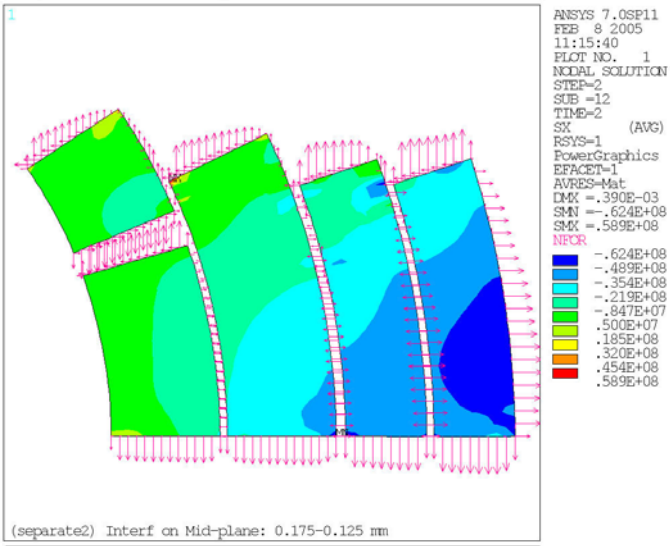

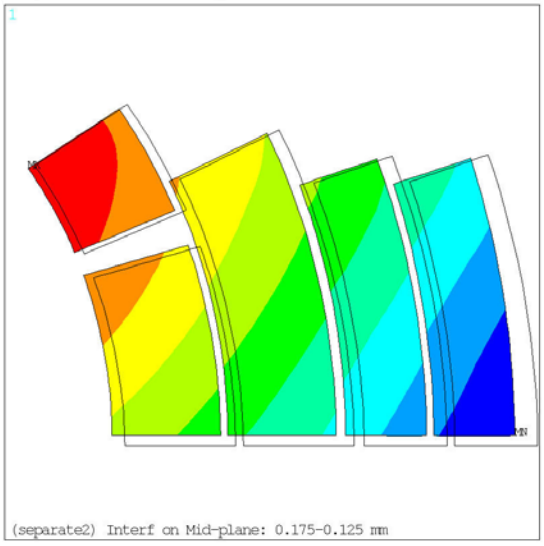

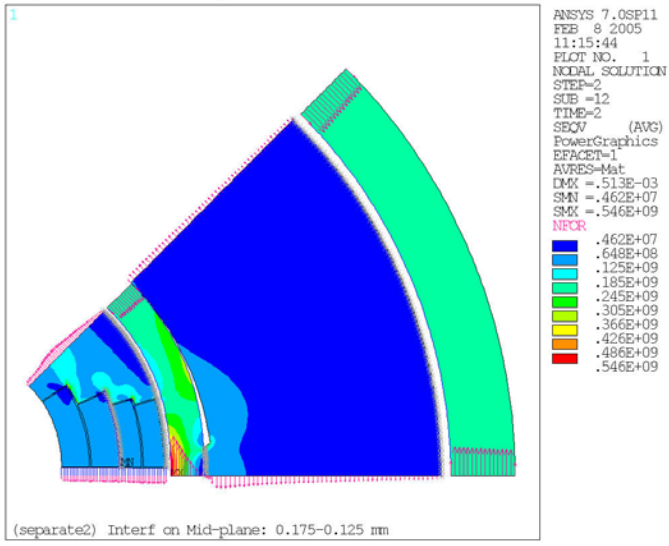

At 228 T/m:

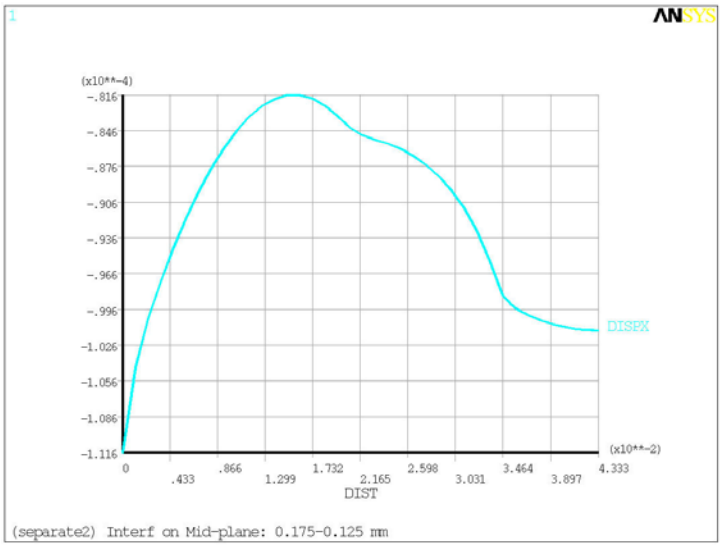
ANSYS
(x10**-4)
-.816
-.846
-.876
-.906
-.936
-.966
-.996
-1.026
-1.056
-1.086
-1.116
DISPX
(x10**-2)
0
.433
.866
1.299
1.732
2.165
2.598
3.031
3.464
3.897
4.333
DIST
(separate2) Interf on Mid-plane: 0.175-0.125 mm

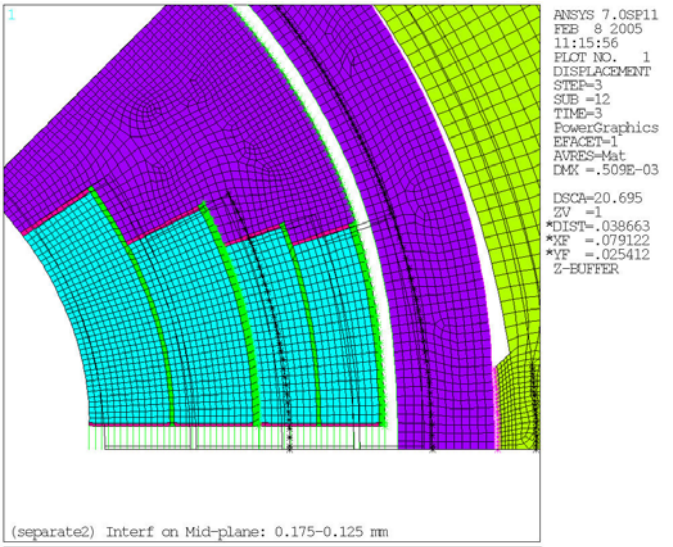
ANSYS 7.0SP11
FEB 8 2005
11:15:56
PLOT NO. 1
DISPLACEMENT
STEP=3
SUB =12
TIME=3
PowerGraphics
EFACET=1
AVRES=Mat
DMX =.509E-03
DSCA=20.695
ZV =1
*DIST=.038663
*XF =.079122
*YF =.025412
Z-BUFFER
(separate2) Interf on Mid-plane: 0.175-0.125 mm

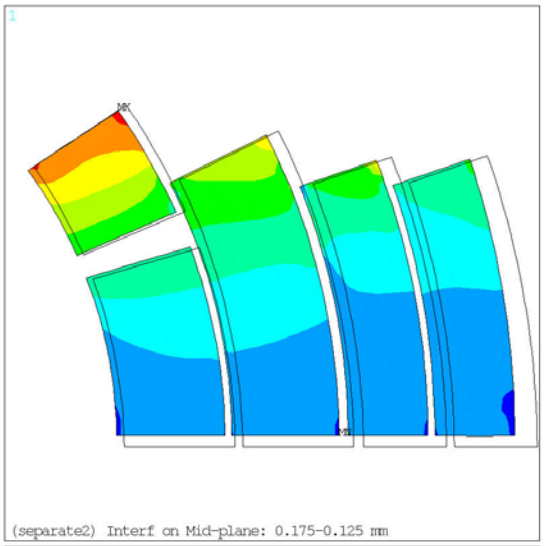
ANSYS 7.0SP11
FEB 8 2005
11:15:57
PLOT NO. 1
NODAL SOLUTION
STEP=3
SUB =12
TIME=3
SY (AVG)
RSYS=1
PowerGraphics
EFACET=1
AVRES=Mat
DMX =.352E-03
SMN =-.169E+09
SMX =.988E+08
-.169E+09
-.139E+09
-.109E+09
-.797E+08
-.500E+08
-.202E+08
.956E+07
.393E+08
.691E+08
.988E+08
(separate2) Interf on Mid-plane: 0.175-0.125 mm

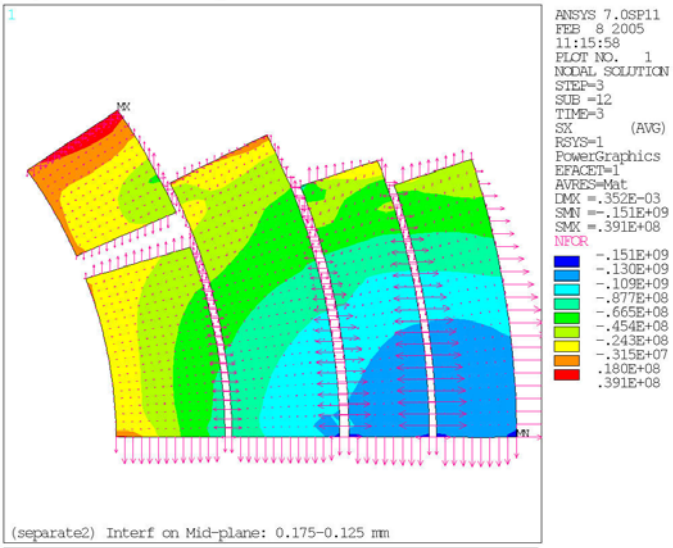
ANSYS 7.0SP11
FEB 8 2005
11:15:58
PLOT NO. 1
NODAL SOLUTION
STEP=3
SUB =12
TIME=3
SX (AVG)
RSYS=1
PowerGraphics
EFACET=1
AVRES=Mat
DMX =.352E-03
SMN =-.151E+09
SMX =.391E+08
NFOR
-.151E+09
-.130E+09
-.109E+09
-.877E+08
-.665E+08
-.454E+08
-.243E+08
-.315E+07
.180E+08
.391E+08
(separate2) Interf on Mid-plane: 0.175-0.125 mm

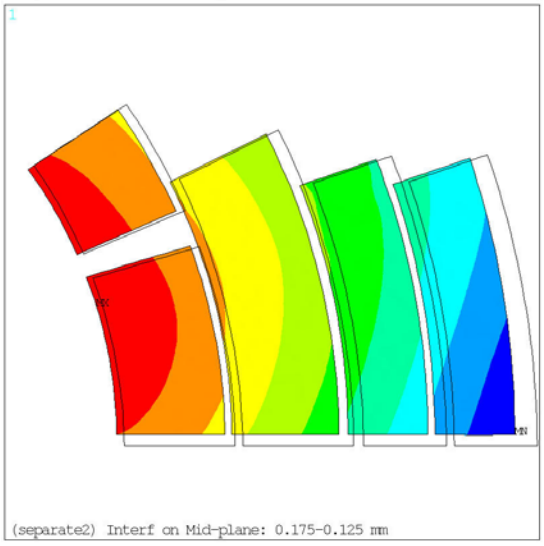
ANSYS 7.0SP11
FEB 8 2005
11:15:59
PLOT NO. 1
NODAL SOLUTION
STEP=3
SUB =12
TIME=3
UX (AVG)
RSYS=1
PowerGraphics
EFACET=1
AVRES=Mat
DMX =.352E-03
SMN =-.313E-03
SMX =-.817E-04
-.313E-03
-.287E-03
-.262E-03
-.236E-03
-.210E-03
-.185E-03
-.159E-03
-.133E-03
-.107E-03
-.817E-04
(separate2) Interf on Mid-plane: 0.175-0.125 mm

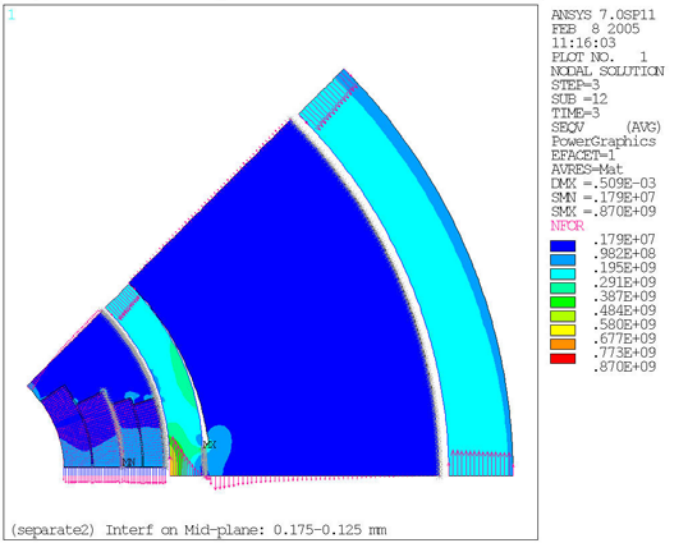
ANSYS 7.0SP11
FEB 8 2005
11:16:03
PLOT NO. 1
NODAL SOLUTION
STEP=3
SUB =12
TIME=3
SEQV (AVG)
PowerGraphics
EFACET=1
AVRES=Mat
DMX =.509E-03
SMN =.179E+07
SMX =.870E+09
NFOR
.179E+07
.982E+08
.195E+09
.291E+09
.387E+09
.484E+09
.580E+09
.677E+09
.773E+09
.870E+09
(separate2) Interf on Mid-plane: 0.175-0.125 mm

9.3 Collar wedge split

The last model has the collar wedge split in two parts. The tip covers the 1st layer (innermost layer) and is glued to it. The rest of the wedge has contact elements at the interface with the wedge tip, the 1st and 2nd layers, and is glued to the remaining layers (for easier convergence). Since layers 3&4 are always under compression, this model can also represent the case in which the collar wedge is not glued to the coil, with the exception of its tip on the 1st layer.

A clearance of 50 μm has been introduced between the 2nd layer and the collar wedge in order to allow more pre-stress of the top of layer 1 than in the latest models. Mid-plane and radial coil-collar interferences are equal to those used in the previous case. The results shown in the following plots show that the azimuthal stresses in the coils are: (i) at the maximum acceptable level after pre-stressing at 300K (the top of layer 1 is actually above 150 MPa); (ii) they decrease during cooldown (less than 122 MPa in layer 1); there is some tension (less than 80 MPa) on the top of layer 1 at maximum gradient. The coil bending in this case has a "C" shape with maximum bending (Rmax-Rmin) of 33 μm. The coil displacement at the mid-plane under magnetic forces is 96 μm.

Equal to 9.2 except for: **Collar wedge separated from layer 1**
Gap on top of layer2: 50 μm

Coil/Coll radial Int : 0.1 mm; Coil 1&2 separate from 2&3; Midplane interf: 175 (1&2) – 125 (3&4) μm

Prestress:

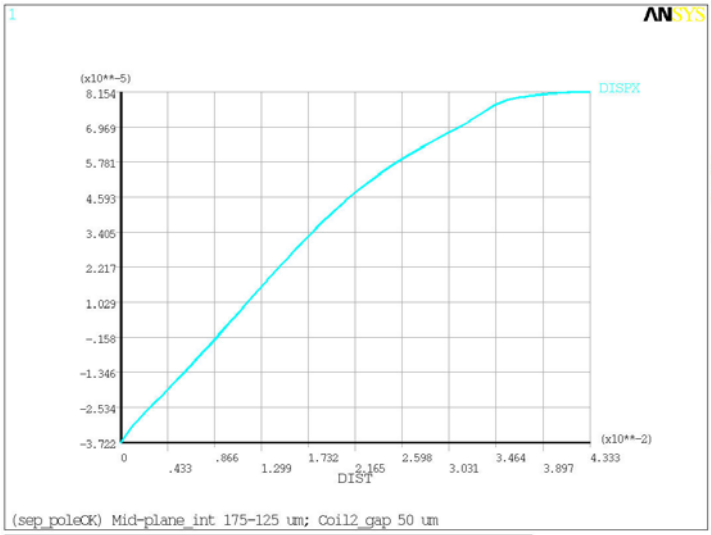

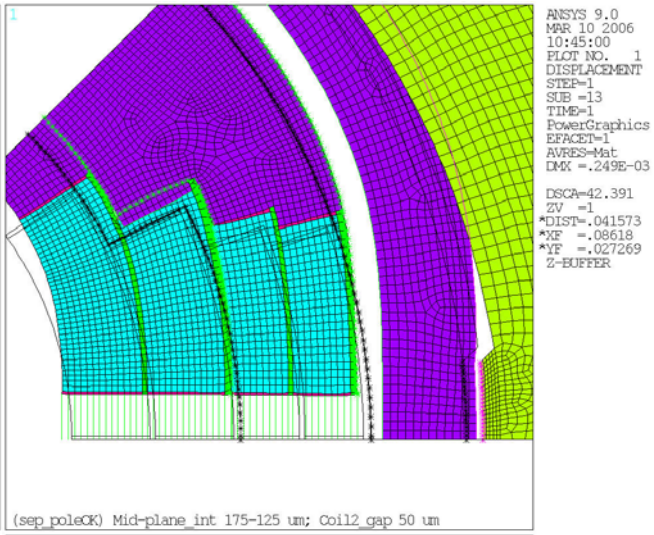

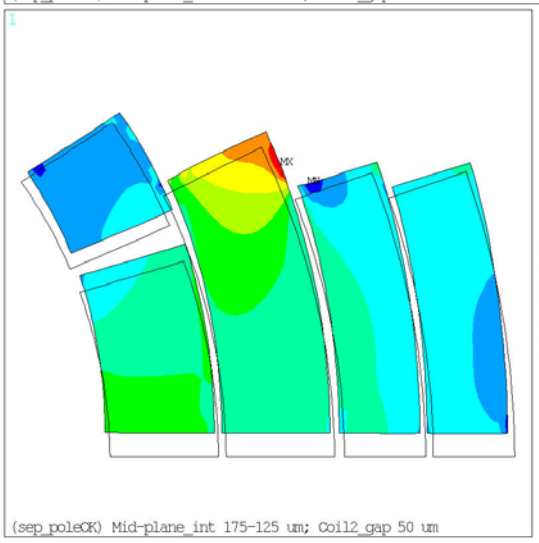

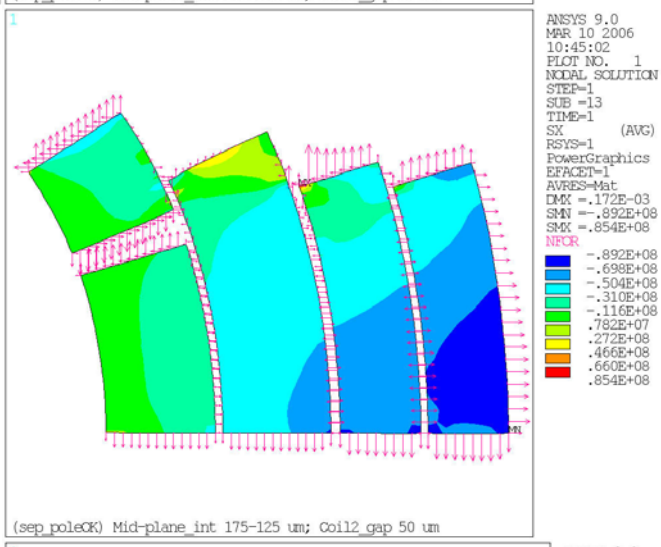

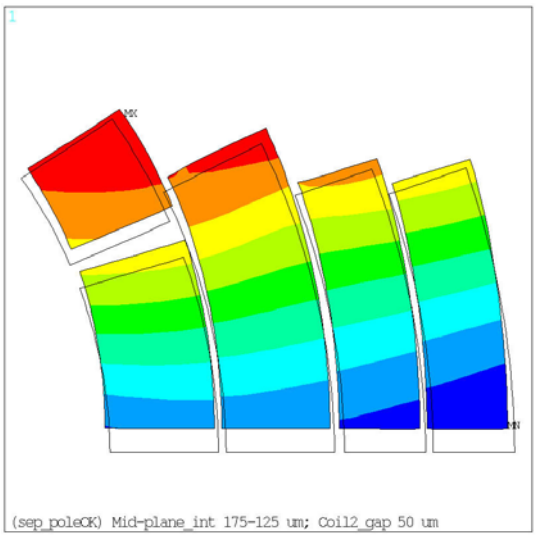

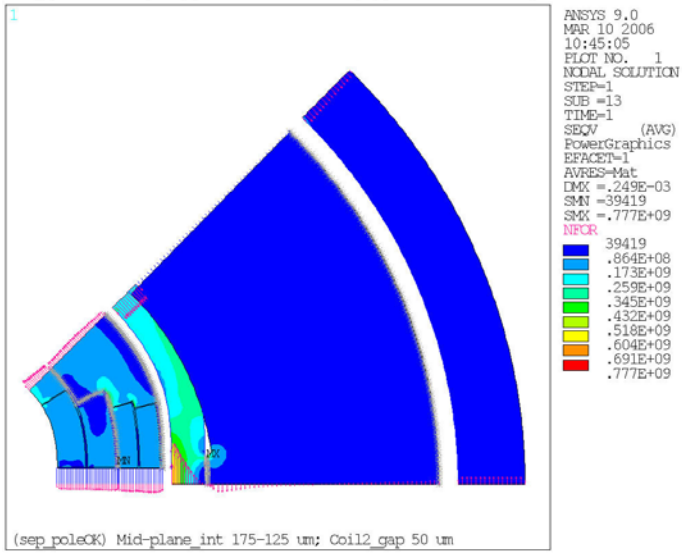

After Cooldown

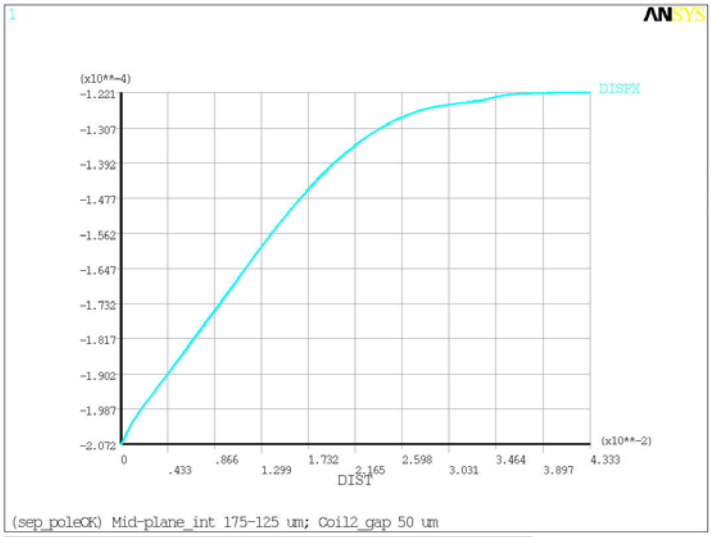

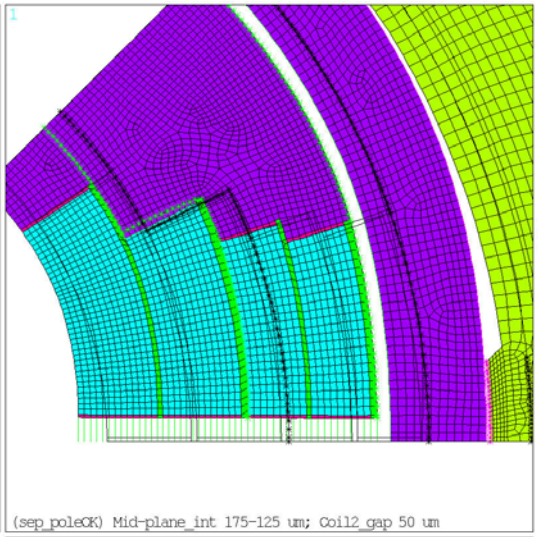

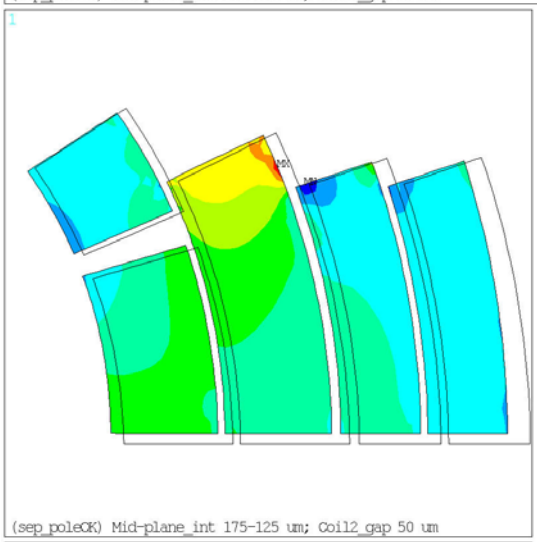

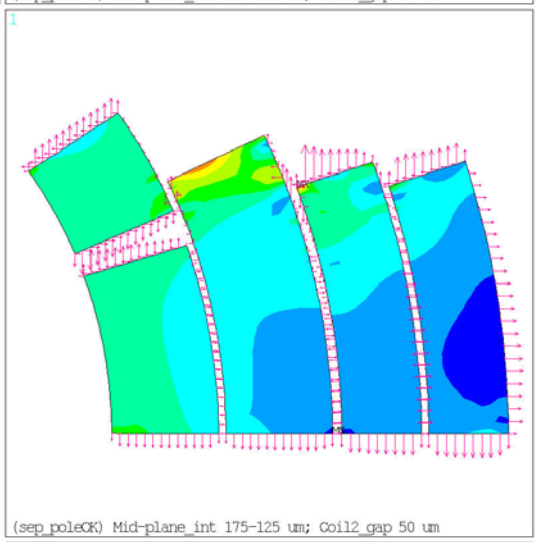

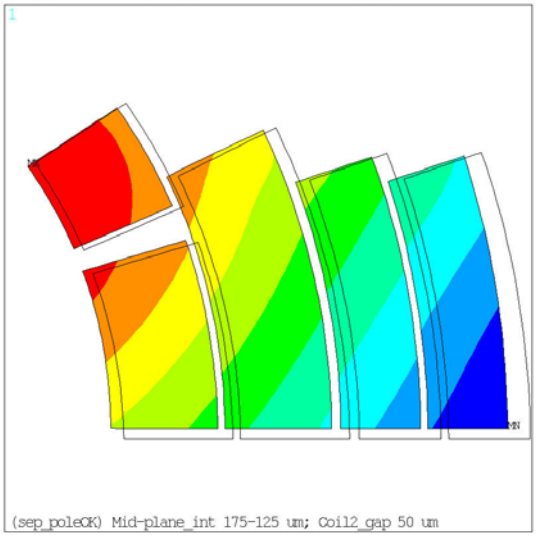

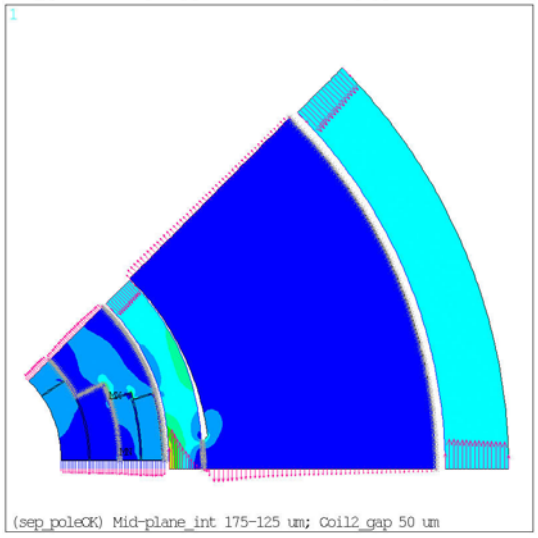

At 228 T/m:

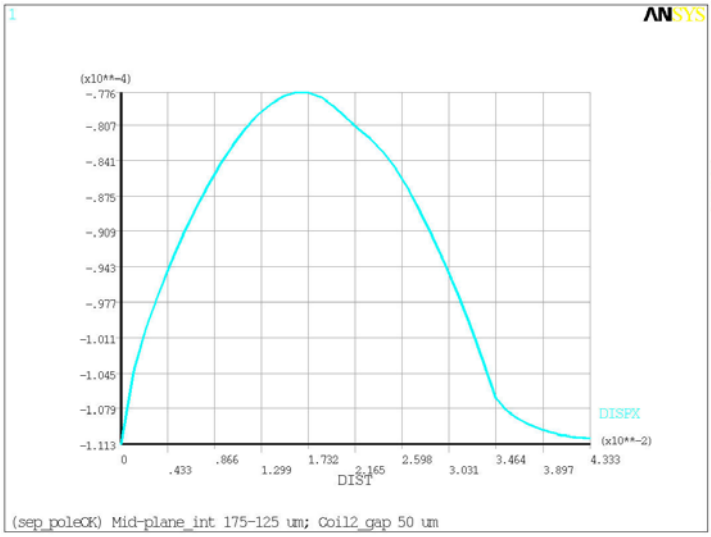
ANSYS
(x10**-4)
-.776
-.807
-.841
-.875
-.909
-.943
-.977
-1.011
-1.045
-1.079
-1.113
DISPX
(x10**-2)
0
.433
.866
1.299
1.732
2.165
2.598
3.031
3.464
3.897
4.333
DIST
(sep_poleOK) Mid-plane_int 175-125 um; Coil2_gap 50 um

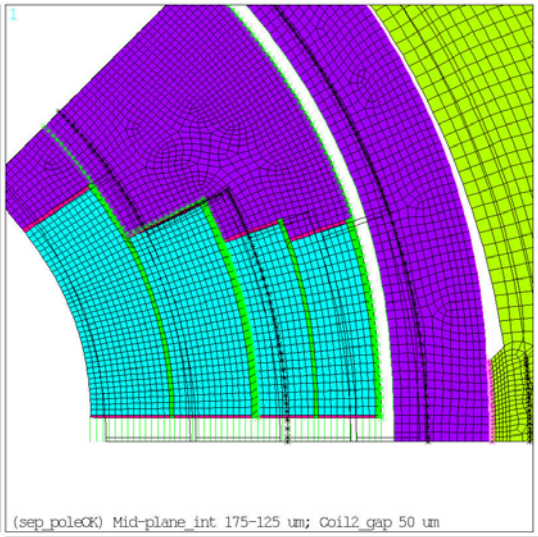
ANSYS 9.0
MAR 10 2006
10:45:23
PLOT NO. 1
DISPLACEMENT
STEP=3
SUB =12
TIME=3
PowerGraphics
EFACET=1
AVRES=Mat
DMX =.509E-03
DSCA=20.699
ZV =1
*DIST=.03869
*XF =.079014
*YF =.025371
Z-BUFFER
(sep_poleOK) Mid-plane_int 175-125 um; Coil2_gap 50 um

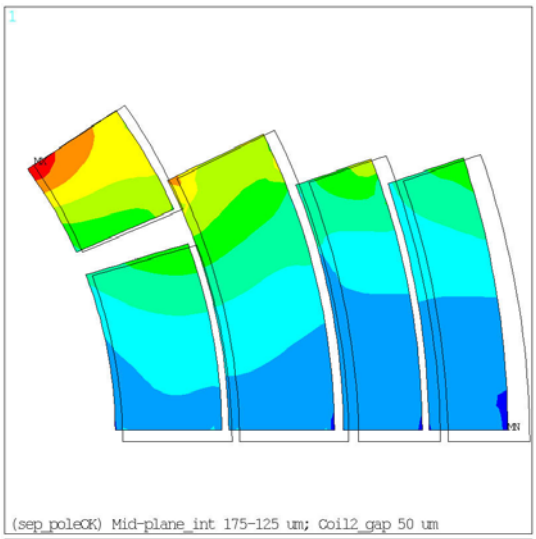
ANSYS 9.0
MAR 10 2006
10:45:24
PLOT NO. 1
NODAL SOLUTION
STEP=3
SUB =12
TIME=3
SY (AVG)
RSYS=1
PowerGraphics
EFACET=1
AVRES=Mat
DMX =.352E-03
SMN =-.170E+09
SMX =.826E+08
-.170E+09
-.142E+09
-.114E+09
-.858E+08
-.577E+08
-.297E+08
-.160E+07
.265E+08
.545E+08
.826E+08
(sep_poleOK) Mid-plane_int 175-125 um; Coil2_gap 50 um

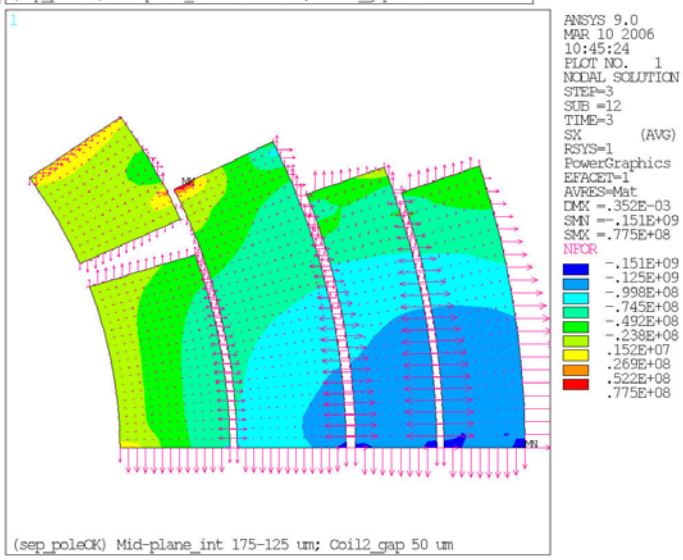
ANSYS 9.0
MAR 10 2006
10:45:24
PLOT NO. 1
NODAL SOLUTION
STEP=3
SUB =12
TIME=3
SX (AVG)
RSYS=1
PowerGraphics
EFACET=1
AVRES=Mat
DMX =.352E-03
SMN =-.151E+09
SMX =.775E+08
NFOR
-.151E+09
-.125E+09
-.998E+08
-.745E+08
-.492E+08
-.238E+08
.152E+07
.269E+08
.522E+08
.775E+08
(sep_poleOK) Mid-plane_int 175-125 um; Coil2_gap 50 um

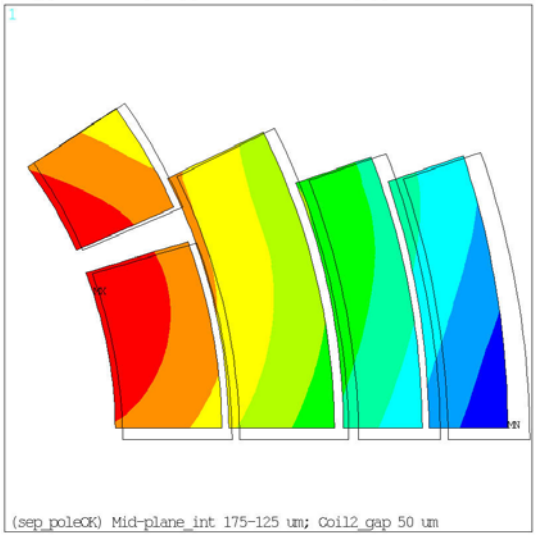
ANSYS 9.0
MAR 10 2006
10:45:24
PLOT NO. 1
NODAL SOLUTION
STEP=3
SUB =12
TIME=3
UX (AVG)
RSYS=1
PowerGraphics
EFACET=1
AVRES=Mat
DMX =.352E-03
SMN =-.313E-03
SMX =-.776E-04
-.313E-03
-.286E-03
-.260E-03
-.234E-03
-.208E-03
-.182E-03
-.156E-03
-.130E-03
-.104E-03
-.776E-04
(sep_poleOK) Mid-plane_int 175-125 um; Coil2_gap 50 um

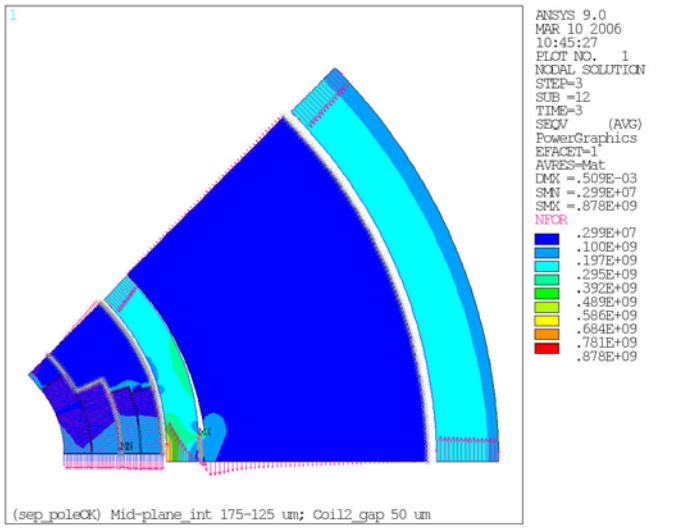
ANSYS 9.0
MAR 10 2006
10:45:27
PLOT NO. 1
NODAL SOLUTION
STEP=3
SUB =12
TIME=3
SEQV (AVG)
PowerGraphics
EFACET=1
AVRES=Mat
DMX =.509E-03
SMN =.299E+07
SMX =.878E+09
NFOR
.299E+07
.100E+09
.197E+09
.295E+09
.392E+09
.489E+09
.586E+09
.684E+09
.781E+09
.878E+09
(sep_poleOK) Mid-plane_int 175-125 um; Coil2_gap 50 um

9.3b Collar wedge split and thicker yoke pusher

The following analysis shows an attempt to improve the last model by increasing the pre-stress at cold without increasing the pre-stress at room temperature. In order to do it the thickness of the yoke pusher (the part of the yoke in contact with the collars) was increased by 50 μm. Since this model uses an aluminum shell the effect of this change should be larger at cold than at room temperature. The following plots show that this attempt, although produced some improvements, wasn't sufficient to fix the problem. The stresses at room temperature didn't increase, but the stresses at cold showed only small increments not sufficient to avoid tension (50 MPa) in the 1st layer at maximum forces. It's not possible to increase any more significantly the thickness of the yoke pusher because this solution shows that the stresses in the 4th layer have passed 150 MPa in a large area.

In this solution the force on the mid-plane is so large that the coil inner radius on the midplane remains smaller than the radius at any other point of the coil inner surface even under maximum forces. The resulting coil bending (Rmax – Rmin) is 43 μm, the coil displacement at the inner radius is 96 μm, and the coil pre-bending after cooldown is 106 μm (the largest pre-bending after cooldown among all cases presented).

The conclusion of this part of the study is that it wasn't possible to find an acceptable solution with pre-load applied by interference on the mid-plane (i.e. simulating shims set on the mid-plane during magnet assembly) with the same amount of effort spent to find an acceptable solution with interference at the coil-pole interface (i.e. simulating shims set between the coil and the pole during magnet assembly). That doesn't mean that it's not possible to find an acceptable solution with interference on the coil mid-plane, but its shows that it's significantly more difficult than in case of applying the pre-stress by interference at the coil-pole interface. We can also guess that if it will be possible to find a solution with interference on the mid-plane, the acceptable tolerance range will be smaller than in case of solutions with interference at the coil-pole interface.

Equal to 9.3 except for the inner radius of Yoke_Pusher that is 117.25 mm (previously was 117.3)

This is an attempt to increase pre-stress at cold but not at 300 K

Coil/Coll radial Int : 0.1 mm; Coil 1&2 separate from 2&3; Midplane interf: 175 (1&2) – 125 (3&4) um

Prestress:

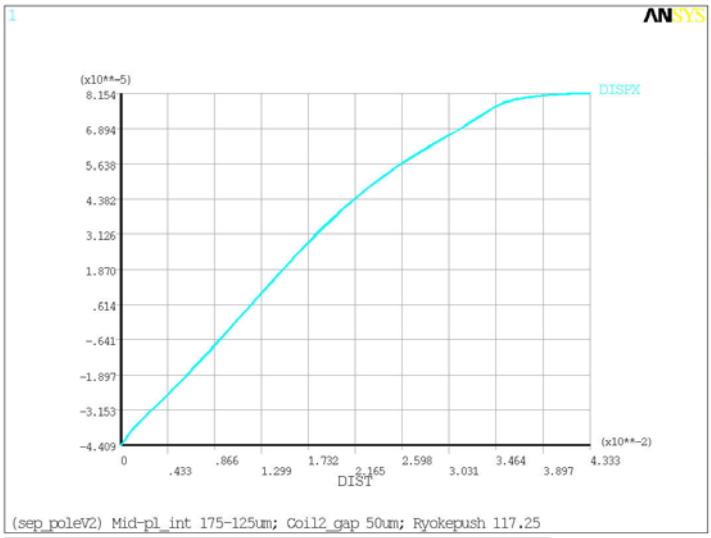

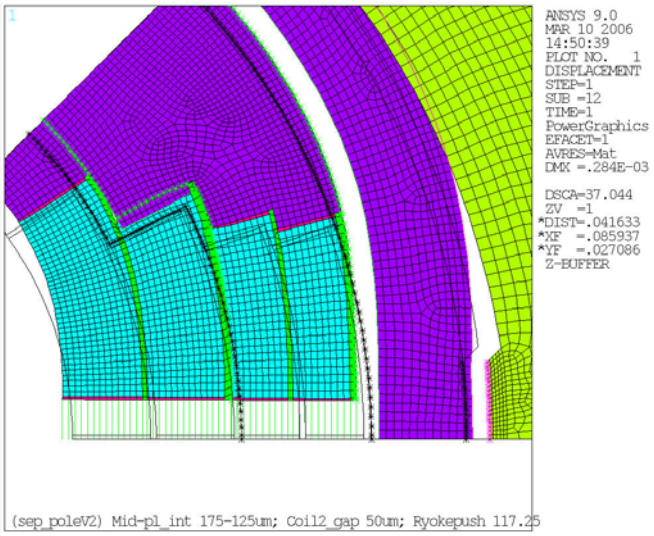

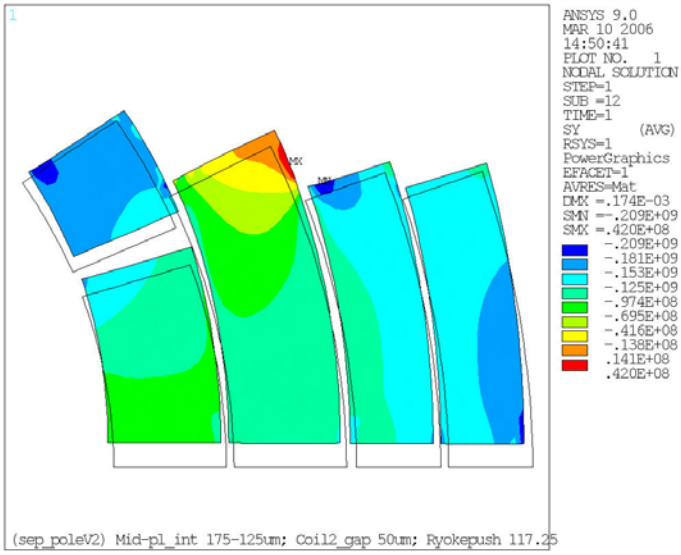

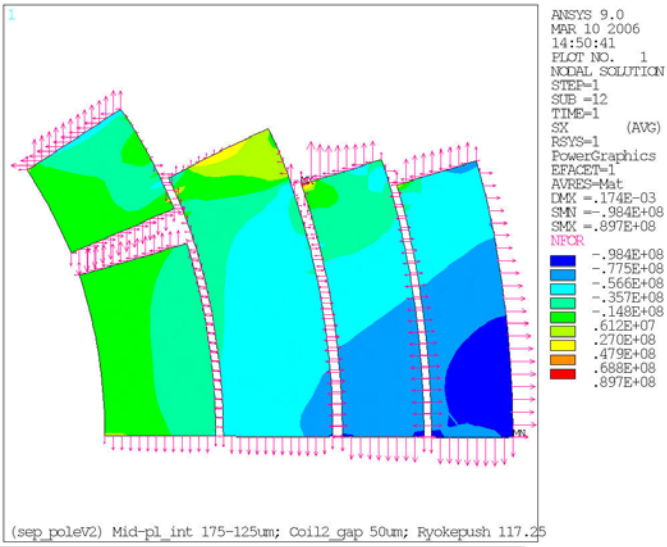

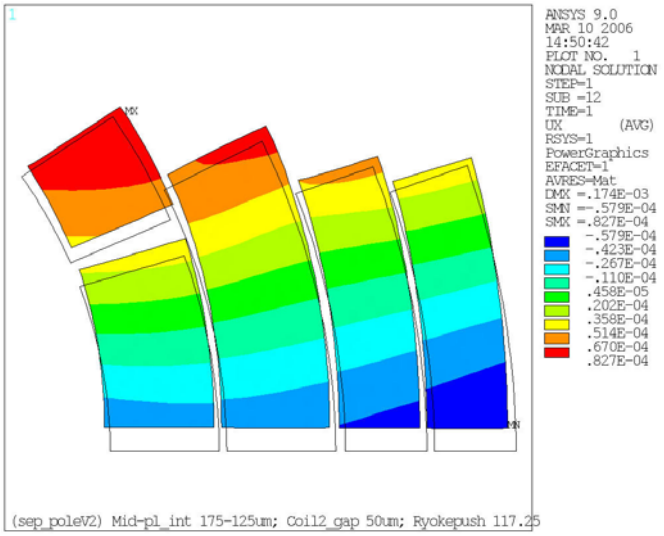

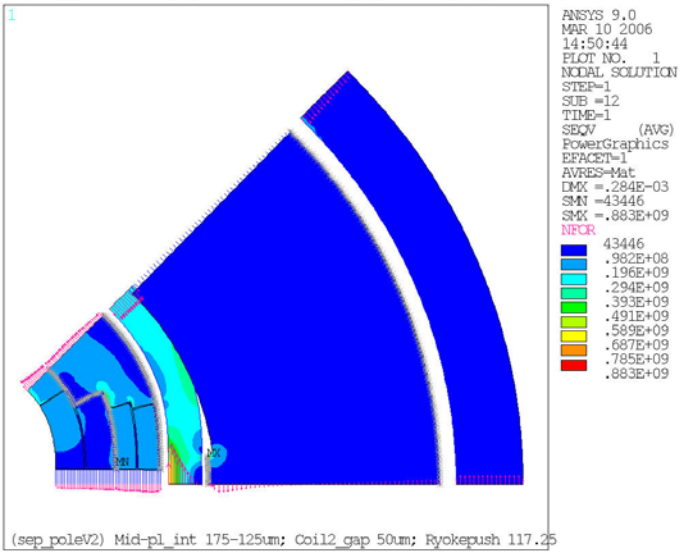

After Cooldown

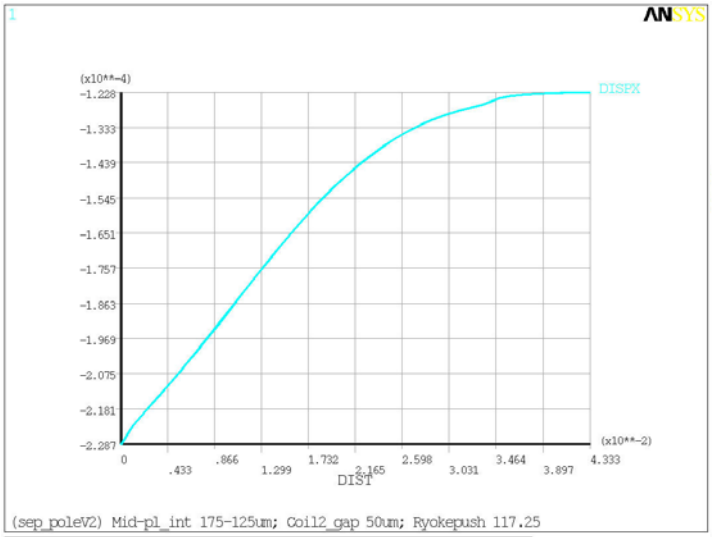

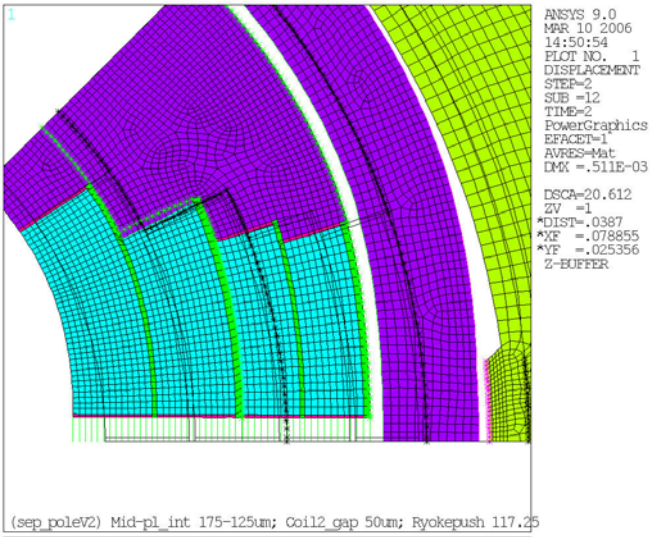

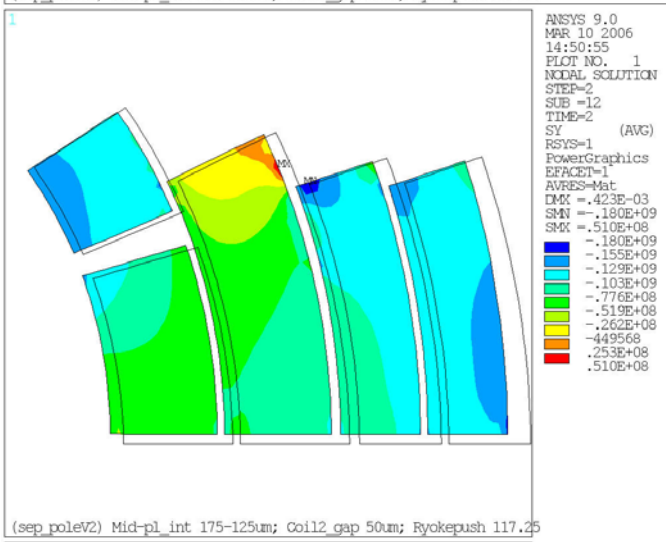

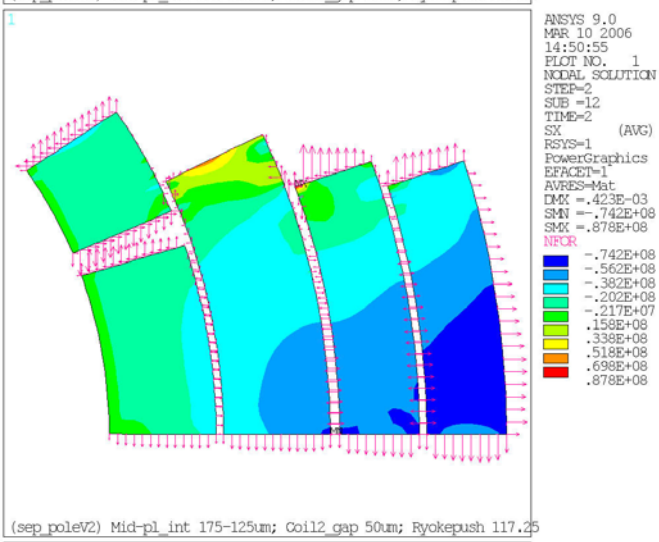

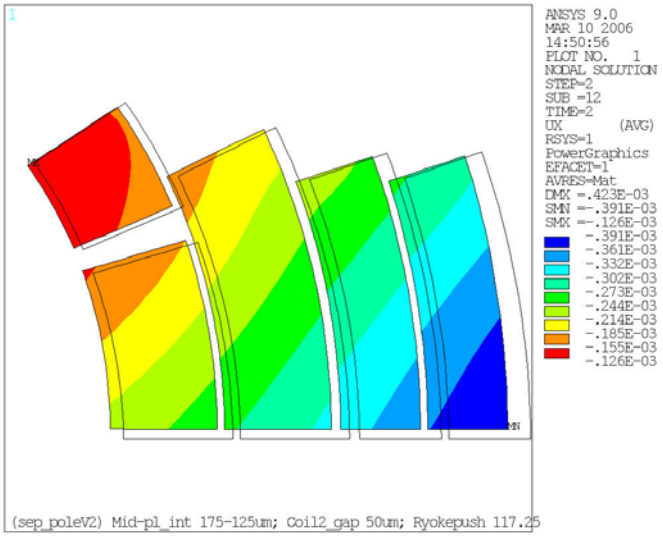

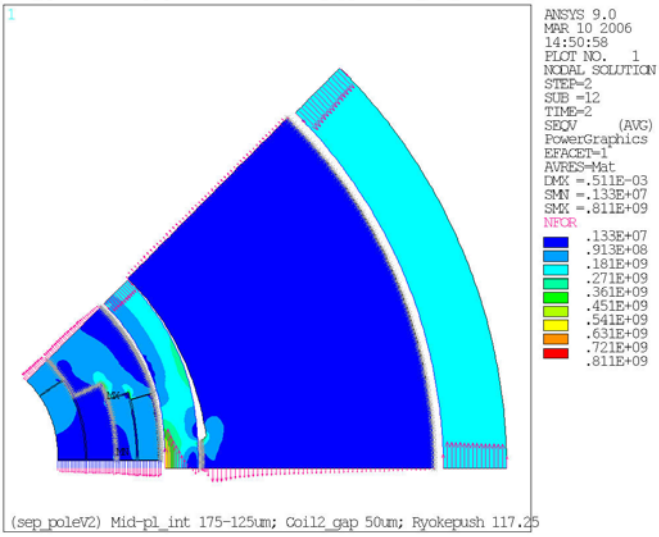

At 228 T/m:

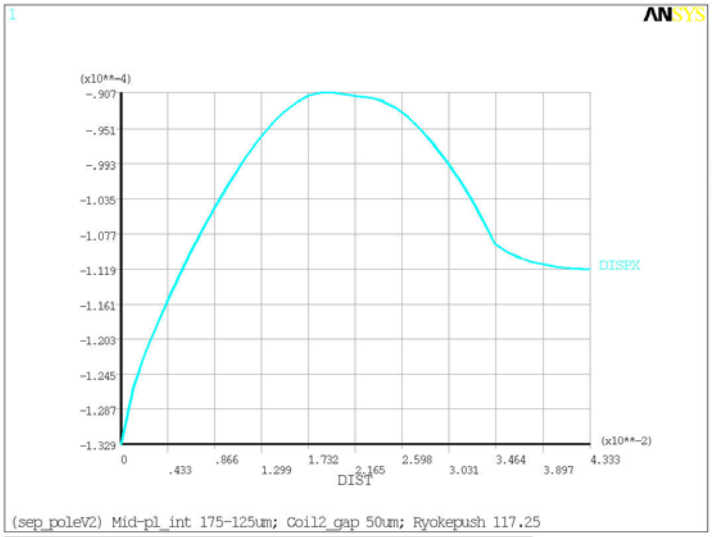
ANSYS
(x10**-4)
-.907
-.951
-.993
-1.035
-1.077
-1.119
-1.161
-1.203
-1.245
-1.287
-1.329
DISPX
0
.433
.866
1.299
1.732
2.165
2.598
3.031
3.464
3.897
4.333
(x10**-2)
DIST
(sep_poleV2) Mid-pl_int 175-125um; Coil2_gap 50um; Ryokepush 117.25

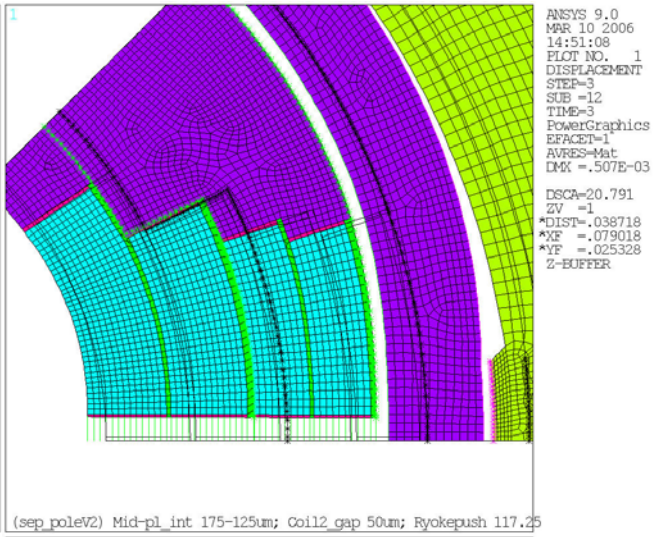
ANSYS 9.0
MAR 10 2006
14:51:08
PLOT NO. 1
DISPLACEMENT
STEP=3
SUB =12
TIME=3
PowerGraphics
EFACET=1
AVRES=Mat
DMX =.507E-03
DSCA=20.791
ZV =1
*DIST=.038718
*XF =.079018
*YF =.025328
Z-BUFFER
(sep_poleV2) Mid-pl_int 175-125um; Coil2_gap 50um; Ryokepush 117.25

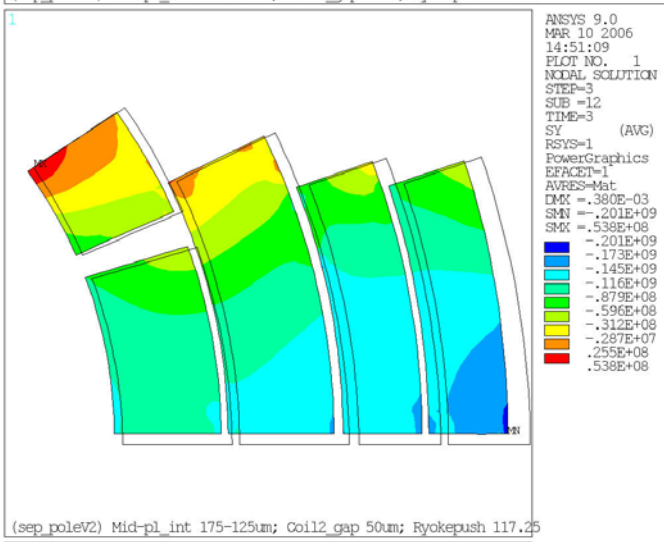
ANSYS 9.0
MAR 10 2006
14:51:09
PLOT NO. 1
NODAL SOLUTION
STEP=3
SUB =12
TIME=3
SY (AVG)
RSYS=1
PowerGraphics
EFACET=1
AVRES=Mat
DMX =.380E-03
SMN =-.201E+09
SMX =.538E+08
-.201E+09
-.173E+09
-.145E+09
-.116E+09
-.879E+08
-.596E+08
-.312E+08
-.287E+07
.255E+08
.538E+08
(sep_poleV2) Mid-pl_int 175-125um; Coil2_gap 50um; Ryokepush 117.25

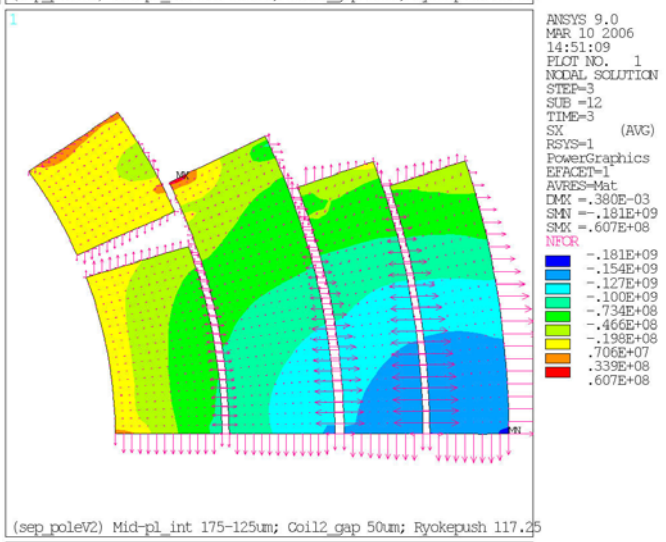
ANSYS 9.0
MAR 10 2006
14:51:09
PLOT NO. 1
NODAL SOLUTION
STEP=3
SUB =12
TIME=3
SX (AVG)
RSYS=1
PowerGraphics
EFACET=1
AVRES=Mat
DMX =.380E-03
SMN =-.181E+09
SMX =.607E+08
NFOR
-.181E+09
-.154E+09
-.127E+09
-.100E+09
-.734E+08
-.466E+08
-.198E+08
.706E+07
.339E+08
.607E+08
(sep_poleV2) Mid-pl_int 175-125um; Coil2_gap 50um; Ryokepush 117.25

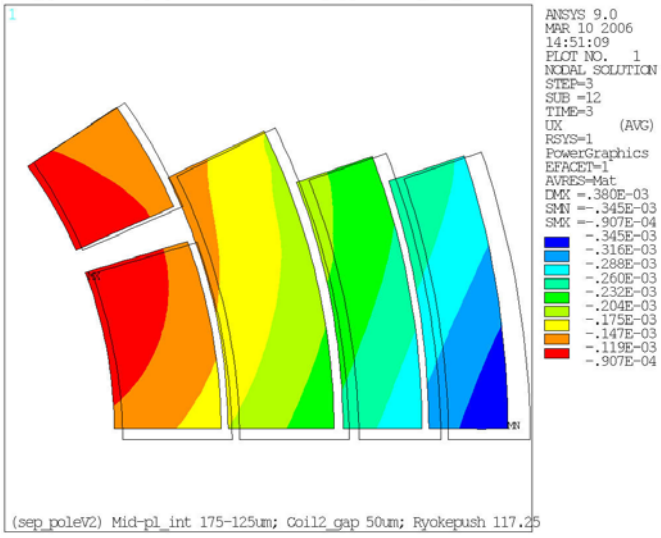
ANSYS 9.0
MAR 10 2006
14:51:09
PLOT NO. 1
NODAL SOLUTION
STEP=3
SUB =12
TIME=3
UX (AVG)
RSYS=1
PowerGraphics
EFACET=1
AVRES=Mat
DMX =.380E-03
SMN =-.345E-03
SMX =-.907E-04
-.345E-03
-.316E-03
-.288E-03
-.260E-03
-.232E-03
-.204E-03
-.175E-03
-.147E-03
-.119E-03
-.907E-04
(sep_poleV2) Mid-pl_int 175-125um; Coil2_gap 50um; Ryokepush 117.25

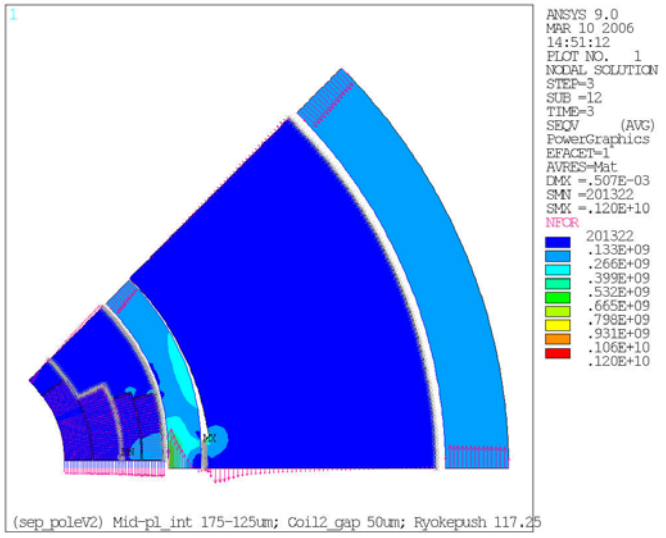
ANSYS 9.0
MAR 10 2006
14:51:12
PLOT NO. 1
NODAL SOLUTION
STEP=3
SUB =12
TIME=3
SEQV (AVG)
PowerGraphics
EFACET=1
AVRES=Mat
DMX =.507E-03
SMN =201322
SMX =.120E+10
NFOR
201322
.133E+09
.266E+09
.399E+09
.532E+09
.665E+09
.798E+09
.931E+09
.106E+10
.120E+10
(sep_poleV2) Mid-pl_int 175-125um; Coil2_gap 50um; Ryokepush 117.25

10. CONCLUSIONS

This study shows that it's possible to design a support structure for a 4-layer, 230-T/m gradient, 110-mm aperture quadrupole with acceptable stresses and coil deformation, but it's quite difficult. The design of the support structure may not allow complete freedom of choice for the coil fabrication and magnet assembly technology, it will require an integrated optimization of the whole magnet design, and may require very tight tolerances. More in details we can conclude that:

- The concept developed in this study (stainless steel collars providing part of the pre-stress, and rigid structure with iron gaps closing during cooldown providing additional support and coil pre-bending on the mid-planes) achieved the goals (acceptable stresses and coil deformation) under some conditions of pre-stress application.
- Acceptable solutions were found when the pre-stress was applied by interferences at the coil-pole interface, because the interference can be optimized for each layer (this as an impact on the coil fabrication technology because it does not allow to glue the pole to the coil).
- Because of the very large forces and internal stresses this magnet requires a very careful optimization of the design.
- The design optimization has to be performed on the whole design (for instance both magnetic and mechanical, because designs with similar magnetic properties may have significantly different mechanical behaviors) and the assembly technology (for instance not glued poles allow pre-stress optimization) in a very integrated effort.
- Sensitivity analysis should be part of the optimization in order to evaluate acceptable tolerances, which may be critical because there is very small margin.

References

1. V.V. Kashikhin, A.V. Zlobin, *"4-layer Nb3Sn IR Quadrupoles for the LHC Luminosity Upgrade"* Fermilab Technical Division note TD-03-003
2. D.R. Chichili, et al., *"Investigation of Cable Insulation and Thermo-Mechanical Properties of Epoxy Impregnated Nb3Sn Composite"*, IEEE Trans. on Applied Superconductivity, Vol. 10, No. 1, March 2000, pp. 1317 -1320.